

# Methodical Approach for Analyzing Process Variables and Optimizing Boundary Conditions in Multi-Axis Robot Programs

Methodischer Ansatz zur Analyse von Prozessvariablen und Optimierung von Randbedingungen in Multi-Achs-Roboterprogrammen

Scientific work for obtaining the academic degree

Master of Science (M.Sc.)

at the TUM School of Engineering and Design of the Technical University of Munich

<b>Supervised by</b>	Prof. Dr.-Ing. Michael Zäh Institute for Machine Tools and Industrial Management (iwb)
<b>Submitted by</b>	Jan Nalivaika Lerchenauerstrasse 10 80809 Munich
<b>Submitted on</b>	March 04, 2024 in Garching



## **Acknowledgment**

I would like to take this opportunity to express my heartfelt appreciation to my two supervisors, Marius Breuer and Ludwig Siebert, for their exceptional guidance and unwavering support throughout the entire duration of my master's thesis. Their expertise, dedication, and willingness to share their knowledge have been instrumental in shaping the direction and quality of this research. Their valuable insights and constructive feedback have significantly contributed to the development of this work. I am truly grateful for their availability, as they were always approachable and ready to assist whenever I encountered challenges or needed clarification. Their prompt response and timely feedback were incredibly valuable in ensuring the smooth progress of this thesis. I am deeply thankful for their remarkable contributions and for being outstanding mentors throughout this journey.



# Scope of Work

## Title of the Master's Thesis:

Methodical Approach for Analyzing Process Variables and Optimizing Boundary Conditions in Multi-Axis Robot Programs

## Titel der Master's Thesis:

Methodischer Ansatz zur Analyse von Prozessvariablen und Optimierung von Randbedingungen in Multi-Achs-Roboterprogrammen

**Author:** B.Sc. Jan Nalivaika

**Issue:** 02.10.2023

**Supervisor:** M.Sc. Ludwig Siebert

**Submission:** 04.03.2024

## Motivation:

Computer-aided manufacturing (CAM) is used to automatically generate tool paths for computer numerically controlled machines. The CAM software considers the models of the raw and finished parts, the constraints of the machine, the tools, and the manufacturing technology. Together with user-configurable parameters, tool paths for 3-axis, 5-axis, or robot-based machine tools are generated. The growing demand for flexibility in machine tools, such as the use of multiple manufacturing technologies in one machine or automated loading and unloading, has led to many machine tools being equipped with additional mechanical axes. Examples include robots mounted on linear axes and rotary-tilt tables. The tool paths created in CAM programs are usually defined by five degrees of freedom. The first three are the translational axes X, Y, and Z. The tilting and inclining of the tool are defined by the A- and B-axes. Occasionally, an additional rotation of the tool (C-axis) around the Z-axis (e.g., for dragging a swivel knife) is defined. Machines with more degrees of freedom than those limited by the toolpath often need user-defined constraints. These constraints are necessary to fully specify the movements of the machine axes. An example is the alignment of a part using the rotary-tilt table so that the Z-axis of the tool always points in the direction of gravity. This is helpful in processes like fused deposition modeling (FDM) and wire arc additive manufacturing (WAAM). It is common practice to set the user-defined constraints based on experience. The definition of these constraints does not affect the relative tool path generated by the CAM software. A preliminary literature review indicates that the configuration of

these degrees of freedom has an impact on the energy demand and stability of the process. As such, a methodical approach to optimize these constraints in terms of efficiency, speed, and energy demand of the machine is required. Currently, no literature provides a comprehensive analysis or methodology regarding this global optimization problem.

**Objective:**

This work aims to attain a methodical approach that analyzes a set of constraints and evaluates the influence of those constraints on a set of defined process variables. It will focus on a 6-axis robot with a rotary-tilt table, whereby the results should also be transferable to other machines. Furthermore, the experiments and validations will be limited to the manufacturing processes of WAAM and milling. First, the influence of the constraints on relevant process variables (energy demand, joint turnover, speed and acceleration peaks, and total joint movements) in a manufacturing process such as WAAM will be assessed. Subsequently, a process evaluation will be elaborated in the CAM software, by means of which the process quality can be determined. Depending on the respective process variables, approximation or machine learning methods will be investigated for the process evaluation. The process quality as a one-dimensional variable will be determined by weighting the process variables. Subsequently, a method for the optimization of the constraints will be elaborated. This task corresponds to an optimization problem in which the process quality will be maximized by selecting suitable constraints.

**Procedure and working method:**

The following work packages are conducted within this thesis:

- Literature research
- Familiarization with WAAM, milling machines, and CAM software
- Selection of suitable process variables
- Elaboration of the proposed method in a suitable programming language
- Verification and validation of the elaborated method
- Documentation of the work

**Agreement:**

Through the supervision of B.Sc. Jan Nalivaika intellectual property of the *iwb* is incorporated in this work. Publication of the work or transfer to third parties requires the permission of the chair holder. I agree to the archiving of the work in the library of the *iwb*, which is only accessible to *iwb* staff, as inventory and in the digital student research project database of the *iwb* as a PDF document.

Garching, 02.10.2023

Prof. Dr.-Ing.  
Michael F. Zäh

B.Sc.  
Jan Nalivaika

## **Abstract**

This thesis discusses a methodology for analyzing and optimizing process variables in manufacturing systems with redundant DoFs. The main focus lies on a 6-DoF industrial robot that traverses a toolpath defined in 5-DoFs (X,Y,Z,A,B). This means that the rotation C, which represents the rotation around the tool symmetry axis, is a redundant DoF and can be chosen freely. The first part of the methodology covers the analysis of process variables, such as direction changes in the joints or the total travel of the joints. The goal is to understand how the redundant DoFs affect the robot's behavior and how they can be used to optimize user-selected process variables. The second part of the methodology proposes a procedure to optimize the user-selected process variables by properly constraining the redundant DoF. After modeling the robot in Python, validation is performed on multiple toolpaths. The results show that the redundant DoFs can significantly affect the process variables. By implementing a PSO algorithm, it is possible to find the ideal setting for the redundant DoFs, thus maximizing the process quality with respect to the process variables.

## **Zusammenfassung**

In dieser Arbeit wird eine Methodik zur Analyse und Optimierung von Prozessvariablen in Fertigungssystemen mit redundanten Freiheitsgraden diskutiert. Der Schwerpunkt liegt auf einem Industrieroboter mit sechs Freiheitsgraden, der eine in Werkzeugpfad abfährt, der nur fünf Freiheitsgrade (X, Y, Z, A, B) definiert. Dies bedeutet, dass die Rotation um Achse C, die die Werkzeugsymmetriearchse darstellt, ein redundanter Freiheitsgrad ist und frei gewählt werden kann. Der erste Teil der Methodik umfasst die Analyse von Prozessvariablen wie Richtungswechsel in den Gelenken oder der Gesamtverfahrwege der Gelenke. Das Ziel ist es, zu verstehen, wie sich die redundanten Freiheitsgrade auf das Verhalten des Roboters auswirken und wie sie zur Optimierung der vom Benutzer ausgewählten Prozessvariablen verwendet werden können. Der zweite Teil der Methodik schlägt ein Verfahren zur Optimierung der ausgewählten Prozessvariablen vor. Nach der Modellierung des Roboters in Python wird die Validierung anhand mehrerer Werkzeugbahnen durchgeführt. Die Ergebnisse zeigen, dass die redundanten Freiheitsgrade die Prozessvariablen erheblich beeinflussen können. Durch die Implementierung eines PSO-Algorithmus ist es möglich, die ideale Einstellung für die redundanten Freiheitsgrade zu finden und somit die Prozessqualität in Bezug auf die Prozessvariablen zu maximieren.

# Contents

<b>List of Abbreviations</b>	<b>xi</b>
<b>1 Introduction</b>	<b>1</b>
1.1 Motivation . . . . .	1
1.2 Problem Formulation . . . . .	2
1.3 Objective . . . . .	4
<b>2 State of Science and Technology</b>	<b>5</b>
2.1 Manufacturing Technologies . . . . .	5
2.1.1 Subtractive Manufacturing . . . . .	5
2.1.2 Additive Manufacturing . . . . .	9
2.1.3 Industrial Robots . . . . .	13
2.2 Computer-Aided Manufacturing . . . . .	22
2.2.1 CAM Software . . . . .	22
2.2.2 Path Planning . . . . .	23
2.3 Optimization Algorithms . . . . .	24
2.4 Comparison of the State of the Art . . . . .	26
2.4.1 Singularity Avoidance . . . . .	26
2.4.2 Optimization of Joint Accelerations and Joint Jerk . . . . .	28
2.4.3 Optimization of Stiffness . . . . .	28
2.4.4 Optimization of Energy Usage . . . . .	29
2.4.5 Summary . . . . .	30
<b>3 Methodology</b>	<b>31</b>
3.1 Introduction . . . . .	31
3.2 General Method for Process Analysis and Evaluation . . . . .	32
3.2.1 General Methodology . . . . .	32
3.2.2 Process Variables . . . . .	34
3.3 User-Defined Weights and Score Calculation . . . . .	37
3.3.1 Local Rating and Global Score . . . . .	37
3.3.2 Local Rating Calculation . . . . .	38
3.3.3 Information Extraction from Time-Series Data . . . . .	39
3.4 Information from Angular Position . . . . .	40
3.4.1 Total Joint Travel and Direction Changes . . . . .	41

3.4.2	Rotation Limits . . . . .	43
3.4.3	Velocity, Acceleration and Jerk of the Joints . . . . .	44
3.4.4	Continuous Energy Usage . . . . .	46
3.4.5	Total Energy Usage . . . . .	47
3.5	Reach, Singularities and Torch Orientation . . . . .	49
3.5.1	Reach and Alignment . . . . .	49
3.5.2	Singularities . . . . .	51
3.5.3	Torch Orientation in WAAM . . . . .	51
3.6	Summary for Boundary Condition Evaluation . . . . .	53
3.7	General Methodology for Process Optimization . . . . .	55
3.7.1	Optimization Without CAM Software in the Loop . . . . .	55
3.7.2	Optimization Loop With CAM Software in the Loop . . . . .	58
<b>4</b>	<b>Implementation and Validation</b>	<b>61</b>
4.1	Simple Implementation . . . . .	61
4.1.1	Modeling a 6-DoF Robot . . . . .	61
4.1.2	Modeling a Basic Toolpath . . . . .	63
4.2	Testing and Validation . . . . .	66
4.2.1	Toolpath Evaluation With one Redundant DoF . . . . .	66
4.2.2	Extracting Process Variables . . . . .	68
4.2.3	Validation on a Production Grade Toolpath . . . . .	72
4.2.4	Toolpath Evaluation With two Redundant DoF . . . . .	75
4.2.5	Boundary Condition Optimization . . . . .	80
4.3	Analysis and Discussion of the Results . . . . .	87
4.3.1	One Redundant DoF . . . . .	87
4.3.2	Production Grade Toolpath . . . . .	88
4.3.3	Two Redundant DoF . . . . .	88
4.3.4	PSO Optimization . . . . .	89
<b>5</b>	<b>Conclusion</b>	<b>91</b>
5.1	Summary . . . . .	91
5.2	Outlook . . . . .	93
<b>Bibliography</b>		<b>99</b>

## List of Abbreviations

AI	Artificial Intelligence
AM	Additive manufacturing
API	Application programming interface
CAD	Computer-aided design
CAE	Computer-aided engineering
CAM	Computer-aided manufacturing
CMT	Cold Metal Transfer
CNC	Computer numerical control
DED	Directed energy deposition
DH	Denavit-Hartenberg
DoF	Degree of freedom
ERP	Enterprise resource planning
FDM	Fused deposition modeling
GMAW	Gas metal arc welding
MBS	Multi-body simulations
ML	Machine Learning
PSO	Particle swarm optimization
RNN	Recurrent neural-network
SLA	Stereolithography
SLM	Selective laser melting
TCP	Tool center point
TWA	Twist decomposition approach
WAAM	Wire arc additive manufacturing



# **Chapter 1**

## **Introduction**

### **1.1 Motivation**

In the age of "Industrie 4.0", advanced technologies like digital twins, have greatly transformed industrial manufacturing (SINGH, FUENMAYOR, et al. 2021). A considerable amount of data can be gathered from various processes, like milling or 3D printing. By analyzing this data, it is possible to find new and optimized methods for improving efficiency as well as streamline and enhancing the manufacturing process (GHOBAKHO 2020). By doing so, a significant amount of resources, like time and money, can be saved while at the same time increasing the quality of the produced product (BIBBY and DEHE 2018; SIMONIS et al. 2016). Computer-aided manufacturing (CAM) has been introduced as a crucial tool to improve productivity and accuracy in creating customized products (FELDHAUSEN et al. 2022). CAM systems automate and optimize tasks such as machining, welding, and assembly (LALIT NARAYAN et al. 2013). One of the key strengths of CAM lies in its precision and consistency, ensuring that intricate components are produced with minimal error. Furthermore, CAM systems contribute to increased efficiency by minimizing material waste and reducing production time (DUBOVSKA et al. 2014). These capabilities play a significant role in achieving a carbon-neutral production process (SAXENA et al. 2020). One of the most important areas of CAM is the calculation of the tool path for computer numerical control (CNC) machines as well as the movement and behavior of multi-axis industrial robots (PAN et al. 2012).

Manufacturing machines are the backbone of modern industrial processes (BI and WANG 2020). These machines encompass a wide range of equipment, from CNC machining centers to 3D printers and automated assembly lines. Their primary ability lies in precision and efficiency. CNC machines, for instance, can repeatedly produce intricate parts with high accuracy ( $\mu\text{m}$ -scale), reducing human error and ensuring consistency (JIA et al. 2018; LIBERMAN and GORBUNOVA 2021). Industrial robots are a dominant part in the area of manufacturing as they can perform multi-axis movements. These capabilities are especially helpful to fulfill the customers wishes for individualized products and one-off parts (SHERWANI et al. 2020). They are cheaper to acquire and easily adapted for different tasks compared to CNC milling machines, but have their own set of disadvantages like for example lower stiffness (IGLE-

SIAS et al. 2015; LIBERMAN and GORBUNOVA 2021). One of the most important advantages of industrial robots is their wide adaptability. They allow for quick reconfiguration to produce different components or products, promoting flexibility in manufacturing (BILLARD and KRAGIC 2019). Further, advancements in robotics and Artificial Intelligence (AI) have broadened their capabilities, enabling tasks that were once deemed too complex or hazardous for humans (GOEL and GUPTA 2020).

Achieving better efficiency and continuous sustainability in the current fast-changing environment, requires a thorough analysis of the interdependent relationships between the manufactured part, the user-defined process parameters, and boundary conditions that govern multi-axis robot programs (GADALETA et al. 2019; PAN et al. 2012). Companies that work with industrial robots can place a strong emphasis on energy reduction, cycle-time minimization, or precision. By defining optimal boundary conditions, it is possible to optimize these process variables. CAM enables the simulation of the planned process, thus adapting any boundary conditions in advance, to fit the selected goals (KYRATSIS et al. 2020; MAITI 2017; PAN et al. 2012; UHLMANN et al. 2016). This thesis is focused on a methodical approach for analyzing process variables and optimizing boundary conditions in multi-axis robot programs.

## 1.2 Problem Formulation

Manufacturing systems that incorporate redundant degrees of freedom (DoFs) offer significant advantages in terms of flexibility and adaptability (ANJUM et al. 2022). One example of a system with redundancy is a 6-DoF industrial robot with a rotary tilt table, which brings the system to eight DoFs. However, these systems also present various conflict points that need to be carefully managed to ensure optimal performance (BOSCAROL et al. 2020).

One of the critical challenges in manufacturing systems with redundant DoFs is singularity avoidance (KIRÉANSKI and PETROVIĆ 1993; WANG et al. 2022). Singularities, which are critical points in the motion of a robot manipulator, arise when the system loses its ability to maintain full control or achieves limited mobility as a consequence of specific joint configurations (MALYSHEV et al. 2022). These configurations result in the loss of a DoF or make the system highly sensitive to small changes, leading to unstable or even unpredictable and dangerous behavior (MILENKOVIC 2021; ZHAO et al. 2021). Limiting the possible positions by adding artificial constraints can help to avoid this problem (FARIA et al. 2018).

Another significant aspect of manufacturing systems with redundant DoFs is joint acceleration and jerk, which is the rate of change of acceleration. The robot must allocate accelerations effectively among its joints to achieve smooth and coordinated motion. Failure to do so can result in jerky or erratic movements, which not only compromises precision but also impacts the efficiency of the manufacturing process (DUONG 2021). Rapid changes in acceleration and jerk can cause mechanical stress and thus, decrease the system lifespan. Ad-

ditionally, the joints can be limited in their ability to keep up with the required speed due to limitations in power (R.V. DUBEY et al. 1988). Therefore, advanced control algorithms and motion planning techniques are necessary to optimize joint motion and minimize conflicts in joint acceleration and jerk (DUONG 2021; VALENTE et al. 2017). As of now, no publication is considering the option of constraining the redundant DoFs, to effectively mitigate the occurring joint accelerations while at the same time considering further process variables.

Extension control, which is a further process variables, is a critical aspect that needs to be addressed in systems with redundant DoFs. Redundant DoFs can provide additional extension capabilities to industrial robots, allowing them to reach difficult-to-access areas (DUONG 2021). However, managing and controlling the extension can be challenging, particularly when precise positioning or maintaining stiffness is required (LIN et al. 2022). The robot must accurately determine the appropriate position for each joint to avoid unnecessary over-extension and collisions with the surrounding environment. The robot pose, which is the combination of position and orientation in three-dimensional space, also has a significant effect on robot stiffness (XIONG et al. 2019). An increased number of joints can introduce more play and reduce overall system stiffness. This can affect precision, accuracy and stability. Robot pose and its DoFs must be carefully considered to ensure the desired level of system rigidity (SHI et al. 2021; WANG et al. 2022). The current state of the art does not provide a methodical approach that, can utilize the redundant DoFs to ensure a most optimal solution for multiple process variables like, robot stiffness or joint movements.

Precision is a crucial element in manufacturing systems, and closely tied to its stiffness. The robot needs to have precise control over the movement of each joint to achieve the desired accuracy in the manufacturing process. However, achieving and maintaining high accuracy and repeatability can be difficult due to the increased complexity (DUONG 2021). Frequent changes in direction in the joints are another factor that affects precision. Due to the serial kinematics of industrial robots, the present play in the motor joints can add up the inaccuracies and impede the manufacturing process (CHEN-GANG et al. 2014; HUYNH et al. 2020). Mechanical stresses, decreased precision, and increased energy consumption can all result from abrupt and frequent direction changes (GASPARETTO and ZANOTTO 2010). Furthermore, effectively coordinating the movement of multiple joints to execute rapid direction changes can prove to be a computationally intensive task (VANDE WEGHE et al. 2007). Poor robot configurations can result in prolonged and unnecessary movements, ultimately hampering the overall productivity of the manufacturing process (REITER et al. 2016). If constrained effectively, the redundant DoFs can serve as helpful tool to reduce the direction changes in the joints of a industrial robot, while its execution of a toolpath.

Energy use is also a significant concern in manufacturing systems employing redundant DoFs (DOAN et al. 2016). The presence of additional joints and their non-optimal usage can require more power to operate, leading to increased energy consumption. As energy efficiency becomes a priority in modern manufacturing, mitigation strategies regarding this problem are necessary (BOSCAROL et al. 2020; BOSCAROL and RICHIEDEI 2019). One possible solution, is the optimal constraining of the redundant DoFs which are not directly defined

by the toolpath. No method is considering the influence of the redundant DoFs on energy consumption, while simultaneously optimizing for the process variables mentioned before.

While redundant DoFs may introduce potential conflicts and require special attention, they can also significantly enhance performance in manufacturing systems (AYTEN et al. 2016). The added DoFs increase flexibility and adaptability, enabling the robot to carry out complex tasks more efficiently. Redundancy enables multiple approaches to achieve a desired end-effector position or orientation. By effectively utilizing the surplus of DoFs, manufacturing systems can enhance their performance, increase efficiency, and exhibit greater process stability while performing diverse tasks (BOSCAROL et al. 2020).

Currently, there is no integrated system that can evaluate a computed tool path based on the configuration of the manufacturing machine as well as the chosen process variables, such as combined direction changes or stiffness. Additionally, there is no published method that provides an optimal or near-optimal solution for defining the necessary constraints for a specific goal like for example, minimizing energy usage while at the same time reducing joint accelerations.

### 1.3 Objective

The definition of the constraints for the redundant DoFs, as mentioned in Chapter 1.2, does not affect the relative tool path generated by the CAM software. As such, a methodical approach to optimize these constraints without altering the toolpath, in terms of energy demand of the machine, accelerations in the joints and further process variables is required. Currently, no literature provides a comprehensive analysis or methodology regarding this global optimization problem. This work aims to attain a methodical approach that analyzes a set of constraints and evaluates the influence of those constraints on a set of defined process variables. This work is focused on a 6-axis industrial robot with a rotary-tilt table, whereby the results should also be transferable to other machines. Furthermore, the validations is limited to the manufacturing processes of wire arc additive manufacturing (WAAM) and milling.

First, the influence of the constraints on relevant process variables (energy demand, joint turnover, speed and acceleration peaks, total joint movements) in a manufacturing process such as WAAM is assessed. Subsequently, a process evaluation is elaborated, by means of which the process quality can be determined. The process quality as a one-dimensional variable is determined by weighting the process variables. Subsequently, a method for the optimization of the constraints is elaborated. This task corresponds to an optimization problem in which the process quality is maximized by selecting suitable constraints.

# **Chapter 2**

## **State of Science and Technology**

The following chapter gives an overview of manufacturing technologies, CAM, and algorithms for optimization problems. Special attention is given to the comparison of optimization problems in manufacturing with redundant DoFs.

### **2.1 Manufacturing Technologies**

Manufacturing technologies encompass a wide range of processes that are used to transform raw materials into finished products. Two major categories within this field are subtractive and additive manufacturing (AM) (IQBAL et al. 2020). Subtractive manufacturing involves removing material from a workpiece to shape it into the desired form (WATSON and TAMINGER 2015). On the other hand, AM, also known as 3D printing, typically involves building up layers of material to create an object. This process offers greater design flexibility and the ability to create complex geometries (DILBEROGLU et al. 2017).

Both subtractive and additive manufacturing play crucial roles in various industries, revolutionizing production methods and offering new possibilities for customization and innovation (BANDYOPADHYAY 2020; VAN LE et al. 2017).

#### **2.1.1 Subtractive Manufacturing**

Subtractive manufacturing, also referred to as subtractive fabrication or machining, is a precise and efficient method utilized in contemporary manufacturing processes (WANG et al. 2023). This approach entails the removal of material from a workpiece, resulting in the formation of a desired shape or product (CALLEJA et al. 2018). In contrast to AM techniques, subtractive manufacturing always relies on material that is removed (ABDULHAMEED et al. 2019).

Subtractive manufacturing involves various techniques such as milling, turning, drilling, and grinding that are mostly performed by using CNC machines (KUMAR et al. 2020). Such

machines are programmed to precisely control the cutting tool movement to clear material from the workpiece based on a predetermined design (AMANULLAH et al. 2017).

The versatility and precision of subtractive manufacturing are two of its significant advantages. A CNC machine can process a diverse array of materials, such as metals, plastics, and composites, with high levels of precision and surface quality, allowing for the creation of intricate and complex components (TOMAZ et al. 2021; YANG et al. 2019). As a result, it finds applications in industries where precision and quality are critical, such as aerospace, automotive, and medical.

The process of subtractive manufacturing starts with the drafting of the intended component using CAD software. Subsequently, CAM software is used to generate instructions that are used to guide the CNC machine (see Chapter 2.2 for more details). The machining process begins with the machine operator setting up and securing the workpiece in the machine and starting the execution of the generated instructions (NEE 2015). The cutting tools then perform various operations, such as drilling holes, creating pockets or slots, and shaping the external contours of the part, by following the predetermined movements. In a typical 3-axis machine, the DoFs are along the X, Y, and Z axes. In a 5-axis machine, two additional DoFs in form of rotations are present. Additionally, recent research is trying to extend the machines possibilities by adding advanced abilities like constantly monitoring and adjusting the cutting parameters on the fly to ensure the most efficient cutting speed, feed rate, and tool engagement while minimizing errors (TIEN et al. 2021).

Subtractive manufacturing provides numerous advantages over alternative manufacturing techniques. This method allows for the creation of intricate and highly customizable components with tight tolerances and complex geometries (JAYAWARDANE et al. 2023). In addition, it results in exceptional surface finish, dimensional accuracy, and consistency, guaranteeing uniform quality across production runs. Moreover, it is cost-effective for small to medium production volumes as it does not necessitate the use of costly molds or part-specific tooling, which makes it a great option to produce a multitude of parts (GU and KOREN 2018).

One of the disadvantages of the process is the possibly long cycle time. Particularly for intricate and large-volume designs with a high material-removal-ratio, the process can result in significant material waste as well as long machining time (FALUDI et al. 2015). Furthermore, it may not be appropriate for high hardness or brittle materials, which can lead to excessive tool wear or breakage (HESSER and MARKERT 2019).

Another common issue in CNC machining is tool vibration. Tool vibration, also called chatter, refers to the unwanted oscillation or movement of the cutting tool during the machining operation (YUE et al. 2019). This phenomenon can have detrimental effects on the quality of the finished part and can lead to various problems, such as poor surface finish, reduced dimensional accuracy, increased tool wear, and even tool breakage (ASLAN and ALTINTAS 2018). Several factors contribute to tool vibration in CNC machining. One of the primary factors are the cutting parameters, which include the cutting speed, feed rate, and depth of cut. When these parameters are not optimized, excessive cutting forces can be generated,

causing the tool to vibrate. It is crucial to find the right balance between economical material removal rates and minimizing tool vibration to ensure optimal efficiency (GIORGIO BORT et al. 2016). The tool holder and spindle also influence tool vibration. A rigid tool holder and spindle are necessary to minimize vibrations while at the same time maintain accuracy during machining (WAN et al. 2019). Any play or misalignment in these components can contribute to tool vibration. Thus, it is paramount to ensure stiffness for high-precision operations. Chapter 2.1.3 and Chapter 2.4.3 give a more in-depth look regarding the stiffens in machining operations executed with industrial robots.

In summary, subtractive manufacturing offers a wide range of applications but should be carefully considered for each situation. CNC technology, in combination with subtractive manufacturing, has become indispensable across a variety of industries. Nonetheless, it is crucial to evaluate its restrictions and suitability for specific design needs and material characteristics.

Figure 2.1 shows the basic design of a 3-axis CNC machine. In this configuration, the workpiece is placed on the worktable and secured using a vice to hold it in place. The worktable has the ability to move in two directions, namely the X and Y directions. This movement allows for precise positioning and maneuvering of the workpiece. On the other hand, the spindle, which is the rotating component responsible for cutting or shaping the workpiece, moves along the Z direction. This vertical movement of the spindle enables it to perform various machining operations at different depths. Additionally, the machine interface serves as the control panel for the CNC machine. It provides the user with options to select and load the desired CNC program.

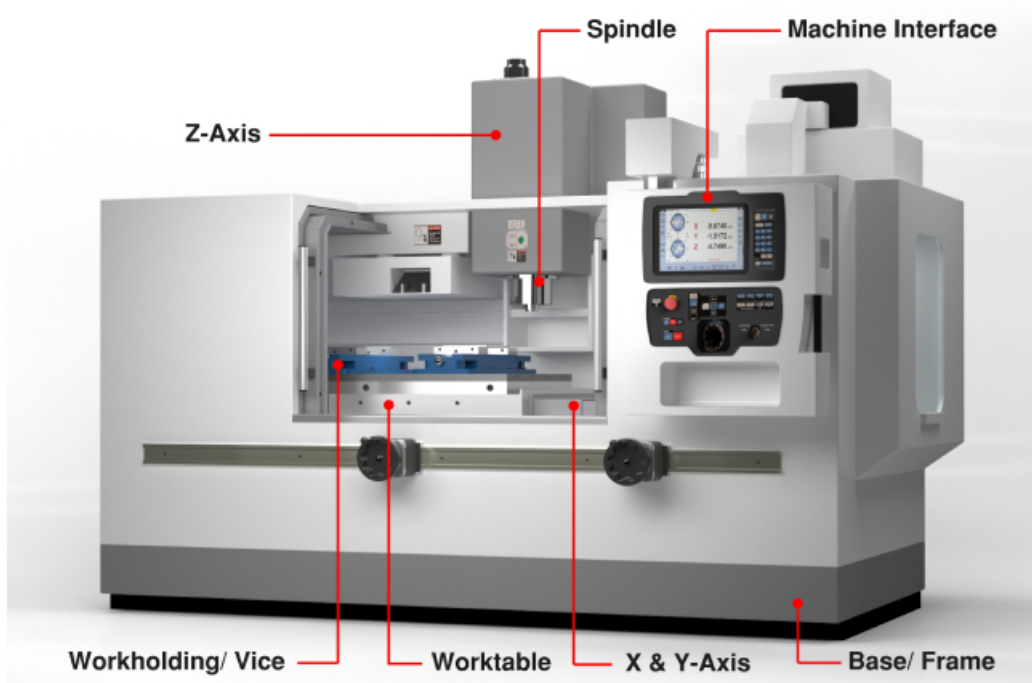
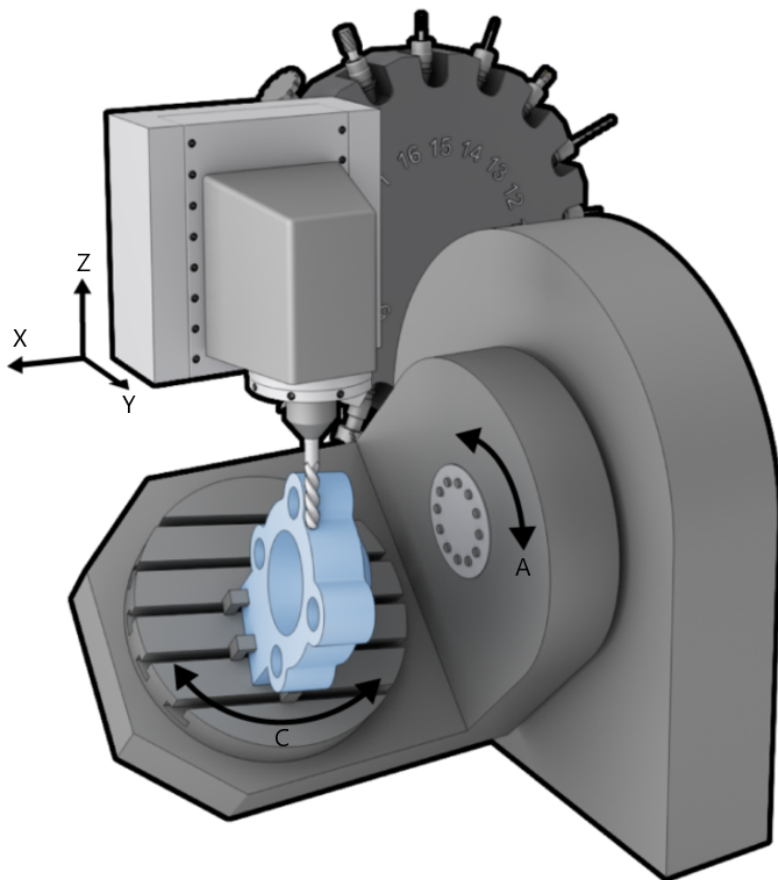


Figure 2.1: 3-Axis CNC Machine (CNC Masters 2022)

Figure 2.2 shows the schematic model of a 5-axis CNC machine. In this particular design, the spindle, which is responsible for cutting the workpiece, has the ability to move along three axes, namely the X-, Y-, and Z-axis. This movement allows for precise control over the position and depth of the tool in relation to the workpiece.

In addition to the spindle movement, the machine features a rotary-tilt table that can adjust two additional axes, namely the A- and C-axis. These axes provide rotational and tilting capabilities to the worktable, allowing for more intricate movements and increased flexibility in part design. By adjusting the A- and C-axis, the workpiece can be positioned and oriented in different angles, enabling the CNC machine to access and machine complex geometries that would otherwise be difficult or impossible to achieve with fewer axes. The inclusion of these two additional DoFs in the 5-axis CNC machine significantly expands the range of operations that can be performed. This increased flexibility and versatility make the 5-axis CNC machine a valuable tool in industries that require high precision and intricate part production.



**Figure 2.2:** 5-Axis CNC Machine (*Manufacturing Guide 2023*)

## 2.1.2 Additive Manufacturing

AM consists of the conversion of digital designs into physical objects by building them layer by layer. This layering approach offers the possibility for creating complex geometries that would be extremely challenging or even impossible to produce using traditional manufacturing methods (PRAKASH et al. 2018). This advantage allows to fabricate intricate structures with internal cavities or undercuts, thus opening up new possibilities in engineering and design (ABDULHAMEED et al. 2019).

Various AM technologies utilize different methods to build the layers. Fused deposition modeling (FDM), for example, involves extruding molten thermoplastic filament through a heated nozzle, which solidifies as it cools, creating the desired shape (WICKRAMASINGHE et al. 2020). Stereolithography (SLA) employs a liquid photopolymer resin that is solidified by a UV laser, while selective laser melting (SLM) uses a high-power laser to selectively fuse powdered materials, such as plastics or metals (MEIER et al. 2017; WANG et al. 2016).

The compatibility of AM with a wide range of different materials is another significant advantage (BOSE et al. 2018). It enables the production of components with diverse properties, including strength, flexibility, conductivity, and heat resistance. AM can accommodate various plastics, such as ABS, PLA, and nylon, as well as metals like titanium, aluminum, and stainless steel. Additionally, ceramics and even biomaterials, like hydrogels or living cells, can be used in AM processes. New materials specifically tailored for AM are continuously developed, expanding the possibilities for unique applications (ATTARAN 2017).

The design freedom offered by AM is a significant selection criterion when choosing a manufacturing method. Traditional methods often have design constraints due to limitations in tooling and manufacturing processes. With AM, designers have greater flexibility to create complex and organic shapes, lightweight structures, and intricate internal features. This freedom leads to optimized performance and improved functionality (PLOCHER and PANESAR 2019).

However, AM also poses scientific challenges. Post-processing requirements, such as smoothing, polishing, or heat treatment, may be necessary to achieve the desired surface finish or material properties (JANDYAL et al. 2022). Additionally, certain applications may have limited material options, particularly in terms of high-temperature or high-strength applications. Production speed can also be a constraint for large or complex parts, as AM processes can be time-consuming compared to traditional manufacturing methods (DILBEROGLU et al. 2017).

As AM technologies continue to advance, they have the potential to transform supply chains. The concept of distributed manufacturing, where products are produced closer to the point of use, becomes feasible with AM (JANDYAL et al. 2022). This reduces transportation costs, lowers carbon emissions, and enables on-demand manufacturing, leading to shorter lead times and increased sustainability (HALEEM and JAVAID 2019).

### Wire Arc Additive Manufacturing

WAAM is a specific type of additive manufacturing process which is part of directed energy deposition (DED) processes (SVETLIZKY et al. 2021). According to the DIN EN ISO 52900 standard, DED involves using focused thermal energy to melt material during the application process to build up the individual layers (DIN EN ISO/ASTM 52900 2022).

The operating principle of WAAM involves the generation of an arc through electrical discharge between an electrode and the workpiece. This arc transfers energy to the workpiece, causing melting in the fusion zone (OU et al. 2018). Additionally, if a welding filler material in the form of a wire is introduced into the arc, it also melts and can be used to deposit additional material onto a metallic substrate (CUNNINGHAM et al. 2018). To ensure a continuous weld seam, a wire feed system must be employed (DING et al. 2015). By placing multiple weld seams over each other, the workpiece is formed layer by layer.

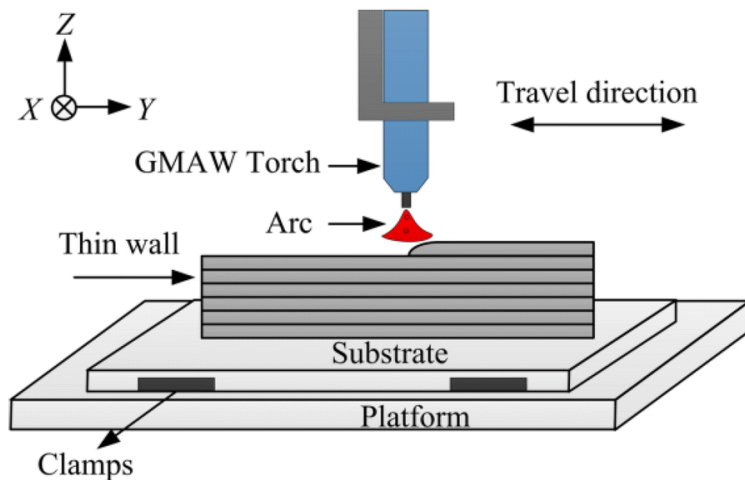
The industrial manufacturing of components using WAAM involves a kinematic system that allows automated movement of the welding torch. This can be achieved using industrial robots or gantry systems (SCHMITZ et al. 2021). Alternatively, a spatially fixed welding torch, combined with robotic kinematics or rotary-tilt table, can be used to move the substrate plate instead (NAGASAI et al. 2022).

WAAM offers several advantages over other additive manufacturing techniques. One major advantage is its high deposition rate, which ranges up to 6 kg/h. This high deposition rate enables the construction of large components in a relatively short amount of time. Components can be produced within a single workday, providing a significant time advantage compared to techniques like SLM, which typically operate at around 0.1 kg/h and thus much slower deposition rates. (IVÁNTABERNERO et al. 2018)

Another advantage of WAAM is its capability to construct large components with almost no limitations on part size. The production volume is only constrained by the working range of the kinematics employed. For example, in the case of an articulated-arm robot, the range is defined by its maximum reach. This means that WAAM has the potential to create components of various sizes without compromising its effectiveness (LI et al. 2019).

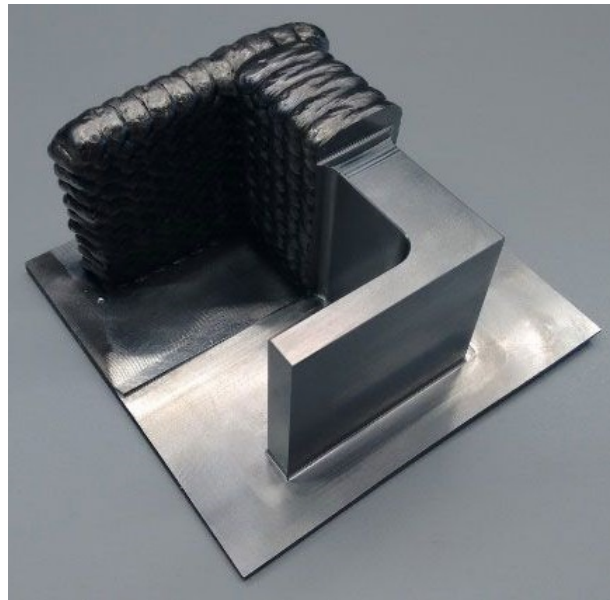
However, it is important to note that WAAM components may have some inherent defects. These include residual stresses, voids and deformations that persist after the production process, as well as relatively low geometric precision and modest surface quality (WU et al. 2018). These limitations should be taken into consideration when utilizing WAAM for manufacturing purposes.

Figure 2.3 shows a schematic representation of the WAAM process. In this process, a wire is fed through the gas metal arc welding (GMAW) torch to supply a continuous stream of material. The wire is then subjected to high heat generated by an electric arc. The wire is melted and then deposited onto a substrate plate. The substrate plate serves as the foundation or base on which the material is built. As the molten wire is deposited, it solidifies and fuses with the previous layers, gradually building up the desired object.



**Figure 2.3:** Schematic representation of WAAM (*Chaurasia et al. 2021*)

Figure 2.4 shows a part produced by WAAM with the addition of a post processing step. The rough surface finish is clearly visible on the non post processed side of the part.



**Figure 2.4:** Part produced by WAAM with post machining (*Lortek 2023*)

### Cold Metal Transfer

Cold Metal Transfer (CMT) welding is a sophisticated process that merges the advantages of multiple welding techniques (DUTRA et al. 2015). It functions based on the principle of controlled short-circuiting, wherein the welding torch generates a short circuit between the wire and the workpiece. This resulting electric arc triggers the melting of the tip of the wire and subsequent detachment. The detachment is assisted by a retraction of the wire. This process is generating a sequence of droplets that are transferred to the weld pool with high

precision (SELVI et al. 2018; SRINIVASAN et al. 2022). This process provides superior heat control with lower heat input than conventional methods. The controlled arc and droplet transfer reduce the risk of overheating and distortion due to internal stresses, making it suitable for thinner materials and heat-sensitive applications (SCOTTI et al. 2020). Additionally, this process minimizes spatter formation, resulting in cleaner and smoother welds and reducing the requirement for post-weld cleaning (SRINIVASAN et al. 2022). CMT welding is ideal for applications that require the highest weld quality which includes structural fabrication and automotive manufacturing (CONG et al. 2016). For dependable weld quality, CMT welding typically integrates advanced process control systems, which utilize adaptive control and real-time monitoring to consistently adjust welding parameters based on sensor feedback. This enhances the precision and dependability (PICKIN and YOUNG 2006).

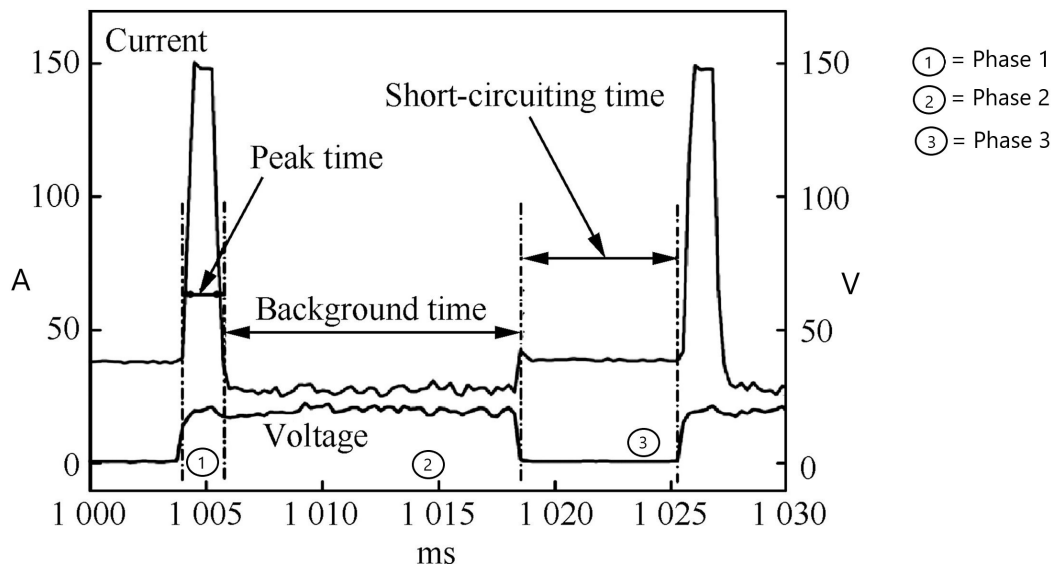
A CMT cycle consists of three phases (SELVI et al. 2018):

1st - pulse phase: A high current pulse leads to the ignition of the arc, which melts the wire electrode. A droplet begins to form at the tip of the wire. The wire is moved forward in the direction of the workpiece.

2nd - arc phase: The arc is kept burning at a lower current. This prevents the melt droplet from detaching prematurely and transferring to the workpiece.

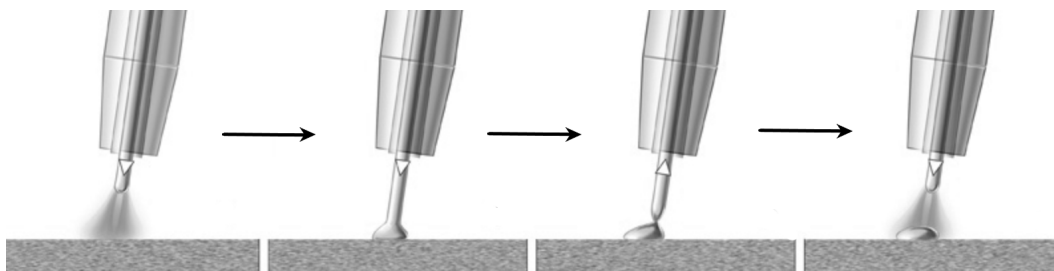
3rd - short-circuit phase: As soon as the wire comes into contact with the substrate, the voltage drops to 0 V and the wire feeder is signaled to withdraw the wire. This supports the droplet detachment from the wire into the molten bath.

Figure 2.5 shows the three Phases of a CMT cycle. The voltage is constant in the first two phases and drops to zero in the short circuit phase. The spike of current is clearly visible in the first phase, which is also the shortest.



**Figure 2.5:** Current and Voltage wave forms of a CMT process (Selvi et al. 2018)

Figure 2.6 shows the clearly distinct parts in a CMT cycle. At first an electric arc is formed and melts the wire. After a short circuit is established the wire retracts and detaches from the molten droplet. After that the cycle restarts.



**Figure 2.6:** Individual sections of a CMT cycle (Dalton 2024)

In summary, WAAM and CMT are highly sophisticated processes that enable the creation of additively manufactured parts with specifically designed parameters. CMT achieves precise welds with low heat input and minimal spatter. It is ideal for thinner materials and applications requiring high weld quality. Advanced process control systems can enhance the reliability of CMT welding (PICKIN et al. 2011; RAHUL et al. 2018).

### 2.1.3 Industrial Robots

Industrial robots are advanced machines designed to perform various tasks in manufacturing and industrial settings. They come in different types, each with its own set of capabilities and advantages. They are crucial to modern manufacturing and automation, transforming production methods and repetitive task performance across diverse industries. Since their inception in the mid-20th century, these machines have undergone significant advancements, evolving into highly adaptive and sophisticated devices that promote productivity, accuracy, and safety within manufacturing processes (JI and WANG 2019). At their core, industrial robots are programmable machines designed to execute tasks with a high degree of accuracy and efficiency. They can carry out repetitive actions consistently, which enhances productivity and reduces the risk of human error (SICILIANO and KHATIB 2016).

One common type of industrial robots are the articulated robots. These robots have rotary joints that allow them to move like a human arm, with multiple links and joints. They can perform a wide range of different tasks, such as welding, material handling, quality control or assembly operations (HANAFUSA et al. 1981; JAIN et al. 2019). Another type is the Cartesian robot, also known as gantry robots. These robots move along three linear axes (X, Y, and Z) to perform tasks. They are commonly used for pick-and-place operations or in applications that require precise positioning (KIM and TSAI 2003).

SCARA robots, shown in Figure 2.7, are designed for fast and precise movements in assembly operations. They have a selective compliance assembly robot arm that allows them to move quickly while maintaining accuracy (DAS and CANAN DÜLGER 2005).

Delta robots, shown in Figure 2.8, robots are used for high-speed pick and place applications, such as packaging or sorting. They are known for their rapid movements and high throughput (BONEV 2001). Collaborative robots, or cobots, are designed to work safely alongside humans. They have built-in safety features, such as force sensors or vision systems, that allow them to interact with humans without causing injury. Cobots are often used in tasks that require human-robot collaboration, such as assembly (LIU et al. 2022).



Figure 2.7: SCARA robot (*Epson 2024*)



Figure 2.8: Delta robot (*Weiss 2024*)

Industrial robots are based on articulated robots and have a wide range of applications across various industries. Depending on the attached tool, they can perform tasks like fastening, welding, or soldering components together. These robots are also commonly used for material handling tasks in warehouses or production lines. Inspection tasks can be automated with robots equipped with sensors or cameras, allowing them to analyze products for defects or perform quality control checks (HÄGELE et al. 2016).

Industrial robots offer several benefits in comparison to manual labor. Firstly, they increase productivity by working continuously, without breaks or fatigue. This leads to higher production rates and shorter cycle times. Additionally, robots can perform tasks with high precision and accuracy, reducing production errors and defects and thereby improving product quality (KUBELA et al. 2016). Safety is another important aspect of industrial robots. They are designed to handle dangerous or hazardous tasks, keeping human workers safe. Robots can work in environments with high temperatures, toxic substances, or heavy loads, minimizing the risk of injury to humans (HEYER 2010). While the initial investment in industrial robots can be high, they offer long-term cost savings. Robots can reduce labor costs by automating repetitive tasks and increasing efficiency. They also offer flexibility, as they can be quickly reprogrammed or reconfigured to perform different tasks, allowing for greater adaptability in manufacturing processes (JUNG and LIM 2020).

When comparing industrial robots to CNC machines, there are a few notable disadvantages for industrial robots. Firstly, industrial robots generally have lower positional accuracy and repeatability compared to CNC machines. CNC machines are purpose-built for precise machining operations and can achieve high levels of accuracy and repeatability (WANG et al. 2023). Secondly, industrial robots typically have a longer cycle time compared to CNC machines for similar tasks. The complex movements and computations involved in robot control can result in slower overall operation speeds, which may not be ideal for high-volume production environments (JOSHI et al. 2021). Additionally, industrial robots can be more complex to program and set up than CNC machines. CNC machines follow a predefined set of instructions, whereas programming industrial robots often requires more advanced programming skills and can be time-consuming (YE 2022). Lastly, industrial robots may have limitations when it comes to handling heavy loads or performing heavy-duty machining operations. CNC machines are specifically designed for heavy-duty cutting, milling, and drilling tasks, whereas industrial robots are better suited for lighter material handling and assembly operations (WU et al. 2022). These differences should be considered when deciding between industrial robots and CNC machines for specific manufacturing applications.

Industrial robots can be programmed using different methods. One common method is using a teach pendant, where operators manually move the robot to record positions and actions. Offline programming is another approach, where programs are created and simulated on a computer before being transferred to the robot. Sensor-based programming allows robots to respond to sensor inputs or interact with the environment (HEIMANN and GUHL 2020).

Serial kinematics is a widely used configuration in industrial robots, where the robot arm is constructed as a sequential chain of joints and links. Each joint provides one DoF, enabling the robot to move and position its end-effector in a controlled manner. The joints can be of various types, including revolute, prismatic, spherical, and cylindrical, providing rotational, linear, and combined movements. The motion of the robot arm is controlled using forward kinematics and inverse kinematics. Forward kinematics calculates the position and orientation of the end-effector based on the joint angles, while inverse kinematics determines the joint angles required to achieve the desired end-effector pose (SINGH, KUKSHAL, et al. 2021).

Figure 2.9 shows the schematic design of a 6-DoF industrial robot with a spindle and force sensor that is used for machining.

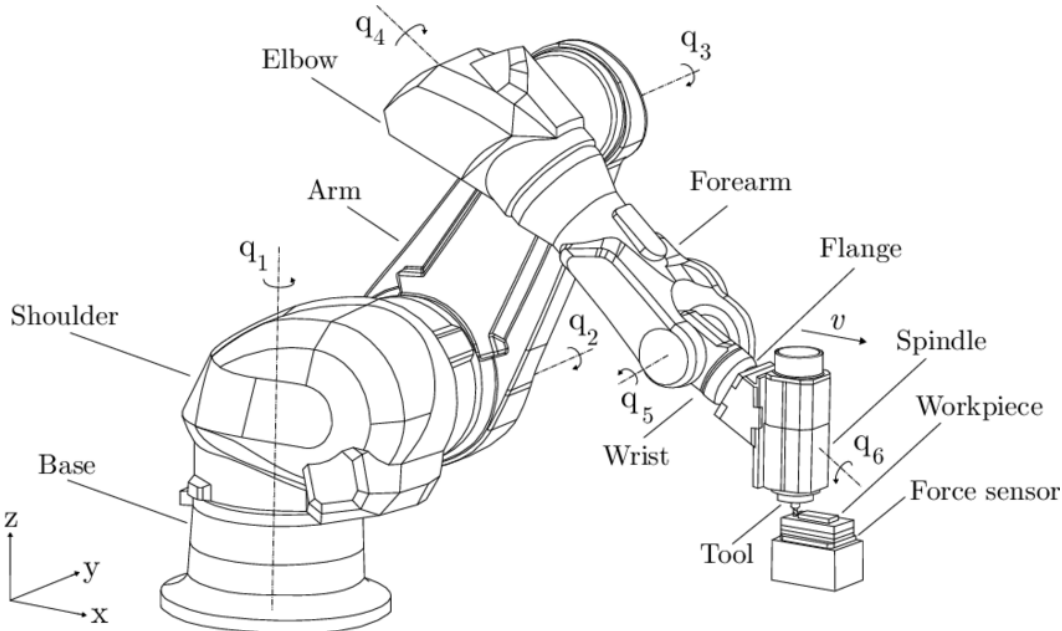


**Figure 2.9:** 6-DoF industrial robot (*Hoai Nam et al. 2018*)

In summary, the robots performance relies on sophisticated control algorithms and feedback systems that allow them to adapt to dynamic conditions, adjust movements in real-time, and maintain a consistently high level of accuracy (LIN et al. 2023). This improves both the quality of the final product and the safety of the manufacturing process, as robots can navigate complex paths without risking collisions or accidents (BOSSCHER and HEDMAN 2011). As this technology continues to advance, industrial robots will play an even more prominent role in shaping the future of manufacturing and automation (DOMAE 2019)

### Redundancy in robotic systems

Industrial robots with redundant DoFs are robotic systems that have been designed with more DoFs than are necessary for a specific task (WANG et al. 2022). These extra DoFs allows the robots to perform additional joint movements or configurations beyond what is required for defined movement or manipulation.

The primary advantage of these redundant systems is their increased flexibility and adaptability (DUONG 2021). Robots with more DoFs can access a wider range of positions and orientations, making it possible for them to complete complex tasks in constrained environments that would have been difficult or impossible otherwise. With this added flexibility, they can avoid obstacles and work around them without disrupting their duties. In industrial settings, redundant manipulators provide significant advantages. Their additional DoFs enable them to improve accessibility to hard-to-reach areas and enhance overall operational capabilities (SHI et al. 2021). Redundancy can take on many different forms in robotic systems. One option is to increase the number of joints in the serial kinematics of an articulated industrial robot (MILENKOVIC 2021).

Another approach to redundancy is the addition of a rotary tilt table, which is commonly used in WAAM in combination with a 6-DoF robot (YUAN et al. 2020). This combined system enables the robot to manipulate the workpiece from various angles, enhancing the manufacturing process. Furthermore, the inclusion of a linear axis that the robot base can traverse on is yet another form of redundant DoF. This additional linear motion provides the robot with extended reach and the capability to access a larger workspace, making it suitable for tasks that require movement along a specific axis (BOSCAROL and RICHIEDEI 2019). Additionally, redundancy can also be observed when using a generic 6-DoF system for operations that only necessitate five or fewer DoFs (for example, milling or WAAM) (HANAFUSA et al. 1981; WANG et al. 2022).

Figure 2.10 shows two industrial robots from the manufacturer KUKA GmbH that are placed on a linear axis. This enables the robots to use the additional and redundant DoF to optimize the process. Multiple robots can be positioned on one linear unit. Figure 2.11 shows how a 7-DoF robot can have multiple poses reaching the same position. In this case, only six DoF are necessary to achieve the position, while one DoF can be defined manually.



**Figure 2.10:** Industrial robots with an additional linear axis (KUKA 2023)

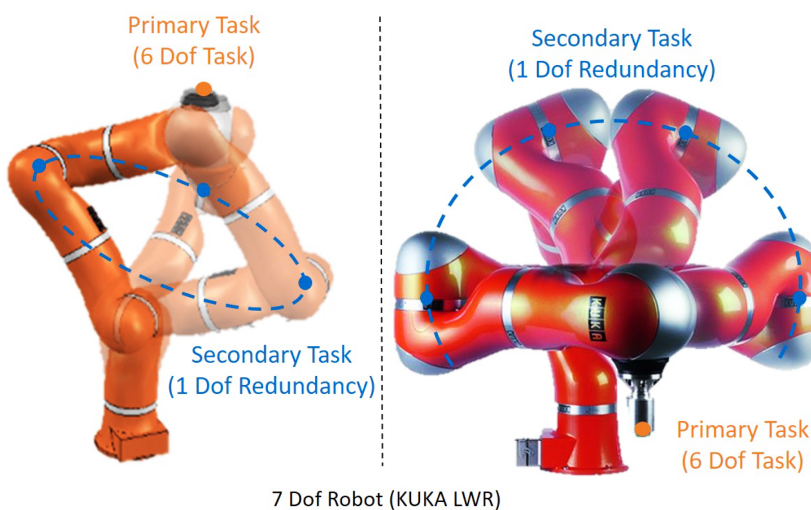


**Figure 2.11:** 7-DoF robot (Hagane et al. 2022)

In summary, redundancy in robotic systems can be achieved through various means, such as increasing joint numbers, incorporating rotary tilt tables, including linear axes, or using a higher DoF system for tasks that demand fewer DoFs. These redundant features enhance the capabilities and versatility of the robot, enabling it to perform a wide range of complex tasks efficiently.

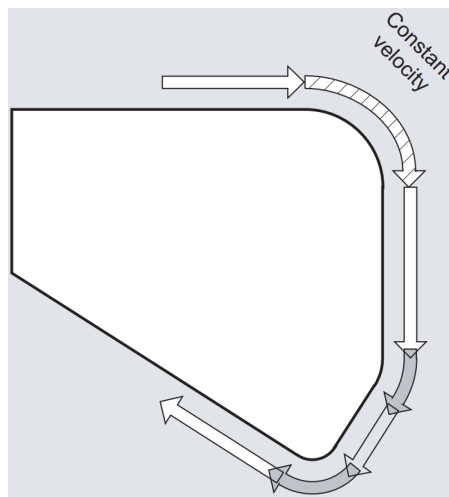
While redundancy in industrial robots can provide increased flexibility and adaptability, it also comes with certain disadvantages. One major drawback is the increased complexity and cost associated with redundant systems (HALEVI et al. 2011). The addition of extra joints, axes or mechanisms, adds to the overall complexity of the robot, requiring more sophisticated control algorithms and hardware (DUONG 2021). This complexity not only increases the initial cost of the robot but also adds to the maintenance and troubleshooting efforts to maintain the system (AHANGAR et al. 2019). Additionally, the presence of redundant DoFs can make the robot more susceptible to mechanical failures as more components are involved. This can result in increased downtime and even higher maintenance costs. Moreover, the increased complexity of redundant systems can make programming and calibration more challenging, requiring specialized skills and expertise (ERDŐS et al. 2016). Therefore, while redundancy can offer advantages in certain scenarios, careful consideration must be given to the cost, complexity, and maintenance implications before implementing it in industrial robotics applications.

### **Continuous-path mode**

In the context of industrial robotics, continuous paths without abrupt direction or velocity changes of a tool play a crucial role in achieving smooth movements of robotic arms along a defined trajectory (JIA et al. 2018). This ensures that the robot can execute complex tasks and movements with accuracy and efficiency. By incorporating continuous path mode into industrial robot programming, manufacturers can optimize production processes and improve the quality of manufactured products (ZHANG et al. 2020). Constant velocity of a tool is especially important in applications like WAAM where the quality of the layer is directly dependent on the feed rate (LI, CHEN, et al. 2018). In CNC machining, discontinuities in velocity, acceleration, and jerk result in non-optimal surface finishes (SUN and ALTINTAS 2021).

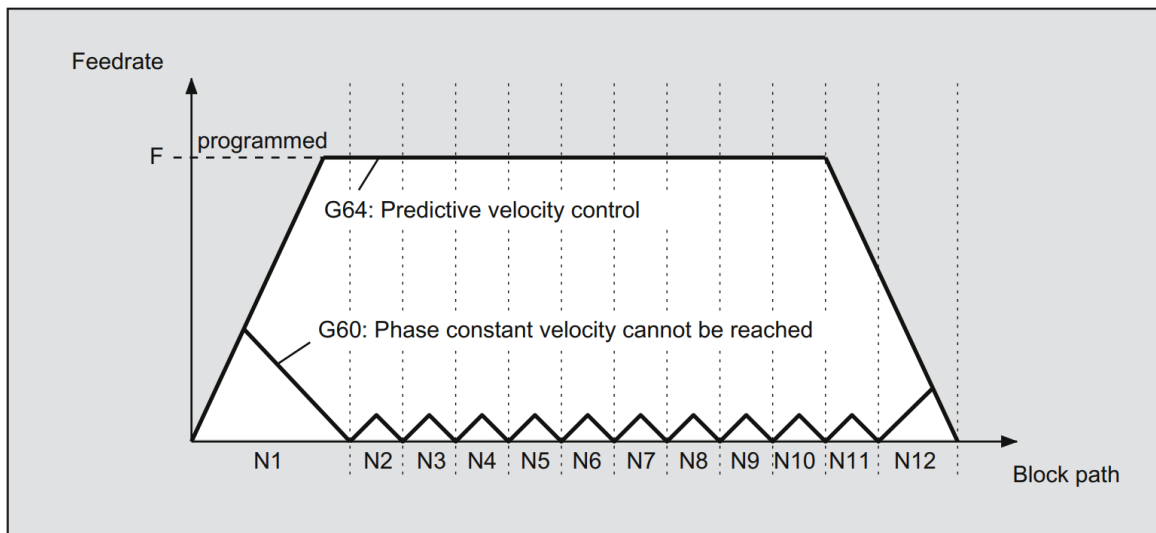
Continuous path mode refers to a mode of operation in high-speed robotics as well as CNC machines where the goal is to achieve a smooth and uninterrupted movement of the machine along a toolpath. In this mode, the machine is expected to follow a path without any sudden changes in direction, velocity or acceleration. The purpose of continuous path mode is to minimize jerk spikes, machine vibrations, and other undesirable effects that can occur when there are discontinuities in the toolpath (JIA et al. 2018; YANG and YUEN 2017).

Figure 2.12 gives a visual example of a contouring toolpath that is defined with a constant velocity. To maintain a constant velocity along sharp corners or small radii, significant deceleration and acceleration may be needed.



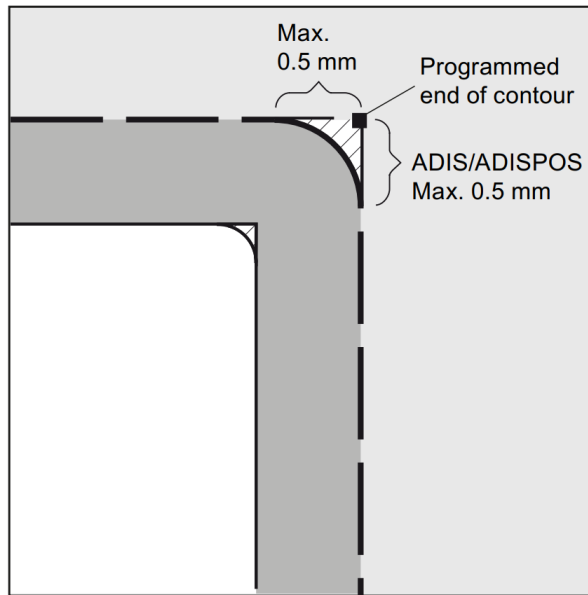
**Figure 2.12:** Desired path with constant velocity (Siemens 2024)

Figure 2.13 shows how specific G-code commands of the SINUMERIK 840D influence the targeted feedrate. N1 to N12 are the individual G-code lines defining the coordinates with the corresponding orientation, also called waypoints, of the tool center point (TCP). When using the G60 command, the points are reached exactly, but the feedrate is reducing to 0 at every waypoint. When implementing the G64 (continuous pathmode) command, the feedrate can be held at the desired value but also requires *LookAhead*-deceleration to maintain precision.



**Figure 2.13:** Influence of G-Code commands G64 and G60 (Siemens 2024)

The SINUMERIK 840D offer more commands to specify how much deviation is acceptable. Figure 2.14 shows how the G-code command G641 ADIS=0.5 is influencing the programmed contour. The rounding of the path begins no more than 0.5 mm before the programmed end of the contour and must finish 0.5 mm after the end of the corner point.



**Figure 2.14:** Predetermined deviation of the programmed path (*Siemens 2024*)

It is also possible to define the precision criterion globally instead of individually at every coordinate. For that the commands G601 and G602 can be utilized. Figure 2.15 shows how these two commands influence the executed trajectory. In this case, two different tolerances, according to the axis-specific tolerance limits, allow the tool to deviate from the programmed path.

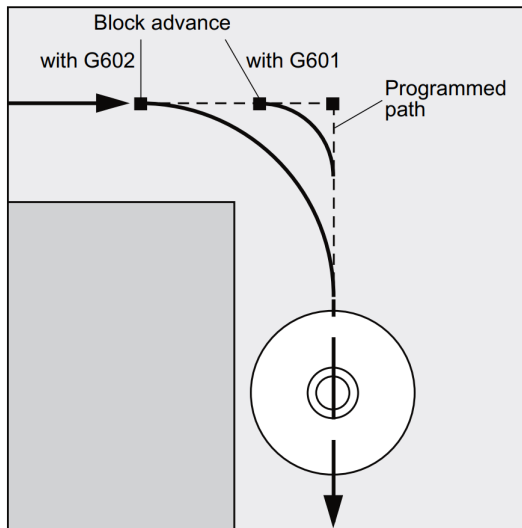


**Figure 2.15:** Influence of commands G601 and G602 (*Siemens 2024*)

Continuous-path mode in CNC machining is a crucial aspect when it comes to processing parts with rapidly varied geometric features. These types of components, often found in high-end equipment, pose challenges due to their intricate structures and strict dimensional requirements. The presence of rapidly varied geometric features, coupled with the continuous-path running characteristic, gives rise to trajectory errors during the machining process, which

severely hampers the overall machining accuracy of such parts (SHAHZADEH et al. 2018). This becomes even more critical in high-speed machining scenarios, where existing studies struggle to effectively reduce this error without compromising machining efficiency (LI, ZHANG, et al. 2018).

In CNC machines, toolpaths are typically composed of lines and arcs (LIU et al. 2020). At the transition points between these elements, careful consideration is required to ensure that the physical limits of the machine are not exceeded. For example, when the machine is moving at a constant feedrate, a sudden change in velocity can occur when two successive non-tangent linear moves meet. This can lead to undesirable effects on the machine and the quality of the cut (BOUJELBENE et al. 2004). Similar issues arise at transitions between lines and arcs or between two arcs, where curvature discontinuities need to be addressed.

Many path smoothing methods have been proposed in the literature, but most of them are limited to linear toolpaths. However, in high-speed CNC machines and industrial robots, the toolpaths often consist of both lines and arcs. Therefore, there is a need for a path smoothing method that can handle both line-to-line transitions and transitions involving arcs (SHAHZADEH et al. 2018). These errors are caused by factors such as servo lag, dynamics mismatch, external disturbances, and more.

To address this issue, various estimation and compensation methods have been proposed for reducing trajectory error. These approaches can be divided into contouring-error estimation and contouring-error reduction approaches (JIA et al. 2018). These approaches include the "Moving frame based method", "Analytical method", "Generalized method" or "Servo-tuning approach". It is important to note that these methods for contouring-error estimation and reduction, only offer relative significance. Each algorithm has its own optimal range of applications and may outperform other methods within that range. Additionally, it is important to note that not every approach can be implemented on every system.

Another approach for achieving continuous path mode is by using biclothoid fillets. These fillets are used for corner smoothing and can be fitted between two arcs or a line and an arc. The main advantage of using biclothoid fillets is that they result in a smoother curvature profile compared to other methods, such as Bezier fillets. Especially with tight tolerance values, only a few biclothoid fillets are needed compared to Bezier fillets. Additionally, the biclothoid approach is more suitable in regards to the jerk and acceleration limits of the driving units. This smoother curvature profile allows for higher feedrates and shorter cycle times, ultimately improving the overall performance of the CNC machine (SHAHZADEH et al. 2018).

## 2.2 Computer-Aided Manufacturing

CAM is a technology that uses computer software to automate and optimize manufacturing processes. It involves the use of computer systems to control and operate machinery, such as CNC machines, robots, and 3D printers. CAM software can generate tool paths and instructions for machines based on CAD models, allowing for precise and efficient production. By reducing manual labor, CAM helps improve productivity, accuracy, and consistency in manufacturing. It is widely used in industries like aerospace, automotive, and electronics to streamline production (BI 2021).

### 2.2.1 CAM Software

CAM software enables manufacturers to generate toolpaths for a variety of manufacturing processes, including milling, turning, drilling, and 3D printing (KUMAR et al. 2019). It takes into account factors such as material properties, tool capabilities, and manufacturing constraints to generate the most efficient and accurate instructions for the machines. CAM software can also simulate the machining process to detect any potential collisions or issues before actual production begins, saving time and resources (BUI et al. 2019).

One of the key features of CAM software is its ability to optimize the machining process. It can automatically optimize toolpaths to minimize machining time, reduce material waste, and improve surface finish. By analyzing the geometry of the part, the software can determine the most efficient toolpath strategies, such as contouring, pocketing, or adaptive machining. It can also optimize tool selection, toolpath sequencing, and cutting parameters to achieve the best possible results (KYRATSIS et al. 2020). Furthermore, CAM software often integrates with other manufacturing software systems, such as computer-aided engineering (CAE) and enterprise resource planning (ERP) systems (RAMAZANOV et al. 2020). This integration enables seamless data exchange, improves collaboration between different departments, and ensures that the manufacturing process is aligned with the overall production goals (KADAM et al. 2023). With features such as optimization, simulation, multi-axis machining, and integration with other systems, CAM software empowers manufacturers to stay competitive in today's fast-paced and complex manufacturing environment (KAPPMEYER and NOVOVIC 2021).

Figure 2.16 shows the interface of Siemens NX, a CAM/CAD software that can be used to design parts and generate machine-specific instructions for manufacturing.

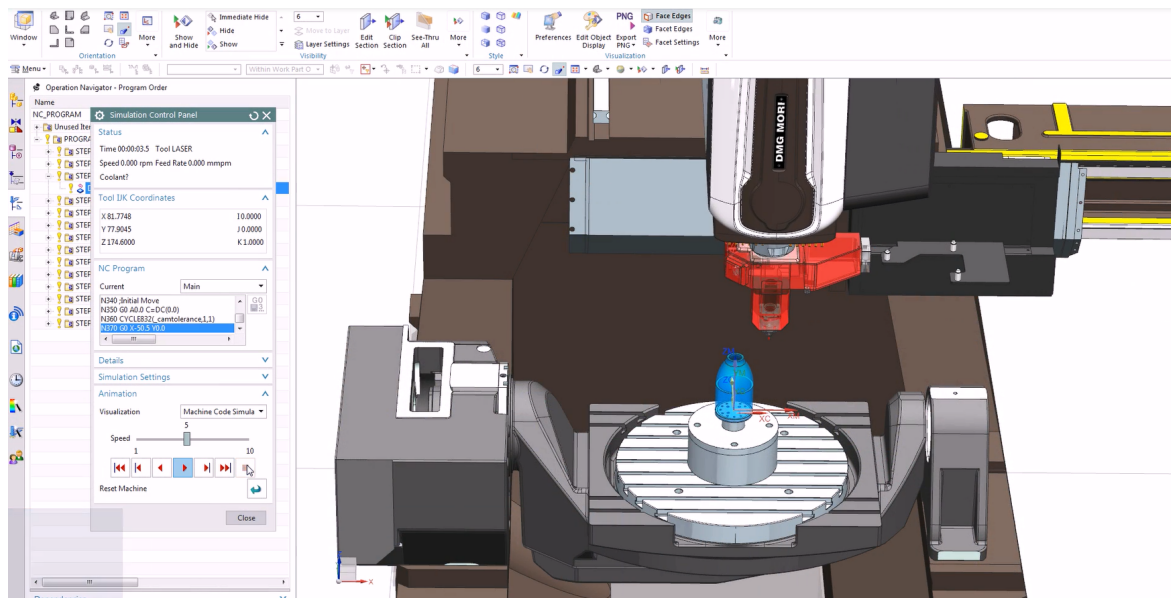


**Figure 2.16:** Interface of Siemens NX (NX 2015)

## 2.2.2 Path Planning

Path planning is a crucial features of CAM. It involves establishing the most effective tool-paths for machining operations, guaranteeing efficient and precise production (BRECHER and LOHSE 2013). It involves determining the optimal sequence of movements for the machining tool to follow while producing a part. It considers factors such as geometry, tool capabilities, machining constraints, and desired parameters. Its goal is to minimize machining time, reduce waste, and improve the finished product (XU et al. 2015). CAM software employs algorithms and mathematical models to determine the tool's position and orientation on the toolpath. Additionally, factors such as cutting direction, feed rate, and tool engagement need to be taken into account (TUNC and STODDART 2017).

Adaptive machining is a critical part of path planning and generation. It enables the CAM software to adjust the toolpath and cutting parameters in real-time based on material properties, tool wear, and other factors. This constant monitoring and adaptation ensure precise and dependable outcomes, even in difficult manufacturing conditions (LIU et al. 2017).

Multi-axis machining is an advanced function of CAM software, ideal for intricate cuts and shapes on complex geometries. By allowing the tool to move simultaneously along multiple axes, it delivers greater precision and accuracy during the machining of curved surfaces, free-form shapes, or parts with undercuts (TAKEUCHI 2014).

CAM software typically includes simulation tools that enable users to visualize and verify the toolpath prior to production. These simulations can detect potential collisions or errors that may occur during machining (DUBOVSKA et al. 2014).

Figure 2.17 shows three different path trajectories for planar milling operations. Depending on the area of application, different paths can be optimal. In generic 3D-printing as well as in WAAM multiple different infill methods, similar to the planar milling operations, can be used to build up and fill the desired geometry.



**Figure 2.17:** Three exemplary tool paths for iso-planar milling (*Zhao et al. 2018*)

## 2.3 Optimization Algorithms

Optimization algorithms are computational methods used to find the best possible solution to a problem within a given set of constraints. These algorithms aim to minimize or maximize an objective function by iteratively adjusting the values of decision variables (SIVANANDAM and DEEPA 2007). They are widely used in various fields, including engineering, operations research, finance, and machine learning, to optimize resource allocation, scheduling, parameter tuning, and other complex tasks. For the problem described in Chapter 1.2 optimization algorithms can be used for determining optimal constraint for the redundant DoFs while considering the defined objective, like reduction of direction changes or energy optimization.

Optimization algorithms are computational techniques employed to identify the optimal solution or set of solutions for a given problem. There are several types of optimization algorithms, each exhibiting a unique methodology and characteristics. Gradient-based optimization algorithms, like gradient descent, update the solution iteratively by following the direction of the steepest ascent or descent of the objective function (RUDER 2017). These algorithms are efficient for convex optimization problems where the objective function is smooth and has a unique global minimum or maximum.

Another type of optimization algorithm is the evolutionary algorithm, which is inspired by biological evolution. Evolutionary algorithms employ mutation, crossover, and selection to progressively shape a population of solutions over time. These techniques are especially applicable to resolving intricate optimization problems characterized by non-linear and non-convex objective functions. By reading a wider range of the search space, evolutionary algorithms can uncover tier-one solutions that draw near to the global optimum, although they may necessitate enhanced computational resources (BÄCK and SCHWEFEL 1993).

Genetic algorithms are evolutionary algorithms that use genetic operators, like crossover and mutation, to evolve solutions in a population. They can handle various types of optimization problems. Genetic algorithms are particularly effective for multi-objective optimization problems. They generate a set of solutions called the Pareto front, which represents the trade-off between conflicting objectives (KATOCH et al. 2021; LAMBORA et al. 2019).

Particle swarm optimization (PSO) is a metaheuristic optimization algorithm based on the collective behavior of a particle swarm. In PSO, each particle represents a potential solution, and it moves through the search space to discover the optimal solution by exchanging information with other particles. This cooperative behavior enables the algorithm to efficiently converge to better solutions. PSO is especially beneficial for continuous optimization problems that have numerous local optima (BÄCK and SCHWEFEL 1993).

In recent years, there has been an increasing interest in metaheuristic optimization algorithms. Examples of such algorithms are ant colony optimization, differential evolution, and harmony search, which draw inspiration from natural phenomena or human behavior. These general-purpose algorithms can be applied to various optimization problems and provide efficient and flexible approaches to finding optimal solutions (YANG 2011).

Optimization algorithms prove to be significant resources for uncovering optimal solutions to intricate issues. Optimization algorithms effectively fine-tune objectives, meet requirements, and refine decision-making processes across a broad spectrum of industries. The algorithm choice relies on the problem's characteristics, the available computational resources, and the desired balance between solution quality and computational efficiency.

## 2.4 Comparison of the State of the Art

In the following, a literature analysis is performed regarding the optimization of various process variables. The focus lies on manufacturing systems with redundant DoFs, specifically for tasks such as milling and WAAM. The main focus lies on the process variables: singularity avoidance, joint accelerations and jerk, stiffness and energy use. In cases where no literature is available that incorporates redundant DoFs, non-redundant systems are analyzed. Additional variables like precision and maximum load capacity can also be analyzed but are omitted from the detailed analysis due to the limitations of scope.

### 2.4.1 Singularity Avoidance

As mentioned in Chapter 1.2, singularities occur when the robot manipulator loses control or achieves limited mobility due to certain configurations (MALYSHEV et al. 2022). This results in the loss of a DoF or makes the system highly sensitive to small changes (MILENKOVIC 2021; ZHAO et al. 2021). Figure 2.18 shows how the 4th joint needs to rotate significantly when moving along a straight line along the Y-axis in Cartesian space. When an additional velocity boundary condition is set that defines the feed rate of that path, the rotation is very difficult to perform as the motor joints cannot keep up with the required angular acceleration. This movement significantly increases energy consumption and increases wear on the joints.

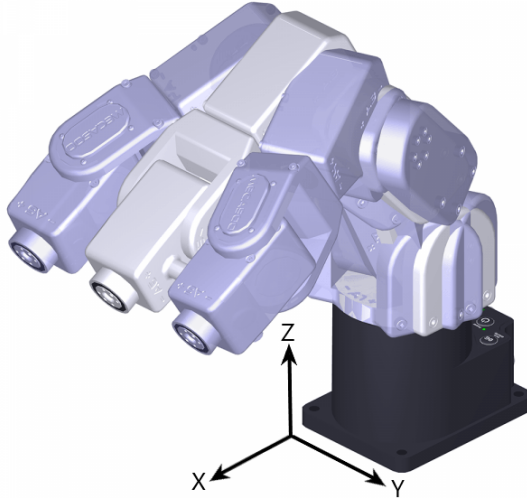


**Figure 2.18:** Passing through a wrist singularity (*Mecademic Industrial Robotics 2023*)

Due to the infinite possible solutions for the inverse kinematics of redundant manipulators, it is exceptionally challenging to predict and prevent the occurrence of singularity configurations during motion planning (SHI et al. 2021). In tasks that involve functional redundancy, as where the manipulator has more DoF than required for the task, the general projection method cannot be applied (WEI et al. 2014). Robotic industrial welding processes often

have functional redundancy due to the presence of symmetry axes when using generic 6-DoF industrial robots. Different approaches have been proposed to solve functional redundancy, including adding a virtual joint to the manipulator or using the twist decomposition approach (TWA).

Most of the research is limited to the mathematical analysis of singularities and does not consider the industrial implementation of the proposed algorithms in an industrial setting. The manipulability measure and maximization of Jacobian minors are commonly used methods to avoid singularities. Other methods, such as condition number and singular value decomposition, can also be used (STEVENSON et al. 2002). Another mathematical analysis performs a differentiation between non-recoverable singularities and configurations where through self-motion recovery into a non-singular configuration is possible (BEDROSSIAN 2002).

Another approach proposes a kinetostatic performance index for evaluating the quality of robotic postures, which includes singularity avoidance and joint limit consideration (HUO and BARON 2008). This method is also transferable to applications like milling. A parameter called "condition number" and "manipulability" are introduced, which are used to calculate the kinetostatic performance index. The presented method can increase the distance from singularities and lower the maximum rotation velocity of the fourth joint. One disadvantage of the proposed method is the manual selection of a parameter. This parameter is responsible for avoiding joint limits and minimizing joint velocities. Manual fine-tuning of that parameter is required for optimal performance.

Further approaches are proposing roll motion around the tool's symmetry axis to counter the loss of a DoF at the singularity. Paths with varying tool roll or fixed roll angles can be chosen, with considerations for tool elevation changes. Selecting paths with a fixed roll angle simplifies implementation for existing robot controllers (MILENKOVIC 2021).

Another approach uses the non-square Jacobi matrix and, after analysis, derives a simplified version through the selection of coordinate systems and primary transformation. By using block matrix analysis, the singularity conditions of the articulated robot are determined. A singular configuration avoidance algorithm is used to avoid singular patterns through constraining redundant DoF (SHI et al. 2021).

Neural networks and other machine learning approaches are commonly used to solve the issue of inverse kinematics. In this case, the optimization variable is not only limited to singularity avoidance but can also be focused on precision or optimization of feed rate (WEI et al. 2014).

### 2.4.2 Optimization of Joint Accelerations and Joint Jerk

Jerk and acceleration control are critical because high values can wear out the robot structure and significantly stimulate its resonance frequencies. Vibrations caused by non-smooth trajectories can harm the robot's actuators and produce substantial deviations compared to the desired path. A recently published approach uses an adaptive greedy algorithm for generating the jerk-optimized trajectory with discrete time constraints.

The proposed algorithm improves the trajectory in an iterative manner after obtaining an initial trajectory by utilizing a graph-search method (DAI et al. 2020). A further method proposes a sequential quadratic programming method. The results show that optimal time-jerk trajectories with traveling time constraints can be obtained. By modifying the weighting coefficients and the elastic coefficient, it is possible to achieve various trajectory planning objectives, such as rapid execution, a seamless trajectory, or a combination of both aspects (JIANG et al. 2017).

Another method is proposing a method of reconstructing the path by a sequence of via-points that define the positions and orientations of the robot's end-effector. Unlike most minimum-jerk trajectory planning techniques, this algorithm does not force an execution time beforehand and takes into account constraints such as upper bounds on velocity, acceleration, and jerk. The algorithm uses a hybrid objective function that balances execution time and smoothness of the trajectory. The output of the algorithm is a vector of time intervals between consecutive via-points that minimizes the objective function (GASPARETTO and ZANOTTO 2010).

The last analyzed method is using an algorithm for adjusting the increments of the generalized coordinate vector. By using a pseudo-inverse of the Jacobi matrix and a Taylor's expansion, the robot's acceleration and jerk can be calculated. Results show that when the end effector is closer to the center of the robot, joint jerk increases. It is also shown that if trajectories are designed on the X-Z plane and directed away from the robot's center, the jerk decreases (DUONG 2021).

### 2.4.3 Optimization of Stiffness

Stiffness plays a crucial role in machining with industrial robots. It refers to the ability of a machine or structure to resist deformation under an applied load. In the context of machining, stiffness directly affects the accuracy, precision, and overall performance of the robot. A high level of stiffness ensures that the robot remains stable and rigid during machining operations, minimizing unwanted vibrations, deflections, and inaccuracies (WU et al. 2022). This is particularly important when dealing with high-speed or heavy-duty machining tasks, as any lack of stiffness can result in poor surface finish, dimensional inaccuracies, and reduced tool life.

One method for evaluating the stiffness of a robot is using a newly defined performance index, which is maximized to optimize the robot's posture. The problem is solved using a discretization search algorithm, taking into account joint limits, singularity avoidance, and trajectory smoothness. Each joint of the robot is modeled as a linear torsion spring, which is transferred into a stiffness matrix. This method is applied to a 6-DoF robot that is used for a milling operation. The goal of this method is to set the redundant DoF in such a way that stiffness is maximized. Simulations and experiments on an industrial robot validate the performance index, demonstrating improved machining accuracy using this method (XIONG et al. 2019).

Another approach is working with a dynamic model to reduce the chatter in a milling operation with a 6-DoF robot. By considering the frequency response function, the maximum possible cutting depth, without the occurrence of chatter can be determined. The cutting depth is a function of the redundant DoF. In this case, the redundant DoF is the rotation around the axis of the spindle. An experimental analysis of a full-slot cut is performed. The results show that a significant reduction in chatter can be achieved by setting the redundant DoF to the optimal value (WANG et al. 2022).

A further publication performs a comparative study of robot pose optimization using static and dynamic stiffness models. The results suggest that the static stiffness model can achieve close to optimal results for pose selection for tasks where the process forces do not approach the resonant frequencies of the robot. It is also discussed that static and dynamic stiffness-based optimizations cannot reduce the deflections of the cutting tool to a range smaller than the robot's repeatability (CVITANIC et al. 2020).

There are many more methods, like finite element analysis, matrix structure analysis, and virtual joint modeling. To enhance stiffness models, further investigation needs to be conducted. The current state of the art shows a need for standardization in stiffness modeling, as there is currently no universally accepted procedure for establishing such models. Developing a modeling process with standard principles, evaluation indicators, and measuring techniques can simplify the selection and application of modeling methods. Additionally, the application of machine learning techniques, such as artificial neural networks, can be explored for stiffness modeling. Processing experimental data using machine learning algorithms is shown to yield high-precision stiffness models (WU et al. 2022).

#### 2.4.4 Optimization of Energy Usage

Energy-efficient usage of industrial robots is essential for achieving cost savings and sustainable manufacturing processes. Manufacturers can achieve this by implementing strategies such as optimizing robot movement paths, reducing idle time, and using energy-efficient components, resulting in significant reductions in energy consumption of their robotic systems. Incorporating advanced algorithms enables robots to adapt to changing conditions and operate at their most efficient levels, optimizing energy usage (UHLMANN et al. 2016).

One publication by Paryanto et al. analyzes the different methods at different development stages of a production environment in regards to energy optimization. The results show that operating speed and payload strongly influence power consumption (PARYANTO et al. 2015). Further analysis in a different publication shows that in a setting where a 6-DoF is used to perform a 5-DoF task, energy savings of up to 20.8% can be expected. The proposed method uses the yaw angle (C-axis) as an optimization variable that can be set to a value in a certain range (BOSCARIOL et al. 2020).

Another publication analyzes the general energy consumption of an industrial robot. The results show that cooling and movement speed have the most significant impact on energy consumption. The axis drives are responsible for 23% of the energy consumption. Based on this result, it is shown that optimizing the robot's movement in regards to optimal movement will significantly reduce its energy usage (UHLMANN et al. 2016).

#### 2.4.5 Summary

Setting the appropriate boundary conditions in form of constraints, directly impacts the performance and efficiency of a production system. By carefully fine-tuning these values, improved process variables such as singularity avoidance, minimization of joint acceleration and jerk can be achieved. Moreover, optimizing energy usage through the adjustment of variables related to movement speed not only contributes to environmental sustainability but also leads to economic benefits by reducing long-term operational costs. Additionally, the consideration of variables like stiffness and joint limits ensures the safety of both the manufacturing system and its operators.

In conclusion, the careful selection and optimization of process variables play a significant role in achieving optimal performance. The discussed publications, work only on the optimization of individual process variables. A method that takes a holistic approach, is not yet published. Additionally no presented method in those publications gives the user the possibility to weigh the individual process variables in relation to each other and optimize the setting of redundant DoFs towards this user-defined goal. The goal of the following proposed method is to fill this demonstrated research gap.

# **Chapter 3**

## **Methodology**

### **3.1 Introduction**

The proposed method aims to provide a framework for optimizing various process variables of a manufacturing system in order to achieve a global optimum. These process variables are numerical values that describe the behavior and attributes of a system during the execution of a manufacturing process. One example of a process variable and a manufacturing system, is the combined angular travel of all joints of an industrial robot that is traversing a defined toolpath. The goal of this method is to effectively utilize the redundant DoFs of a system, as mentioned in Chapter 1.3, to optimize the process variables that are important to the user. This method is suitable for robotic milling operations, robotic WAAM processes, and other systems that have redundant DoFs. Implementing this method can improve the overall performance and efficiency, ultimately leading to increased productivity.

The method is divided into two parts. Firstly, for a specific toolpath with user-defined boundary conditions (constraints for the redundant DoF), a set of selected process variables are analyzed. The user has the option to assign a relative importance to the process variables and thus specifying a personal priority rating. Based on the numerical values of the process variables and their relative importance, it can be determined how optimal the set boundary conditions are.

Secondly, the optimization of these boundary conditions is carried out. In this step, the aim is to find the most optimal setting for the redundant DoFs in order to optimize the selected process variables. In other words, the aim is to maximize a score describing the process. This goal can be, for example, the reduction of acceleration peaks in the robot's joints as well as minimizing direction changes of the driving motors.

This method is transferable to any manufacturing system that is used to perform a task with more DoFs than required by the toolpath. In robotic cells specifically, this form of redundancy can be in form of rotary-tilt tables, linear-axes or simply traversing a 5-axis toolpath with a 6-axis industrial robot.

## 3.2 General Method for Process Analysis and Evaluation

In the following, the general methodology, the process variables and score calculation is discussed. Chapter 3.2.1 gives a general introduction, while Chapter 3.2.2 discusses the individual process variables and their numerical form.

### 3.2.1 General Methodology

In a manufacturing setting with redundant DoFs, multiple elements are in interdependence. These elements include: the toolpath, manufacturing machine, material, part geometry and manually set boundary conditions. It is important to understand how each element is influencing the resulting manufacturing process and what values can be adjusted to achieve an optimal outcome in regards to selected process variables.

The manufacturing machine plays a crucial role in defining the toolpath as it determines parameters such as the total working volume, DoFs, maximum feed rates, and whether the manufacturing process is additive or subtractive. This machine can be a 6-axis CNC machine or an 8-DoF industrial robot. The redundant DoFs, which are not bound by the toolpath, are especially important, as they serve as the future adjustment point for the process variables.

The part geometry refers to the finished geometry as designed in CAD, while the material is the user-defined element from which the part is manufactured. These elements, along with the machine, directly influence the toolpath that is then used in the manufacturing process. For instance, the machine's specifications determine whether the spindle or the work piece itself needs to be tilted during machining to achieve the desired geometric features.

In addition to the machine, part geometry, and material, there are further factors that impact the toolpath. These include the availability of end-mills, the desired depth of cut, the machining strategy, and the operation sequence. These factors are considered as adjacent parameters within the overall manufacturing process. Since the toolpath is a movement relative to the work piece, the user must specify additional parameters before initiating the manufacturing process. One example is the positioning of the raw stock material or substrate plate within the machine and establishing the coordinate system that serves as a reference for the TCP. These settings are also part of the adjacent parameters and need to align with the capabilities of the machine. Correct settings of these parameters may necessitate a comprehensive understanding of both the machine and the specific manufacturing process being performed.

The next element that must be defined, are the constraints for the redundant DoFs. These settings are referred to, as user-defined boundary conditions. A straightforward example to illustrate this constraining is when a 6-DoF robot is used for milling operations. In milling, the TCP position is determined by three coordinates: X, Y, and Z, as well as the tiling and inclination around the X- and Y-axes. Thus only five out of six DoFs are defined by the toolpath. For a full specification, the last DoF which is the rotation around the Z-axis, must

be defined manually. With the addition of this constraint, the pose of the robot is fully defined. Since the spindle is rotationally symmetric around its axis, its setting does not affect the toolpath. The rotation around the Z-axis can theoretically be set to any value, but can significantly affect the overall process. In practical applications, this rotation value is limited due to factors such as cable routing to the spindle or joint limits. These same limitations apply in WAAM, where the wire feed system combined with the torch position restricts the possible orientations that can be achieved. Once the constraints are established and the toolpath is generated, various process variables can be analyzed (see Chapter 3.2.2 for more details).

The goal is now to optimize these process variables by selecting the most optimal boundary condition. Some notable variables include the total angular travel of a specific joint or the occurring angular acceleration. Alongside these resulting numerical values that describe the process, the user has the option to assign specific importance or weight to those variables. By weighting selected process variables, an overall objective with a preference of the user is defined. For example, reducing acceleration peaks is twice as important as reducing the number of direction changes in the joints. With the help of the defined importance factors, a score for the determined toolpath with the set boundary condition can be calculated.

The flowchart displayed in Figure 3.1 illustrates the mentioned interdependence of the different elements and the resulting process variables. In the following steps of the method, the adjacent parameters, machine, part geometry and material are excluded in the presentation, as they considered fixed elements and do not directly impact the optimization of the manufacturing process as explained in Chapter 1.3. These elements serve as hard constraints that define the feasible toolpath and are not directly linked to the redundant DoFs. However, it is important to acknowledge that these adjacent parameters can still greatly enhance areas such as cycle time or surface finish of the manufactured part. The main focus of the presented method is placed on the user-defined boundary conditions, user-defined weights, and the resulting process variables.

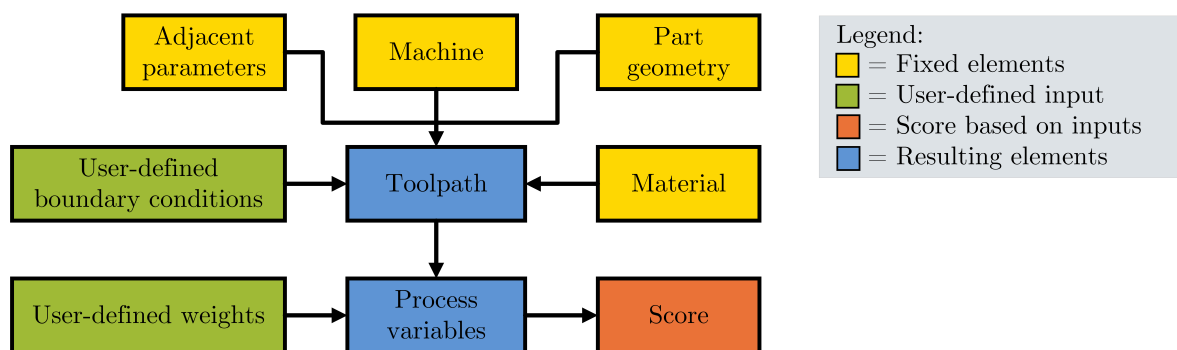


**Figure 3.1:** Interdependence of various parameters and elements

### 3.2.2 Process Variables

Table 3.1 presents an overview of a select group of the various process variables and their numerical form. These process variables can be derived from a toolpath with defined boundary conditions that is executed by an industrial robot. Due to the limited scope of this thesis, only this selected group of process variables is discussed in detail. Further process variables are mentioned in Chapter 5.2.

The first group of process variables covers the position, velocity, acceleration, and jerk of the individual joints. These parameters are closely related to the joint position, as they are derived from it. The second group includes the number of direction changes of a joint during operation and the total travel of a joint. The third group comprises the continuous and total energy usage of the manufacturing system during production. The last group consists of the reachability index, singularity analysis, and torch orientation. In the following section, each of these process parameters, their numerical form and required post processing is discussed in detail.

**Table 3.1:** Process variables and their numerical form

Process variables	Numerical form
Angular position of each joint	Time-series
Angular velocity of each joint	Time-series
Angular acceleration of each joint	Time-series
Angular jerk of each joint	Time-series
Direction changes of each joint	Scalar value
Total travel of each joint	Scalar value
Continuous energy usage	Time-series
Total energy usage	Scalar value
Reachability index	Binary value / Time-series
Singularity Analysis	Scalar value / Time-series
Torch orientation	Time-series

#### Position, Velocity, Acceleration and Jerk

One of the primary variables in a robotic manufacturing system is the joint positions. This process variable is recorded as a one-dimensional array comprising the rotational position or extension values of each rotary or linear joint at each time step. This data serves as the foundation for calculating subsequent variables like velocity, acceleration, and jerk. Analyzing these variables is crucial to ensure that the joints are not excessively strained during the manufacturing process, thus prolonging their service life as much as possible. To extend the lifespan of an industrial robot, it is essential to take into account the load on individual joints.

### Direction Changes and Total Travel

An important factor in assessing joint load is the number of direction changes that occur during operation. High-frequency rotational changes can lead to degradation and reduced precision in manufacturing processes. This process variable, referred to as the number of direction changes, is a scalar value that can be derived from the angular position of each joint. By analyzing the joint position data further, the total travel of a joint can be determined by integrating the joint velocity over time. Furthermore, it can be important to analyze if velocity changes consistently occur at the same position, leading to wear on the same tooth flank of the gears. This can cause significant localized wear and shorten the lifespan of the joints. Programs or toolpaths that require less overall joint travel are generally preferred. By minimizing the number of direction changes and optimizing joint travel in regards to acceleration and jerk, stress and wear on the robot joints can be reduced, ultimately extending the overall lifespan of the system.

### Energy Usage

Estimating energy usage in industrial robot applications is increasingly important in the current manufacturing environment. One accurate method to estimate energy consumption is through multi-body simulation (MBS), which requires a correct 3D model incorporating information about the weight and distribution of the robot joints. Another approach is to utilize Machine Learning (ML) techniques in combination with the joint positions over time or other intermediate analyses. Moreover, in cases where the industrial robot is used for WAAM, the power required for welding can be determined by analyzing the duration during which the welding torch remains active, which can be extracted from the G-code. Similar to the variables mentioned earlier, the continuous energy usage is also stored in the form of an array to capture variations over time.

Total energy usage, measured in kilowatt-hours (kWh), is a crucial variable that can be directly extracted after finishing the manufacturing process. It offers valuable insights into the overall energy consumption of the industrial robot system. These variables can be obtained by recording the overall energy usage as a single value or by integrating the time-series data of continuous energy consumption. By analyzing energy usage, manufacturers can identify energy-intensive processes or operations, optimize energy consumption, and implement strategies to reduce overall energy consumption. This not only leads to cost savings but also provides environmental benefits.

### Reachability

The reachability index is a binary variable used to assess the feasibility of executing a program in an industrial robot system. It determines whether all the necessary points defined in the toolpath are within the robot's working volume and can be reached by its TCP. This variable

ensures that the robot can physically access all required positions in the work area. If any point is found to be outside the reachable workspace, adjustments are necessary. Reachability can also be influenced by additional factors such as cable routing. Even if all the traversed points are within the robot's working volume, factors like wire-feed systems or optical fibers used for laser transmission may have limitations on bending degrees. When analyzing cable routing in relation to orientation, the reachability index can be represented as a time-series that records the deviation of the cable's bending angle from the optimal angle.

### Singularity Analysis

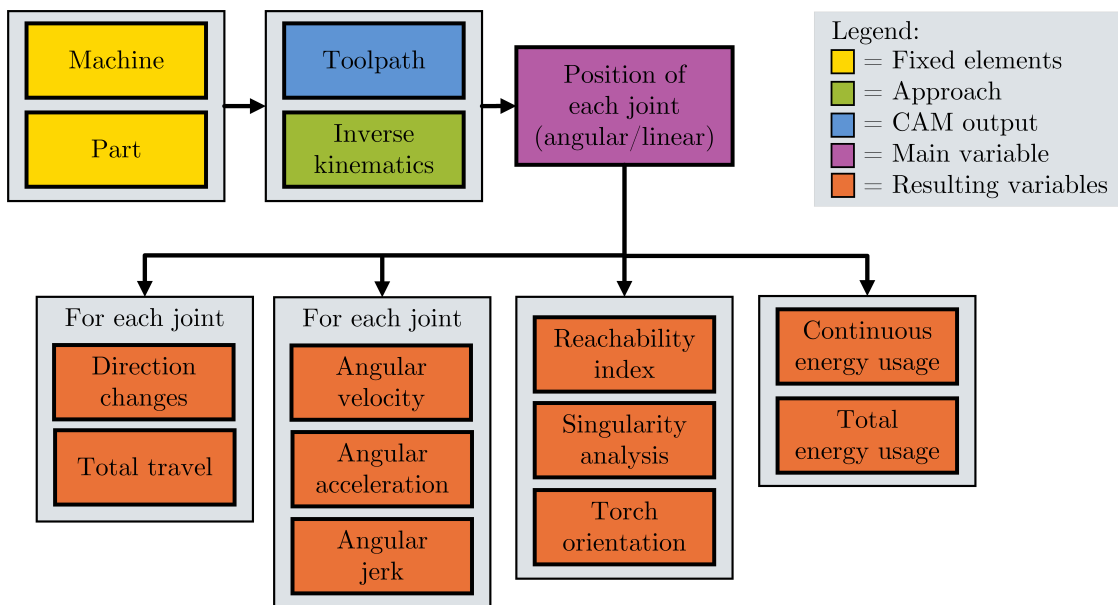
The singularity analysis variable can be represented either as a time-series or as a single numerical value. It is derived from the smallest eigenvalue of the Jacobian matrix, which is calculated using the current configuration of the robot. This variable can be stored in an array format, capturing the variations in singularity analysis over time. Alternatively, only the smallest eigenvalue encountered throughout the entire toolpath can be recorded. Analyzing the singularity time-series enables the optimization of non-optimal poses, ensuring that the robot avoids singular configurations that may result in reduced performance or unexpected behavior.

### Torch Orientation

Torch orientation is a crucial variable in WAAM, as it tracks the tilt angle of the welding torch during the process. Achieving optimal performance requires that the material deposition always occurs in the direction of gravity. When the welding head is positioned upside down, it represents a worst-case scenario where the welding process takes place against the force of gravity. Significant deviation of the tilt angle from the gravity vector makes it challenging to maintain the stability of the molten metal pool, potentially leading to defects such as sagging. To ensure proper monitoring of torch orientation, a time-series is used to record the deviation of the torch angle from the gravity vector. Analyzing this information helps identify any deviations or that may impact the quality of the deposition process.

### Flowchart of process variables

Figure 3.2 illustrates the interconnections of the different variables. It is evident that all variables can be derived from the position of the joints. This highlights the significance of this information. The position data is vital for analyzing and optimizing the robot system's performance. By monitoring and analyzing the joint positions, users can gain insights into various aspects of the robot's operation and make informed decisions to enhance productivity.

**Figure 3.2:** Parameter flowchart

### 3.3 User-Defined Weights and Score Calculation

#### 3.3.1 Local Rating and Global Score

In order to evaluate whether the boundary conditions for a toolpath are optimal or can be improved, it is necessary to have a score or rating value that considers the process variables and their importance. Assigning relative importance to different variables can involve subjective judgments, expert knowledge, and consideration of specific manufacturing constraints. For instance, in some cases, minimizing joint jerk may be the main objective, while in others, energy usage may be more important. To quantify the performance of a toolpath, the user can assign weights or importance factors to each variable based on their specific requirements. These weights reflect the relative significance of each variable in achieving the desired optimum. A weighted sum or scoring method can then be used to evaluate and compare the toolpath with varying constraints based on the aggregated scores of the individual process variables. It's important to note that the subjective weighing of variables can vary between different manufacturing scenarios and requires continuous evaluation and adjustment based on changing priorities or goals.

The score of a toolpath with its boundary conditions is calculated as shown in table 3.2. Each process variable is assigned a local rating ranging from 0 to 100, where 0 represents the least optimal and 100 represents the best-case solution. This local rating is multiplied by the corresponding importance factor, resulting in a local score. The local scores for all variables are then summed to obtain the overall global score for that specific boundary condition.

It is crucial to ensure that the sum of all defined importance values equals 1, so that the toolpath with the most optimal boundary conditions yields a global score of 100.

**Table 3.2:** Calculation of a global score for a specific boundary condition

Process variable	Local rating	Importance factor	Local score
Process variable Nr. 1	74	0.5	37
Process variable Nr. 2	34	0.1	3.4
Process variable Nr. 3	65	0.1	6.5
Process variable Nr. 4	22	0.3	6.6
Global score			53.5

### 3.3.2 Local Rating Calculation

Calculating a local rating is not a straight-forward approach. The first problem is, that based on a singular value like "direction changes," it is not possible to determine a local rating as it is not clear if that value is close to optimal or far from it. To address this issue, one possible solution is to analyze the same toolpaths with multiple different boundary conditions or constraints, for example different rotation around the Z-axis, and compare the results.

Figure 3.3 shows how a local rating can be calculated by means of variation. Each variation of the boundary condition results in a different number of direction changes in joint 1 of an articulated robot. The local score can be determined by essentially applying a Min-Max scaler, which normalizes the values between a minimum and maximum value. The range is set from 0 to 100 as described in Chapter 3.3.1.

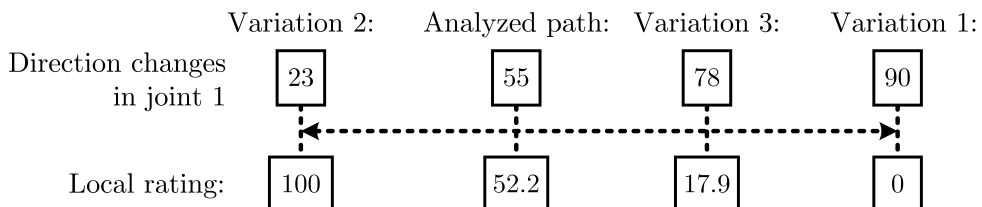


**Figure 3.3:** Calculation of the local score through variation

It is important to note that increasing the number of variations performed before calculating the local score will enhance the accuracy of this approach. If only a few variations are executed, there is a possibility that only similar outcomes will be found, which significantly affects the result. Furthermore, the user needs to specify whether a high or low scalar value of a process variable is desired. The Min-Max scaler should return the local score accordingly.

Another factor that needs to be analyzed is whether the variations in the boundary conditions lead to process variable values that exceed a certain standard deviation. Figure 3.4 illustrates how a local rating of 70 for the total energy consumption is calculated, despite the presence of very small absolute differences. In this case, the standard deviation is only 0.369.

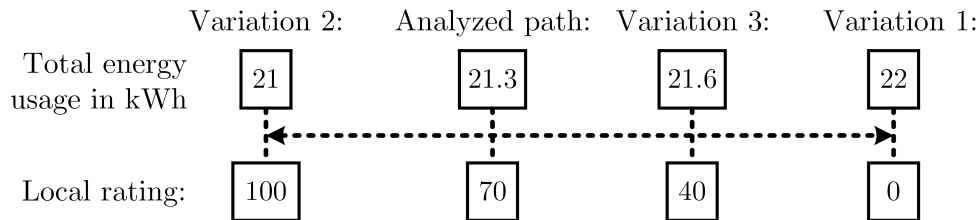


**Figure 3.4:** Variations of a process variable with low standard deviation

On the other hand, Figure 3.5 demonstrates how the same local rating of 66 is calculated, even though the absolute differences are significantly higher. Here, the standard deviation is 36.996. The local rating should only be used as input for the local score if the standard deviation exceeds a predetermined threshold. If the standard deviation criteria are not met, the corresponding process variables and its local score should be excluded from the calculation of the global score. In the following chapters, each process variable and its conversion into a single scalar value is discussed in more detail.

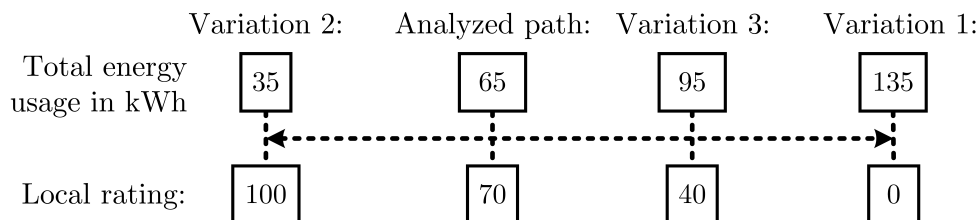


**Figure 3.5:** Variations of a process variable with high standard deviation

### 3.3.3 Information Extraction form Time-Series Data

It is important to note that, as discussed in Chapter 3.3.2, the computation of a local score requires transforming time-series data into a single scalar value. This transformation can be accomplished by directly manipulating the time-series data, such as summing up all values, or by conducting subsequent analyses. Since each time-series captures distinct physical phenomena, each one necessitates a unique process for converting it into a scalar value.

### 3.4 Information from Angular Position

In its isolated form, the rotational or angular position of a joint does not provide much information to enable extensive qualitative analysis. However, when supplemented with temporal information, it becomes a valuable source of information. By considering the angular position in conjunction with the temporal dimension, a more comprehensive understanding of joint behavior can be obtained, allowing for more in depth analysis. Figure 3.6 visualizes what information needs to be added to enrich the analysis of these process variables that are directly related to the angular position of joints.

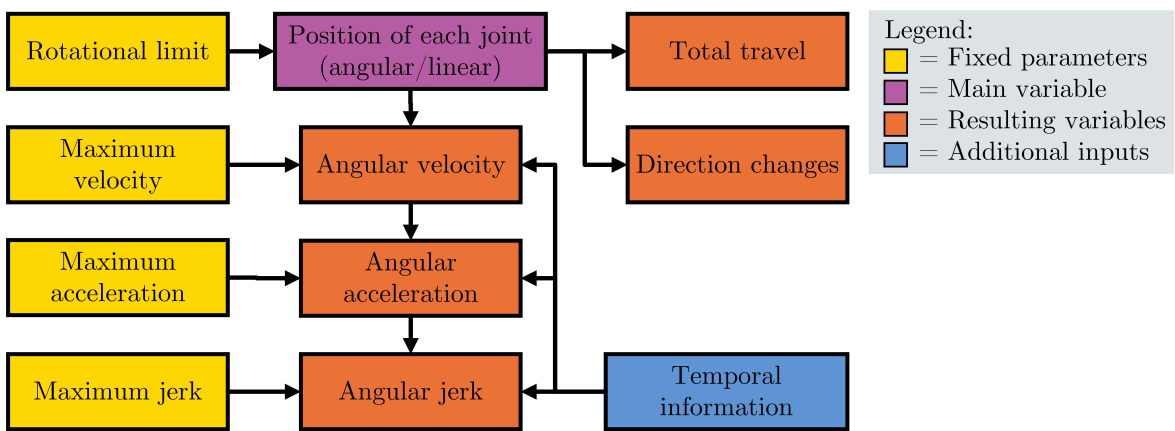


**Figure 3.6:** Additional information for angular position of each joint

The first additional required piece of information is the temporal element, which specifies the exact time when a joint should be in a specific rotational position. This information can be recorded in small equidistant time intervals or only record the positional changes. Recording only the change in position is not ideal because it does not accurately represent the physical aspect of the system. In reality, the position cannot change significantly from one time interval to the next. Additionally, this method does not provide information about the rotational velocity at which the joint should change position. On the other hand, continuous recording in small equidistant time intervals can result in a higher number of recorded values and, consequently, a longer time-series. By deriving the position with time, one can determine the velocity, acceleration, and jerk. With knowledge of the maximum capabilities of the motors, such as maximum velocity or maximum acceleration, it is possible to compare whether the toolpath is feasible for execution. If the limits are exceeded, the behavior of the robot will not be as expected.

Figure 3.7 illustrates the rotational position of a rotary joint over time in degrees. The left side of the figure illustrates the position recorded with equidistant fine grained time intervals, while the right side displays a time-series where only the destination positions and their corresponding times are recorded. Both series have very similar characteristics but offer a significantly different information density.

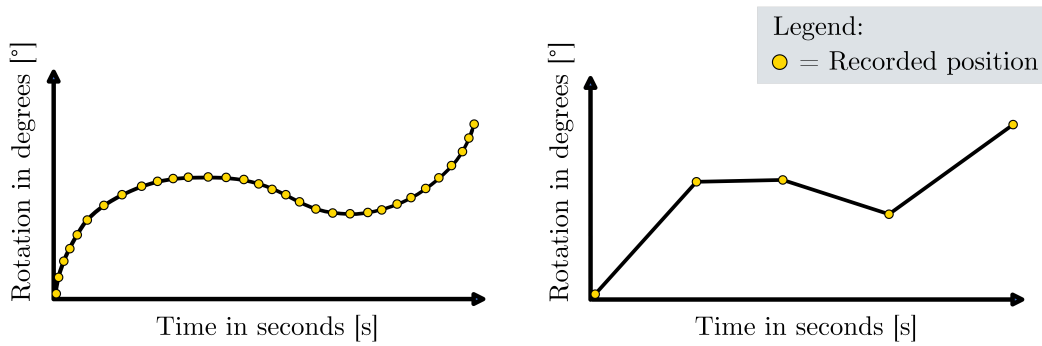


**Figure 3.7:** Two option for recording the joint position in a time-series

### 3.4.1 Total Joint Travel and Direction Changes

Variables that can be analyzed without the need for any additional information include the number of direction changes and the total travel of a joint. The total travel can be determined by subtracting the position of two consecutive recorded points and summing up the absolute values. Furthermore, additional information can be derived by separately summing up the clockwise and counterclockwise rotations. By combining the absolute values of these rotations, the overall travel of the joint can be obtained.

Figure 3.8 provides a visual representation of the calculation of total travel. The total forward rotation (clockwise) can be determined by summing up the lengths of the green arrows, while the total backward rotation (counterclockwise) is obtained by summing up the lengths of the orange arrows.

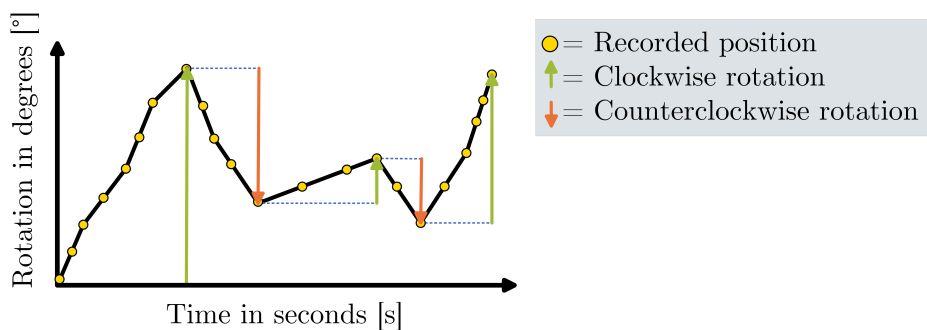


**Figure 3.8:** Summing up the rotation in the clockwise and anti-clockwise direction

The number of direction changes is a variable that can be determined by analyzing the joint position alone, without the need for temporal information. This can be accomplished by identifying points where the position before and after either decreases or increases. However, it is important to note that this method may not be applicable to points where multiple positions are recorded at the same value consecutively. To address the issue of multiple positions recorded at the same value, a potential solution is to introduce a tracking value that indicates whether the previous change in direction of two consecutive positions was

either upward or downward. If the direction of two positions is different from the tracking value, the direction change counter is incremented by 1. However, if the direction is the same as the previous points or if the positions are identical (neutral), the direction change counter and tracking values remain unchanged. Figure 3.9 provides a visual representation of the points where the direction change counter is incremented.

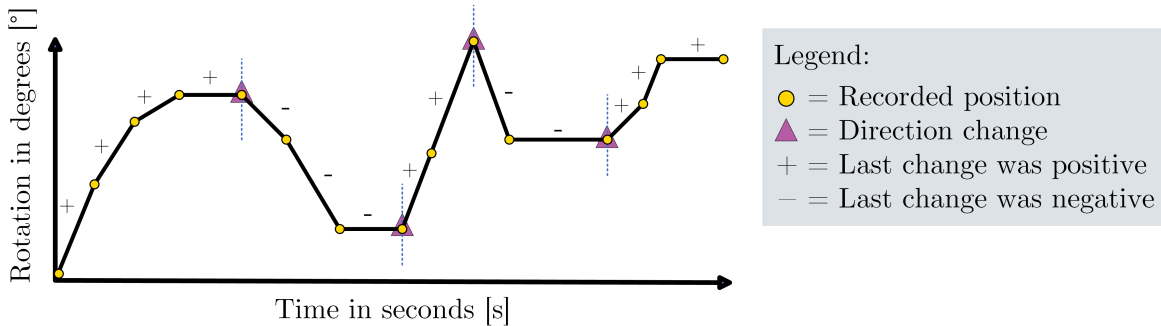


**Figure 3.9:** Calculating direction changes from a time-series

The counters for direction changes and total travel of each joint can be easily transformed into a local rating, as explained in Chapter 3.3.2. This local rating can then be multiplied by an importance factor to calculate the local score. The direction changes can be summed up over all joints, or they can be specifically grouped based on certain criteria or categories.

Table 3.3 provides an example of how a global score can be calculated based solely on the number of direction changes and total travel. The table illustrates how different joints and variables can be weighted and grouped together to calculate the global score. By assigning different importance factors to each variable, the overall global score can reflect the desired optimum. It is important to note that only the local ratings are multiplied by the importance factor, not the actual counted direction changes or total travel values, to form the local scores. This allows the local score to range from 0 to 100. In this example, due to the high local rating and importance factor for the direction changes in joint 1, the overall global score is also very high. This clearly shows the significance of the importance factors in the calculation of the scores.

**Table 3.3:** Calculation of a score regarding only direction changes and total travel

Process variables	Local rating	Importance	Local score
Direction changes in joint 1	95	0.7	66.5
Direction changes in joint 2-6	45	0.1	4.5
Total travel in joint 4	34	0.1	3.4
Total travel in joint 1-3 and 5-6	46	0.1	4.6
Global Score			79

In certain cases, adjusting the boundary conditions may not be sufficient to reduce the num-

ber of direction changes, but can offer an improvement in a different area. It is important to note that having the same number of direction changes does not necessarily mean that two time-series are identical. Figure 3.10 visually demonstrates two time-series with the same number of direction changes but distinct characteristics.

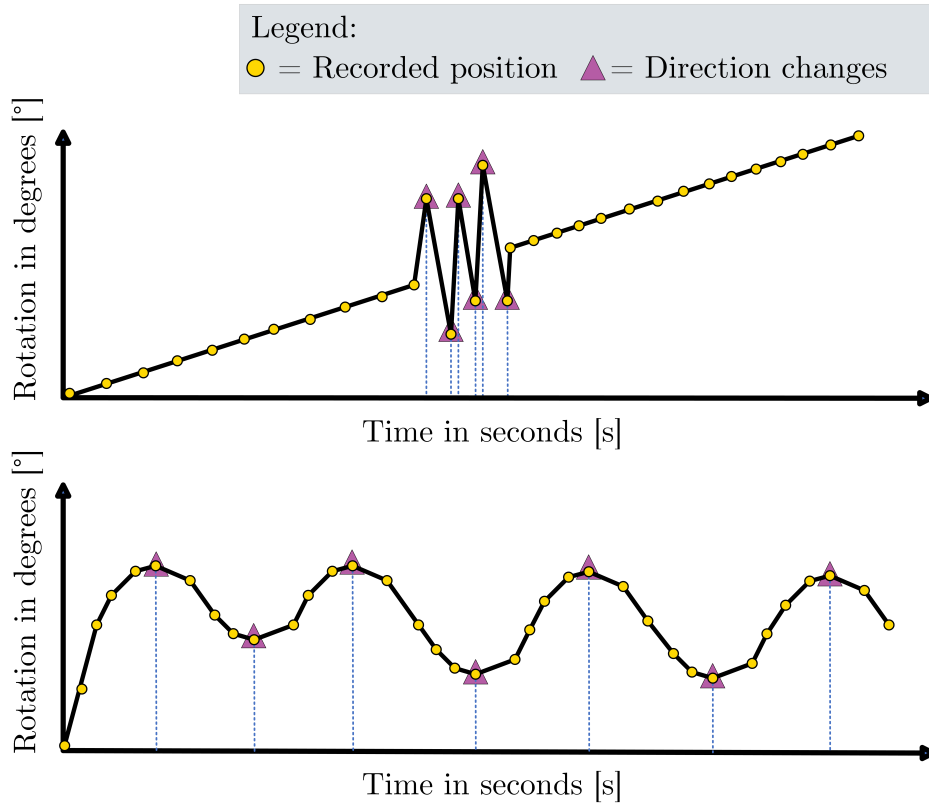


**Figure 3.10:** Two time-series with equal number of direction changes but different characteristics

To distinguish between these cases in the local rating, the standard deviation can be utilized. By incorporating the standard deviation, toolpaths that result in frequent and closely spaced direction changes can be identified and are generally considered less desirable. By combining the standard deviation of the timely occurrence with the number of direction changes, they can be integrated into a single variable. This can be achieved by dividing the number of direction changes by the standard deviation. This approach provides an evaluation method that takes into account both the quantity of direction changes and the variability within the time-series data. When there are only a few direction changes but with a high variance, the resulting variable value will be very low. Conversely, when there are numerous direction changes but with a low variance, the variable value will be high.

### 3.4.2 Rotation Limits

Additionally, a straightforward analysis of rotational limits can be conducted, requiring knowledge of four distinct values. The first two values are the upper and lower physical limit that

a joint cannot exceed, as surpassing those limit can cause significant damage to the robot. The other two values are potential soft limits put in place to prevent over-rotation of the joint beyond its physical limits. To validate whether any joint positions approach or exceed these limits, a simple comparison of all values can be performed. In cases where it is known that a joint is most stable within a specific range, additional limits can be defined accordingly.

Once a toolpath with defined boundary conditions is established, the joint angles can be analyzed through a simple comparison process. If the joint positions exceed the soft limits or deviate excessively from the desired orientation, a "No-Go" exception is triggered. It is important to note that the analysis of rotation limits does not contribute to the calculation of the global score but serves as a validity assessment to determine if the required movement for the toolpath is physically feasible.

Figure 3.11 visually illustrates an example of how the analysis includes the hard and soft limits, as well as the desired position range, of a specific joint. If the limits are not exceeded, the toolpath with the set boundary conditions is deemed safe to be executed. At each time step, the amount by which the joint exceeds the desired area can be summed up to form a scalar value, which can then be used to calculate the local score. By doing so, the toolpath with the most optimal boundary conditions will ensure that the joint positions remain within the desired area.

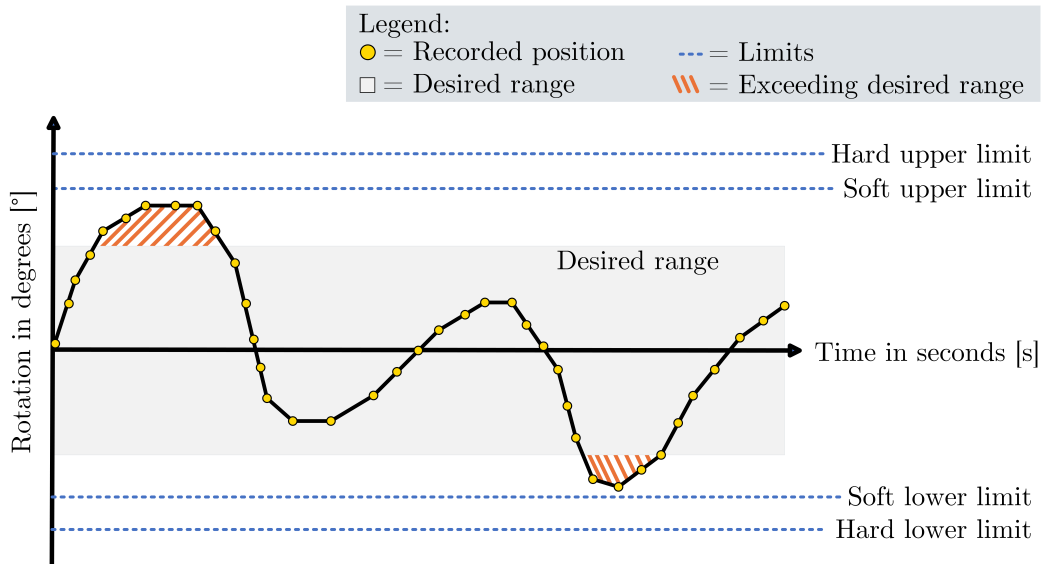


**Figure 3.11:** Hard and soft limits with desired range

### 3.4.3 Velocity, Acceleration and Jerk of the Joints

To conduct a specific analysis of the rotational velocity, acceleration, and jerk of the joints, a time derivative needs to be applied. By performing simple comparisons of the time-series values, it becomes possible to determine whether the maximum capabilities of the motor driving the joint are being exceeded.

Figure 3.12 demonstrates how the velocity aspect can be transformed into a scalar value, which can then be utilized in the calculation of a local rating. Firstly, the joint velocity is obtained by taking the absolute time derivative of the joint position. Subsequently, an analysis is conducted to determine the duration for which the absolute velocity exceeds a certain threshold value. In the given example, the threshold is set at 80%.

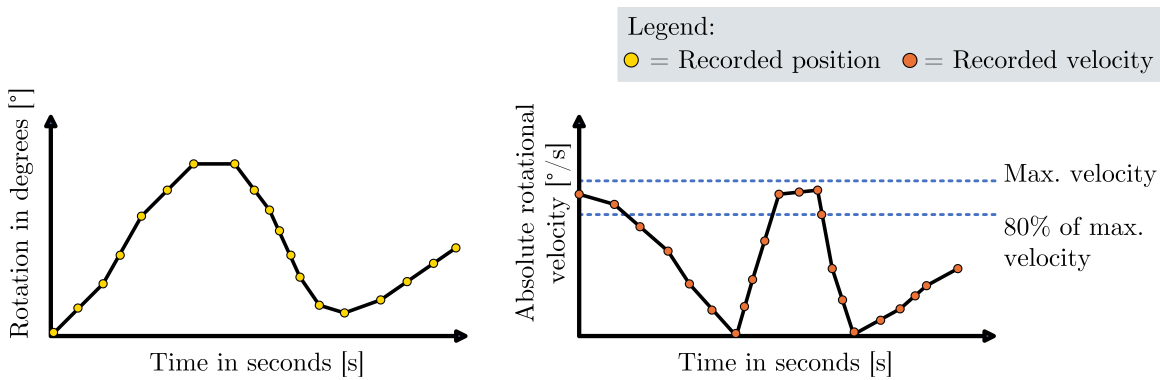


**Figure 3.12:** Calculating velocity from the joint position over time

Additionally, it is feasible to incorporate multiple thresholds and assign linear or exponential weights to them relative to each other. The combined outcome is then utilized to calculate the local rating. For example, if the 80%-threshold is exceeded for 15 seconds and the 90% threshold is exceeded for 5 seconds, the a scalar value is calculated by multiplying the corresponding time and threshold and summing them up. In this case the result is  $80 * 15 + 90 * 5 = 1650$ . This number is then used in the variation approach to calculate the local rating.

It is also possible to determine whether a short but significant peak over the threshold values is more desirable than a constant but small overstep. Figure 3.13 provides a visualization of these two cases.

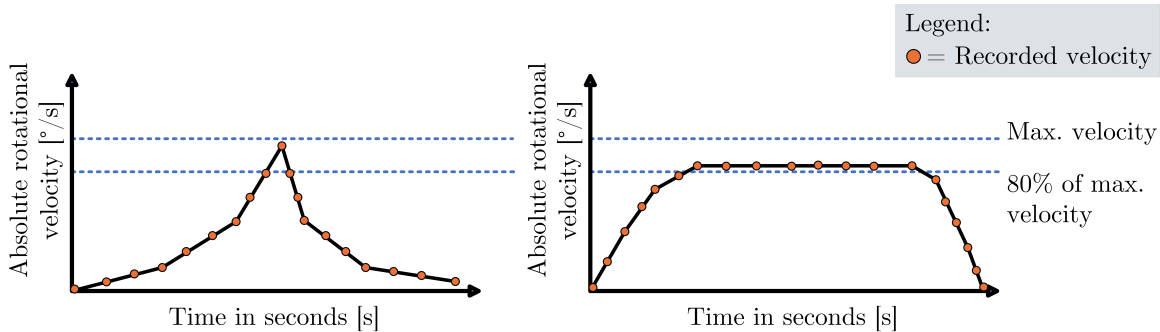


**Figure 3.13:** Overstepping the threshold value

In the former case, where peaks are more desirable, it is sufficient to sum up the area between the velocity and the set threshold. If avoiding peaks is the top priority, all elements in the velocity time-series can be cubed and summed up. By cubing the values, peaks will be exponentially weighted, making them easier to optimize for.

The simplest approach, however, is to square all values and take the sum. This method eliminates the need to define multiple threshold boundaries. Additionally, high peaks will have a greater impact on the resulting value compared to small, constant values, without overshadowing the final result. If the velocity exceeds the maximum velocity, a "No-Go" exception must be triggered, indicating that the movement is not possible. The same rating principle can be applied to acceleration and jerk. Acceleration is obtained by taking the derivative of velocity, while jerk is obtained by taking the second derivative. Individual limits and thresholds can be set to determine the optimality of the robot's movement. If the maximum acceleration or jerk is exceeded, a "No-Go" error is also triggered.

Table 3.4 presents the calculation of a global score, which incorporates a weighting that prioritizes low acceleration in joint 2 and allows for high velocity in all joints. The acceleration in joint 1 and joints 3 to 6 are considered to be of lesser significance. The jerk is completely omitted from the rating in this example. Due to the close-to-optimal acceleration in joint 2 and its high importance value, the overall score of the toolpath with the defined boundary condition is also very high.

**Table 3.4:** Calculation of a score regarding only velocity, acceleration and jerk

Process variables	Local rating	Importance factors	Local score
Velocity in joints 1-6	45	0.1	4.5
Accelerations in joint 2	90	0.8	72
Accelerations in joint 1 and 3-6	15	0.1	1.5
Jerk in joints 1-6	4	0	0
Global Score			78

### 3.4.4 Continuous Energy Usage

Tracking energy consumption can be achieved through a straightforward method of monitoring the velocity and acceleration of individual joints. The energy demand is composed of two components: the rotational movement of a joint at a predetermined speed and the joint's acceleration.

To determine the energy consumed by each joint, the time-series data of joint velocity and acceleration can be multiplied by the average energy consumption value, either in  $\frac{\text{kWh}}{\text{m/sec}}$  or  $\frac{\text{kWh}}{\text{m/sec}^2}$ , associated with that particular joint. By summing up these resultant time-series, an energy consumption profile for each joint can be obtained. The newly obtained time-series represent the energy consumption to move from one pose to another. Aggregating the time-series data from all joints into one time-series provides an overall estimation of the robot's energy consumption. This approach offers a notable advantage in its simplicity. Nevertheless, its primary limitation stems from the potential inaccuracies that may arise when working with an average scaling value. If this value is derived by averaging all possible positions, but only a

limited number of positions are actually traversed by the robot, significant discrepancies can occur. To address these limitations, more advanced approaches are necessary. For instance, the utilization of multi-body simulations (MBS) in CAM software enables a direct analysis of the exact energy requirements for a robot to move between different poses. This method requires precise modeling of weight distribution to achieve accurate outcomes. However, it is important to consider that implementing this approach may require substantial computation and development time.

Another viable option to consider, is the utilization of a ML approach for estimating energy consumption during transitions between discrete poses. By employing a supervised learning technique, where the input data includes the current joint positions and velocities as well as the target pose, an ML model can be trained to predict the energy required for each transition. This approach offers the advantage of leveraging ML algorithms to provide accurate energy consumption estimates in a more efficient manner. However, it is important to note that generating high-quality training data and training the ML model can be a time-intensive processes.

Figure 3.14 illustrates the three aforementioned options along with their key requirements. It is important to note that these examples only give an excerpt on how to get an energy estimation and do not cover all possible solutions to address this problem.

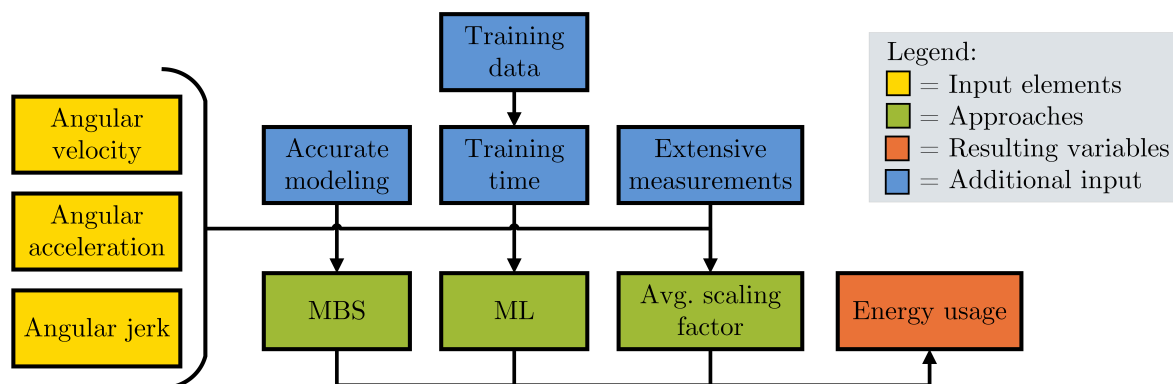


**Figure 3.14:** Exemplary methods for energy usage calculations

Once the time-series data for energy consumption is obtained, it becomes possible to identify peaks and associate them with specific movements. In line with the optimization objective, it is also feasible to establish threshold values, as discussed in Chapter 3.4.3, to optimize for a constant energy consumption.

### 3.4.5 Total Energy Usage

When the aim is to obtain a single scalar value for the total energy consumption, the same procedures outlined in the preceding chapter can be applied, and the values from the time-series can be aggregated through summation.

In situations where the temporal information in energy consumption is considered irrelevant, alternative ML approaches can be employed. For example, Recurrent neural-networks (RNNs) can be utilized, as they have the ability to take an entire time-series as input and generate a scalar value representing the total energy consumption. RNNs excel at capturing dependencies and patterns in sequential data. By training an RNN model using a time-series dataset, it can learn to predict the total energy consumption based on the provided input. However, it is important to note that, like most ML approaches, this method requires substantial effort and time for generating training data and conducting the training process.

In WAAM, it is important to consider the energy consumption associated with the welding process itself. The determination of energy use in welding involves various factors. The G-code, which comprises instructions for the welding process, can provide information on the wire-feed, voltage and the desired power input. By analyzing this code, it becomes possible to estimate the energy consumption during each welding operation. Alternatively, these parameters are often pre-defined as constants on the welding appliance, with the G-code solely specifying the turn-on and turn-off points. Figure 3.15 gives an example on how the turn-on (N10) and turn-off points (N70) can be defined in the G-code.

```
N10 WAAMSTART; - starts welding process
N20 G1 X=-19.988 Y=49.221 Z=56. A=0.0 B=0.0 C=10.0
N30 G1 X=-19.988 Y=46.19 Z=56. A=0.0 B=0.0 C=10.0
N40 G1 X=-19.988 Y=44.371 Z=56. A=0.0 B=0.0 C=10.0
N50 G1 X=-19.988 Y=41.34 Z=56. A=0.0 B=0.0 C=10.0
N60 G1 X=-19.988 Y=39.521 Z=56. A=0.0 B=0.0 C=10.0
N70 WAAMEND; - ends welding process
```

**Figure 3.15:** Turn-on and turn-off points in the G-code used in WAAM

By considering these factors, it is possible to accurately assess the energy usage during welding operations. However, this specific part of the total energy consumption cannot be optimized by defining the boundary conditions of redundant DoFs. The energy required for the welding process is solely defined by the welding parameters and the final part geometry.

## 3.5 Reach, Singularities and Torch Orientation

The following discusses the robot poses with respect to reach and alignment, singularity avoidance, and torch orientation. These factors are essential in ensuring successful and efficient robotic operations, especially in WAAM.

### 3.5.1 Reach and Alignment

As mentioned in Chapter 3.2.2, the analysis of the reachability index can be conducted in various formats. The first format involves a simple analysis to determine if all the points that the robot needs to traverse, lie within its work volume without any self-collisions or exceeding the soft and hard joint limits. This aspect is closely related to the joint limits, as discussed in Chapter 3.4.2. Additionally, it is necessary to analyze that there are no collisions between the robot and the workpiece. If all these conditions are met, a binary index can be used to indicate the feasibility and safety of executing the program. However, this index cannot be used for optimizing the robot's movement, as the parameters influencing this index are mostly defined by the G-Code.

When utilizing a robotic system with a specific tool, such as a milling spindle or a welding torch for WAAM, it is crucial to consider the boundary conditions and limits associated with that tool. Figure 3.16 illustrates a case where the rotation around the Z-axis of the welding torch can be manually defined. Each position leads to different strains on the wire-feed system and power-cables.

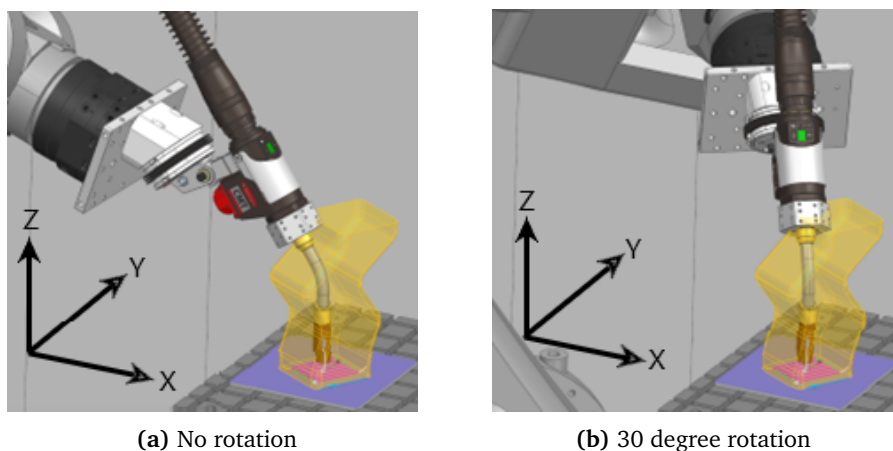


**Figure 3.16:** Rotation around the C-axis of a welding torch

In most cases, the spindle and welding torch come with cables that provide power from an external power supply. These cables have an optimal orientation where bending and wear are minimized. By positioning the cables in an optimal orientation, the robotic system can operate efficiently and effectively without any interference or limitations due to cable

movement, potential damage, or excessive bending or twisting. To assess the optimality of the robot's cable pose, it is important to consider additional information. In certain cases, it is preferable to route the cables in a specific alignment along a spatial vector, allowing for parallel translation or movement in the direction of that vector. In this case, the angle between the planes of the robot's base coordinate system and the optimal translation vector remains constant. Figure 3.17a provides a visual representation of this example. The wire, shown in red, has an optimal alignment along a vector where the least amount of strain is present. Any position along that vector where the cable transitions to the welding torch tangentially is considered optimal. It is worth noting that this vector can be translated parallel in space while still maintaining its optimal status.

In other scenarios, it is more optimal to route the cables towards a specific point in space, such as a mounting point on a wall or ceiling. Figure 3.17b illustrates an example where the optimal alignment of a milling spindle is directed towards a designated point where the cables originate. In this case, any position is considered optimal as long as the extended spindle vector aligns with the vanishing point.

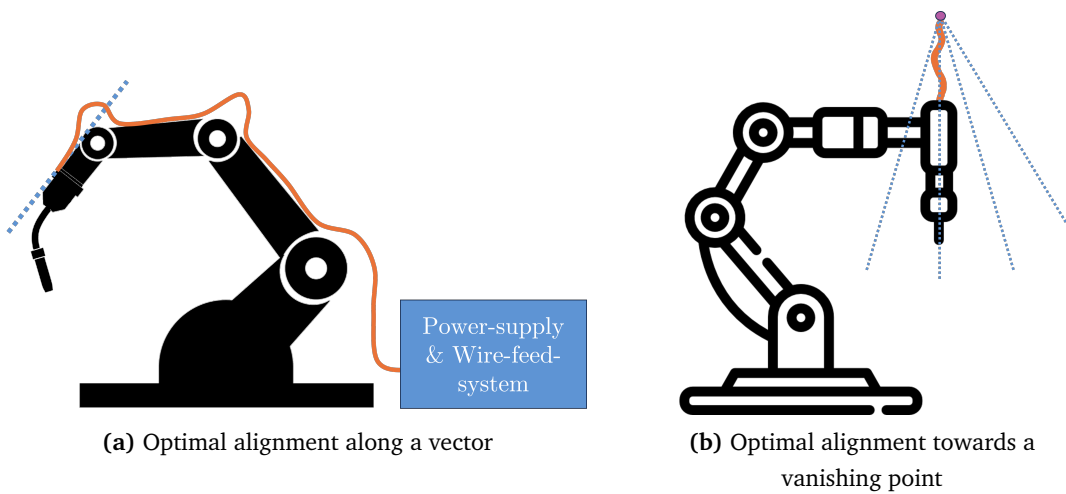


**Figure 3.17:** Two examples for optimal alignments along a vector in 2D

To minimize the deviation from the optimal vector or vanishing point, the redundant DoFs can be utilized. One approach is to analyze the deviation and track it over time, creating a time-series. Each element in this time-series can be squared or cubed, depending on the weight assigned to small and constant deviations versus large but short offsets. The time-series is then summed up to form a scalar value, which can be used to calculate the local score through the variation method. Table 3.5 illustrates an example of how the scalar value is calculated. It is evident that when cubing the time-series, more importance is placed on the larger deviations rather than small deviations. The deviation in time-step 6 is making up approximately 80% of the summed value when squared and 94% when cubed.

**Table 3.5:** From time-series of the deviation vector to scalar value

Time-step:	1	2	3	4	5	6	7	8	
Deviation:	1°	2°	2°	2°	3°	10°	0°	2°	
Squared:	1	4	4	4	9	100	0	4	Sum: 126
Cubed:	1	8	8	8	27	1000	0	8	Sum: 1060

### 3.5.2 Singularities

In Chapter 2.4.1, the concept of singularities in robotic systems is discussed. Singularities occur when the robot's joints align in a way that limits its motion by reducing one or more DoF. To avoid singularities, it is important to optimize the boundary conditions in the redundant DoF. The singularity analysis, as described in Table 3.1, can be represented either as a scalar value or as a time-series that classifies each position based on its proximity to a singularity.

The scalar value can represent the overall smallest eigenvalue of every Jacobi matrix. For this, every pose needs to be analyzed. After calculating the Jacobi matrix, all eigenvalues encountered are examined, and only the smallest one is recorded and used to calculate the local score. This approach allows for an analysis of the overall toolpath rather than specific poses.

Alternatively, a time-series can be used where the determinant, not the eigenvalues, is recorded and stored. By analyzing this time-series, it becomes possible to directly associate the robot's movements with its proximity to a singularity. This enables a more precise understanding of where the robot's motions are close to a singularity, allowing for subsequent optimizations. To transform the time-series into a scalar value, the same threshold method described in Chapter 3.4.3 can be applied.

### 3.5.3 Torch Orientation in WAAM

The torch orientation variable in WAAM, similar to the cable routing orientation variable, analyzes the angle at which the welding torch is positioned during the process. This variable is specific to WAAM and ensures that the torch is at the optimal angle for welding. Achieving material deposition in the direction of gravity is crucial for obtaining the best results. The orientation of the TCP, which represents the welding torch tip, can be determined either through the forward kinematics approach or by extracting it directly from the G-code.

In both the forward kinematics approach and the G-code, the rotation is described as the rotation of the A-, B-, and C-axes. However, the necessary information for torch orientation is simply the angle between the tilted Z-axis of the tool and the vector of gravity. To obtain this information, a dot product is performed between the rotation matrix and the Z-axis of the base coordinate system. This yields a vector corresponding to the tilted Z-axis of the

tool. The enclosed angle can then be calculated using the scalar product. This step assumes that the defined base coordinate system is oriented in a way that aligns the Z-axis parallel to the gravity vector. Figure 3.18 gives a visual example in 2D on how the Z-axis of the tool is deviating from the vector of gravity.

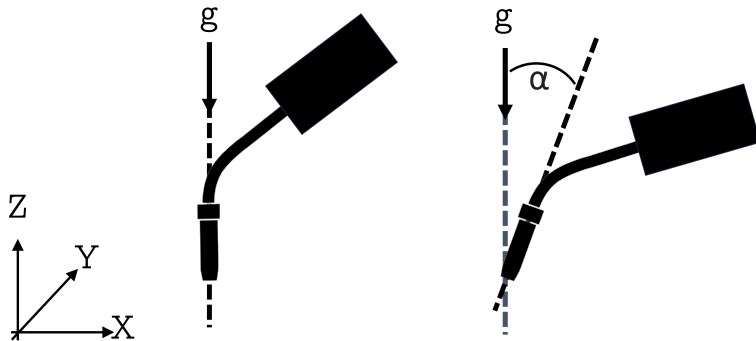


**Figure 3.18:** Example of optimal and non-optimal tilt in the welding torch

To quantify the torch orientation variable, it is recorded in a time-series format. To obtain a scalar value for this process variable, all the values can be squared, cubed, or subjected to other mathematical operations, and then summed up. This process is similar to the one described in Chapter 3.5.1 for the cable routing orientation variable. It is important to note that the tool orientation variable can be in direct conflict with the alignment variable. This conflict is particularly noticeable in cases where the optimal alignment vector does not correspond with the optimal tool orientation vector. In such cases, it is crucial to have knowledge of the parameters of the manufacturing system and adjust the importance factors of the process variables accordingly.

## 3.6 Summary for Boundary Condition Evaluation

Figure 3.19 gives a summary and visual representation, in form of a flowchart, on how a toolpath with defined boundary conditions is evaluated by calculating the individual local scores for the process variables that can be influenced by the redundant DoFs.

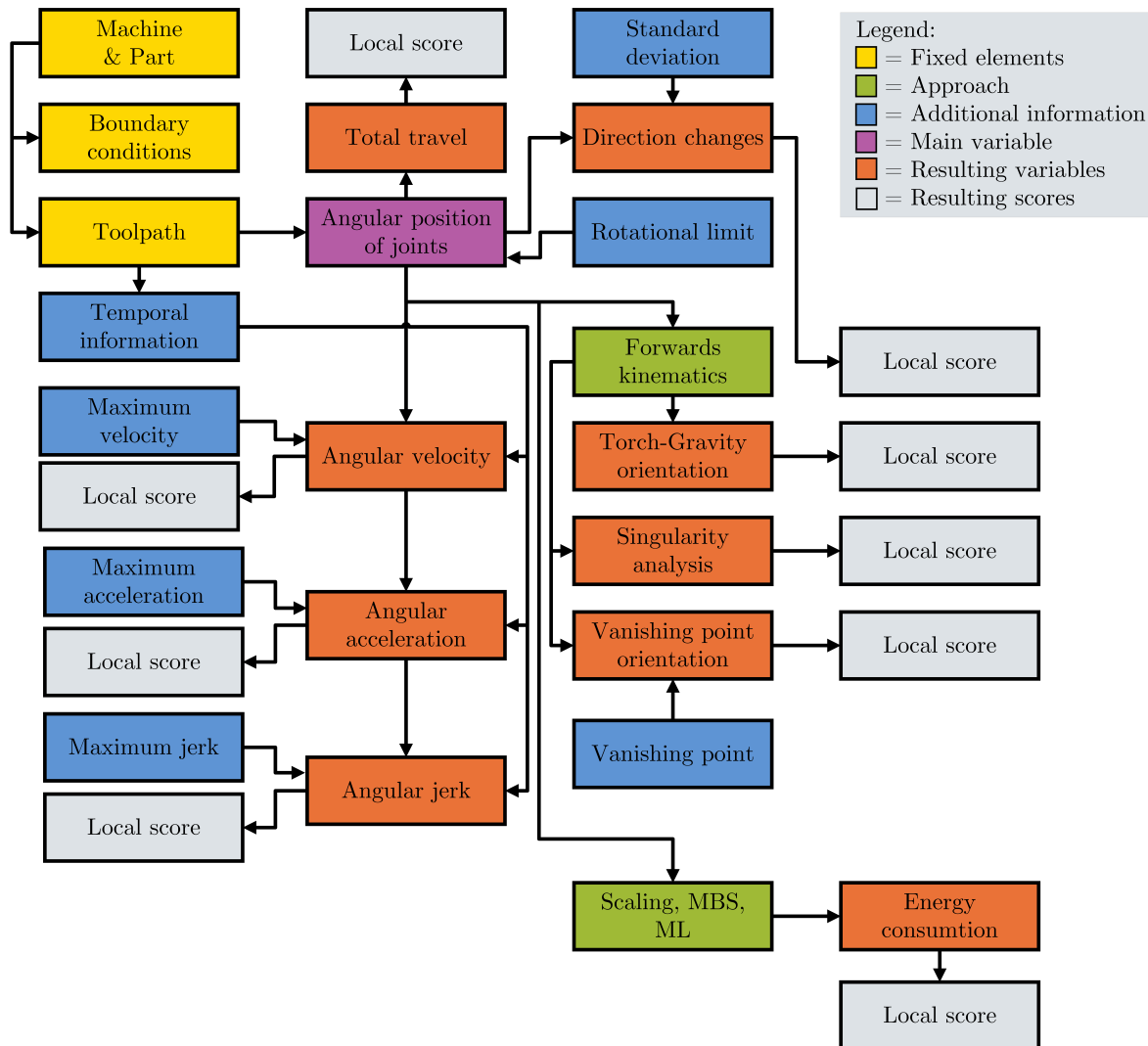
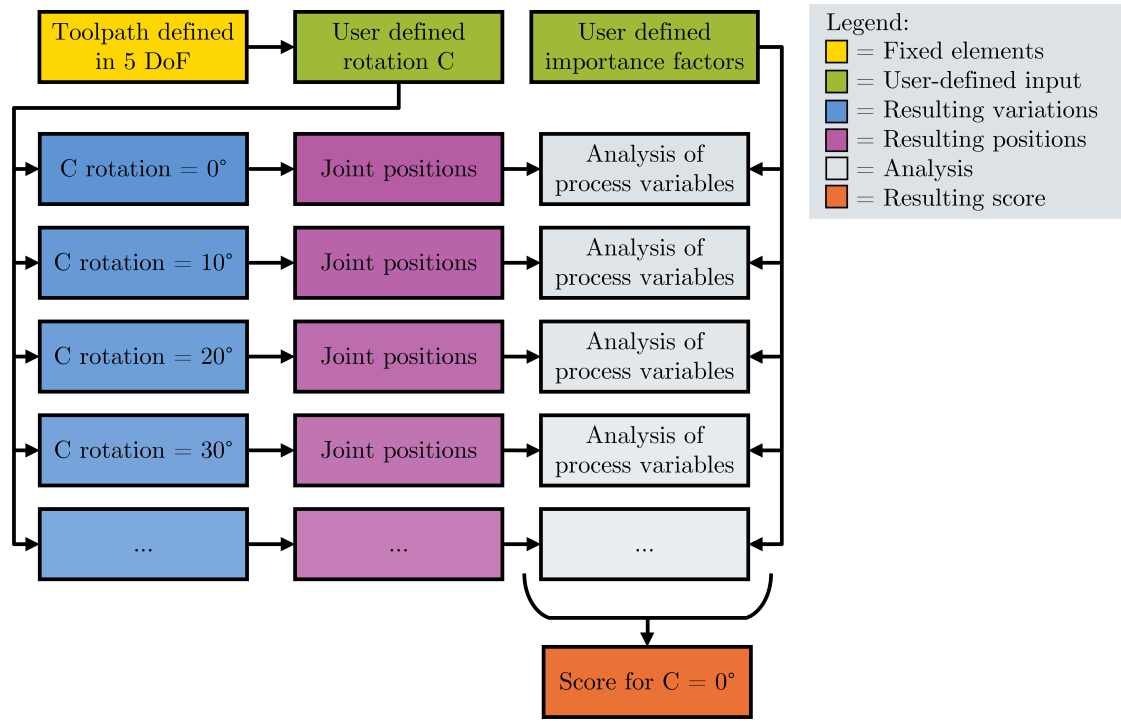


Figure 3.19: Evaluation of a toolpath

It is important to note that for a local score calculation the user defined importance values need to be multiplied with the local rating that results from the numerical values of the process variables. The local scores are then summed up to create the global score.

Figure 3.20 illustrates how a boundary condition for a toolpath can be evaluated with the mentioned variation method (see Chapter 3.3.2). In this case, the toolpath is defined using only 5 DoFs, including X-, Y- and Z-coordinates as well as the rotation around the X- and Y-Axis. However, the C-axis (rotation around the Z-Axis), which is the axis of symmetry for the tool, is not defined and must be specified manually. Once this boundary condition is estab-

lished, the joint positions are analyzed and individual variables, such as direction changes, can be extracted. In this example, the objective is to assess the optimality of a rotation angle of zero degrees of the C-axis. To calculate a local score, additional variations of the rotation around the C-Axis are analyzed. With the help of user-defined weights, the local ratings are weighted and summed up to form the global score for the boundary condition (see Chapter 3.3).



**Figure 3.20:** Process of evaluating a defined boundary condition

## 3.7 General Methodology for Process Optimization

So far only the analysis of a toolpath with set boundary conditions is discussed. In the following sections, two methods for optimizing boundary conditions towards a specific goal is presented. The main difference between these two methods lies in the different incorporation of a CAM software.

It is important to note that optimizing certain process variables may have a direct negative impact on others. For example, optimizing the tools orientation towards a specific vanishing point can significantly increase the total number of direction changes in the joints. Therefore, the user must be aware of these cross-influences and adjust the weights accordingly.

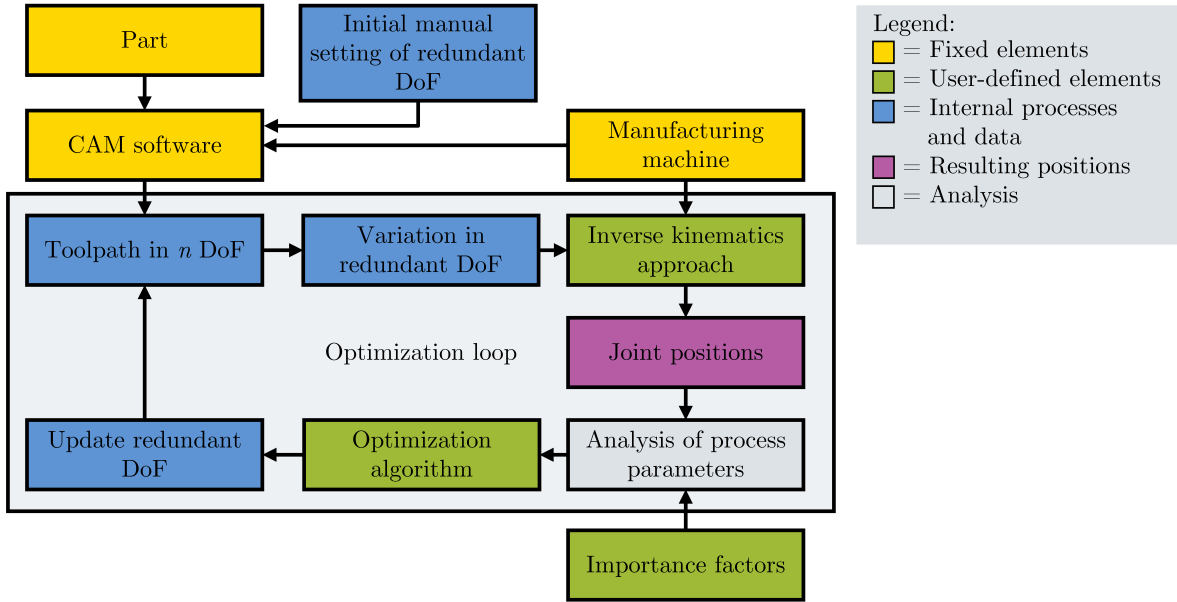
### 3.7.1 Optimization Without CAM Software in the Loop

Figure 3.21 illustrates the process of optimizing the redundant DoFs based on a predefined goal determined by weighing the process variables. In this method, the part and the manufacturing machine are fixed components that are loaded into the CAM software. Before generating a toolpath, the redundant DoFs must be set manually. These constraints can be set based on prior experience, as long as they do not lead to any "No-Go" exceptions caused by collisions or exceeding the joint limits.

When the toolpath is generated, it is defined in all available DoFs of the manufacturing machine. This information is now in form of a G-code. To evaluate the set boundary conditions, the information from the G-code is extracted and the redundant DoFs are varied, resulting in multiple toolpaths with multiple boundary conditions. In some cases, this variation simply involves varying the rotation around the Z-Axis, while keeping all the X-, Y- and Z-coordinates defined in the G-code, unchanged. In other cases, the redundant DoFs involve the rotation and tilt of a rotary-tilt table. In such situations, every single coordinate in the G-code needs to be rotated around the tilting-axes of the rotary-tilt table. After obtaining the multiple toolpaths, each one is subjected to an inverse kinematics algorithm. This algorithm utilizes the machine's parameters, for example, arm length and joint sequence, to calculate the joint positions to reach every point in the different G-Codes. From these values, the score of the originally set boundary condition can be determined. By utilizing a external inverse kinematics approach, the CAM software is not part of the optimization loop. This approach give the user to work with any CAM software.

Following the score calculation, an optimization algorithm (see Chapter 2.3) is employed to generate a new boundary condition for the redundant DoFs. This cycle of optimization continues either for a predetermined number of iterations or a specified duration.

Alternatively, a desired minimal score can be defined as the target, that the toolpath needs to achieve. Once the most optimal or close-to-optimal boundary condition is found, it is used as input for the CAM software to validate that no collisions or other exceptions are triggered. After this validation process, the G-code can be utilized in production.



**Figure 3.21:** Schematic process of optimization without CAM software in the loop

In this method, the optimization of boundary conditions occurs externally to the CAM software. The CAM software is solely utilized for generating the initial toolpath and validating the most optimal boundary condition that is returned by the optimization algorithm. The inverse kinematics process is performed outside of the CAM software and can be implemented in various programming languages such as Python or C++. The same is applicable to the optimization algorithm.

The advantage of this approach is that the external algorithms are independent and can be easily exchanged or modified. It does not necessitate in-depth knowledge or access to the source code of the CAM software. Therefore, any CAM software can be utilized with this approach, providing flexibility and compatibility.

However, it is important to note that one drawback of this approach is that the complete closure of the loop can only be achieved if the most optimal boundary condition can be automatically fed back to the CAM software for the final validation. If there is no application programming interface (API) available or accessible for the CAM software, this step may need to be performed manually. This manual intervention can introduce additional time and effort into the optimization process.

Depending on the chosen optimization algorithm, it may be necessary to calculate multiple scores for multiple boundary conditions before generating a new suggestion. In this scenario, the variations in the redundant DoFs can be utilized to calculate multiple scores relative to each other. These scores can then be used as input for the optimization algorithm, allowing

for a more comprehensive evaluation and selection of the most optimal boundary condition. By considering multiple scores, the algorithm can effectively explore different possibilities and make informed suggestions for improving the boundary conditions.

Another drawback of this approach, is that for the variation of the redundant DoFs the G-Code file is utilized. For that a dedicated software-program is necessary that can read the G-Code and adapt the individual coordinates accordingly. Another level of complexity can occur, if the G-Code is utilizing non-standard or user-defined commands. Many edge cases need to be considered before such a program is deemed save for production.

Figure 3.22 illustrates the process of varying a simple toolpath. In this specific example, the toolpath is defined in six DoFs, with the redundant DoF being the rotation around the Z-axis. Initially, the toolpath is set at its original configuration with C = 0.0°. To explore different possibilities, three variations of the toolpath are created by incrementing the rotation by five degrees for each variation. These variations allow for an examination of the impact of different orientations on the overall process. By systematically adjusting the rotation, the algorithm can evaluate the performance of each variation and suggest even better values.

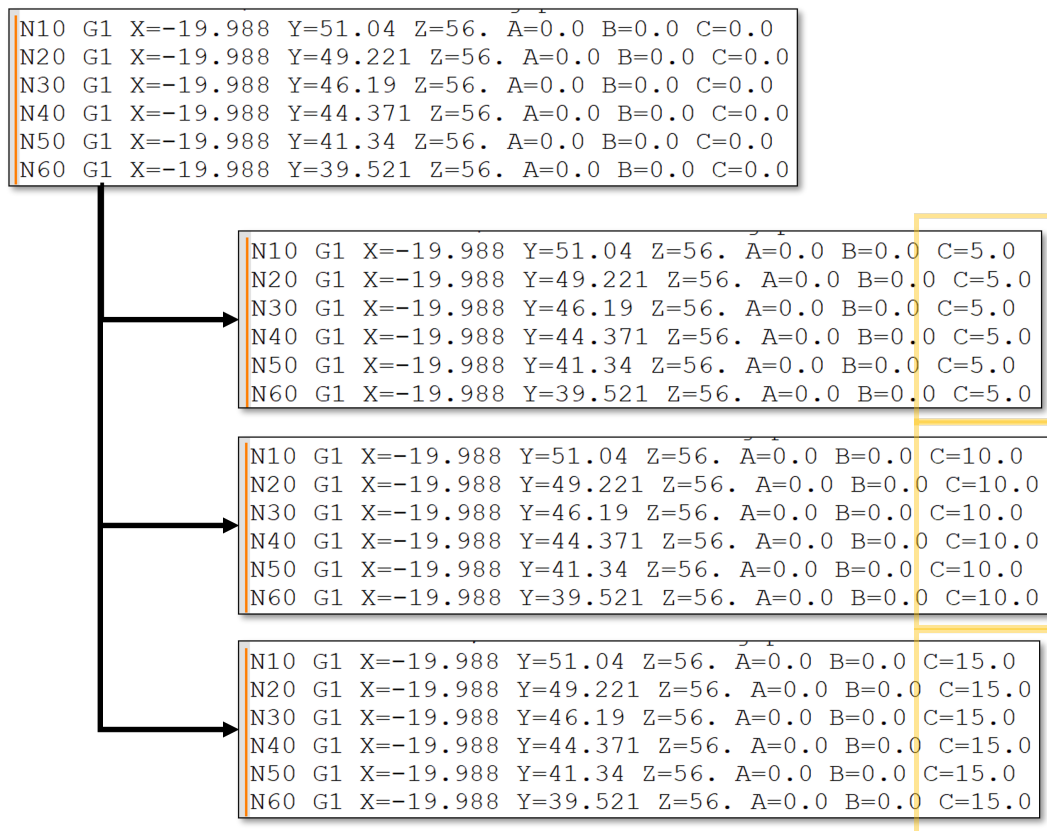


**Figure 3.22:** Variation of the redundant DoF in the G-code

### 3.7.2 Optimization Loop With CAM Software in the Loop

The previously mentioned optimization approach in Chapter 3.7.1 describes a process that does not involve a CAM software within the optimization loop. However, another method can be employed that directly incorporates a CAM software into the optimization process and thus allows for seamless integration. By directly including the CAM software, the optimization loop becomes more tightly knit, enabling seamless feedback and iteration between the toolpath generation and the optimization of constraints for the redundant DoFs. This approach can significantly enhance the overall optimization process and significantly improves the quality and efficiency of the final toolpath.

In this method, the CAM software plays a crucial role in the optimization process. It first generates the initial toolpath by automatically setting the redundant DoF based on the given part geometry and machine configuration. Unlike traditional approaches, the CAM software does not export G-code but utilizes its internal resources and algorithms to calculate the joint positions via a internal inverse kinematics algorithm. The optimization process is performed iteratively, involving multiple variations in the redundant DoFs. Each variation generates a different toolpath, which in turn results in different joint positions of the manufacturing machine. The process variables are then analyzed to calculate a score that represents the quality of the toolpath. Figure 3.23 shows the schematic representation of the optimization loop.

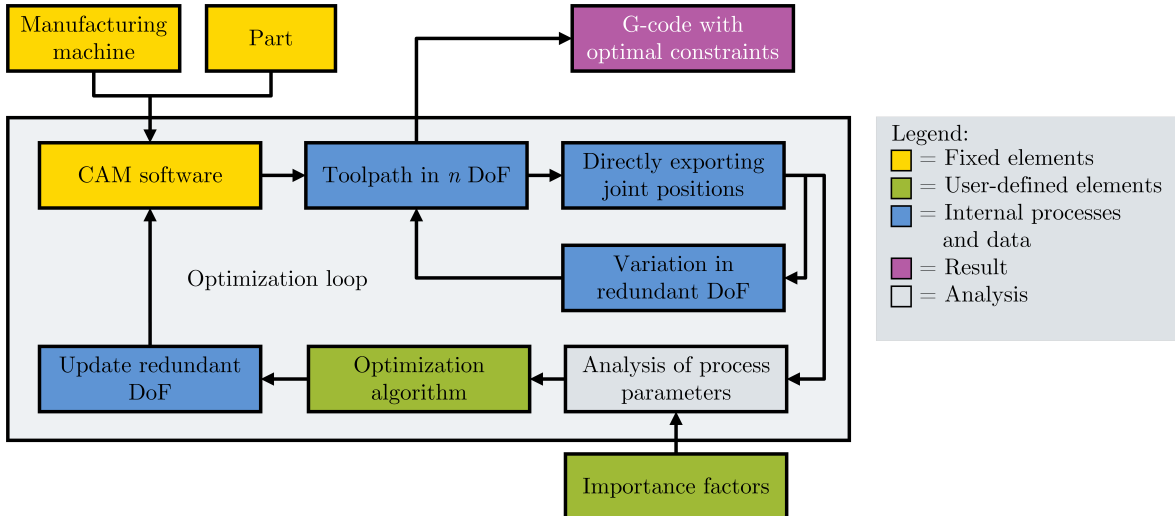


**Figure 3.23:** Schematic process of optimization with CAM software in the loop

The optimization algorithm, seamlessly integrated within the CAM software, utilizes the obtained scores to propose a new setting for the redundant DoFs. This new setting aims to improve the toolpath and optimize the process variables further. The iteration continues until a defined score or a predetermined number of iterations is reached, indicating that the optimization loop has converged. Once the optimization loop is terminated, the CAM software exports the G-code with the best-found boundary conditions, representing the opti-

mized toolpath.

The advantage of this approach lies in leveraging the CAM software's specialized capabilities and features for toolpath generation and optimization. By directly integrating with the software, the optimization process becomes more efficient and streamlined, eliminating the need for external scripts or algorithms.

However, a significant disadvantage of this method is the requirement for access to the source code of the CAM software to add the optimization algorithm and the specific post-processor that calculates the joint positions. Adding the necessary features and functionalities necessitates modifying the software, which may not be feasible or practical in all situations. For that reason, this approach has to be implemented by the provider of the CAM software.



# Chapter 4

## Implementation and Validation

The first step in the validation process involves selecting a manufacturing machine and constructing a fundamental model in the programming language *Python*. In this case, a simple articulated robot is chosen as the manufacturing machine. The programmed model captures the kinematics and dynamics of the modeled industrial robot. It allows for a in depth analysis of its movement and behavior as well as the optimization of its performance.

To test the method in a straightforward scenario, initial tests are conducted on a 6-DoF model with a 5-DoF toolpath. The sixth DoF, which represents rotation around the Z-axis, is freely defined and utilized for optimization purposes. The validation consists of traversing a predefined toolpath and analyzing the individual joint positions over time. Once this simple model is successfully validated, an additional redundant DoF is introduced by incorporating the tilt of a rotary-tilt table.

After establishing the basic model, an optimization algorithm is implemented to determine the optimal values for each redundant DoF in order to optimize the user-selected process variables. This optimization algorithm takes into consideration the specific constraints and objectives of the industrial robot, such as minimizing direction changes or joint accelerations.

The modeled robot, the optimization algorithm as well as the visualizations and plots are constructed using *Python 3.11* with the help of the libraries *visual\_kinematics*, *matplotlib* and *numpy*.

### 4.1 Simple Implementation

#### 4.1.1 Modeling a 6-DoF Robot

To test the proposed method, a simplified articulated industrial robot with 6-DoF is used as a model. A visual representation of this robot modeled in *Python* can be seen in Figure 4.2. The Denavit-Hartenberg (DH) parameters for this robot are provided in Table 4.1. These parameters are essential for describing the geometry and kinematics of the robotic arm. They

define the relationship between adjacent links in the kinematic chain of the robot. The parameter "a" represents the link lengths between adjacent joints. The rotations around the Z-axis between adjacent joints is represented by the parameter "alpha". The parameter "d" represents the link offsets along the Z-axis between adjacent joints. The units of "a" and "d" are in millimeters, while the rotation "alpha" is defined in degrees.

**Table 4.1:** DH-parameters for the modeled robot

Parameters	Values
a in [mm]	[200, 800, 150, 0, 0, 0]
alpha in [°]	[90, 0, 90, -90, 90, 0]
d in [mm]	[400 0, 0, 600, 0, 200]

The schematic of the modeled robot can be seen in Figure 4.1. In this particular configuration, all joints are in their initial positions with no rotation applied.

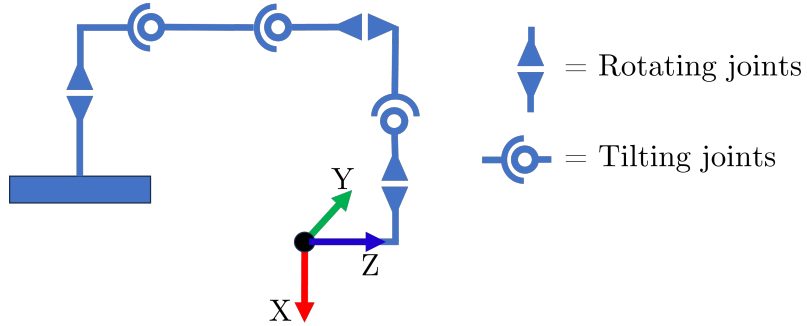


**Figure 4.1:** Schematics of the modeled robot

Figure 4.2 depicts the modeled robot using *Python* in combination with the *matplotlib* library. The joint positions, in degrees, are as follows: [0, 135, -45, 0, 0, 0], corresponding to joints 1 to 6, respectively. The black coordinate system represents the world coordinate system, while the colored coordinate system originating from the TCP and represents the TCP coordinate system. The first link of the robot, originating from the point X=0, Y=0, Z=0 in the world coordinate system, is displayed in green. The individual joints are represented by red dots. The end-mill is marked as a orange dot.

The next step is to model a spindle that is attached to the flange, which is at the end of the last link, and apply a transformation matrix from the flange to the tip of the end-mill. The length of the spindle is set to 300 mm, and the length of the end-mill is set to 80 mm. The transformation matrix applies a rotation and shift from the coordinate system at the flange, which is determined by the rotation "alpha" (see Figure 4.1), to the tip of the end-mill. This establishes a tool coordinate system at the correct position with the desired orientation.

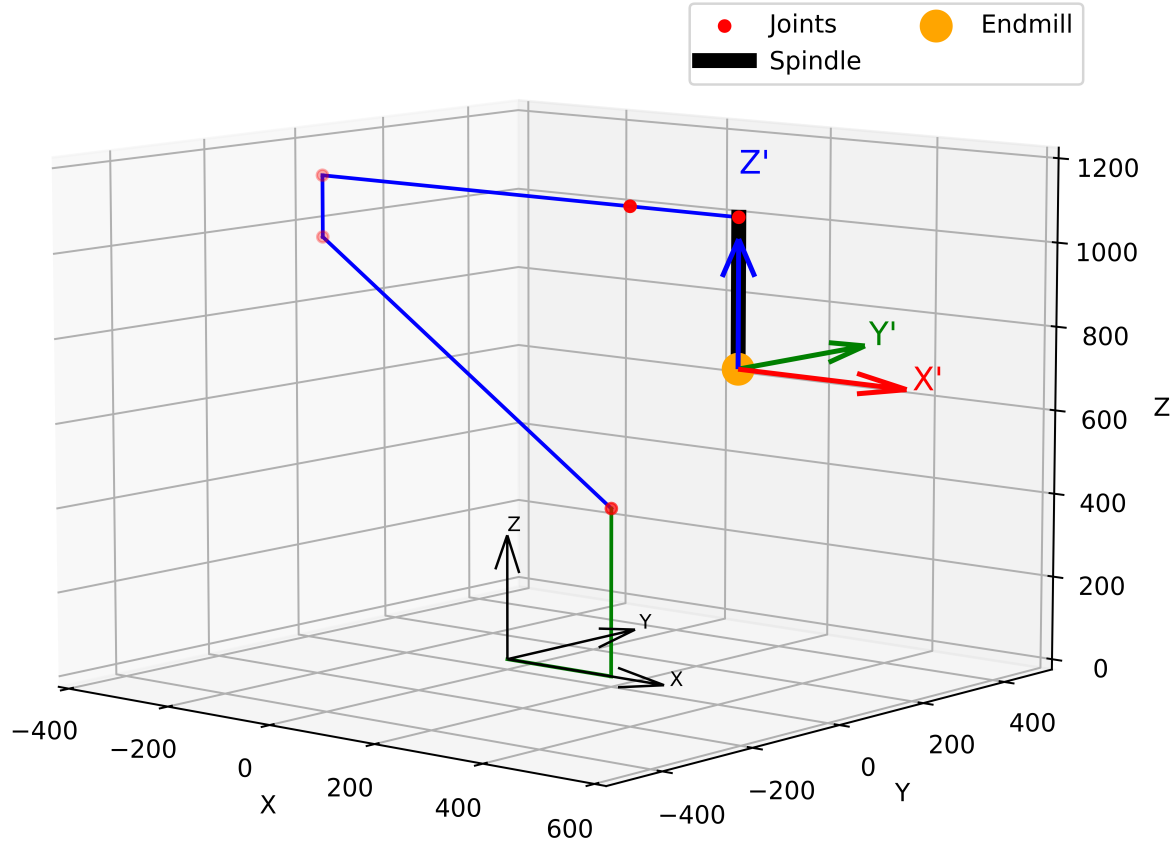


**Figure 4.2:** Visualization of the modeled robot in Python

#### 4.1.2 Modeling a Basic Toolpath

Before analyzing the process variables of interest, it is necessary to define a toolpath for the TCP to follow. For that case, three exemplary toolpaths are presented, each consisting of 3000 points. To validate the proposed method more broadly, each of those manually created toolpaths has individual characteristics. It should be noted that in the first analysis, the redundant DoF is the rotation around the Z-axis. This rotation will be adjusted to determine the optimal value for the desired outcome. A and B are held at 0°.

The first toolpath, depicted in Figure 4.3, represents a converging spiral that is shifting to the side. Figure 4.4 illustrates the second path which is a converging-diverging infinity-loop, and Figure 4.5 displays a forward-moving sinusoidal curve that is following a parabolic profile. Each path consists out of 3000 coordinates.

Figure 4.6 illustrates the robot and Toolpath 1 at the final position of the toolpath. The origin of the toolpath is shifted by  $X=+800$  and  $Z=+400$  relative to the world coordinate system. No rotations are applied around the X-, Y-, and Z-axes, resulting in A, B, and C being zero. As a result, the coordinate axes of the TCP are parallel to the axes of the world coordinate system.

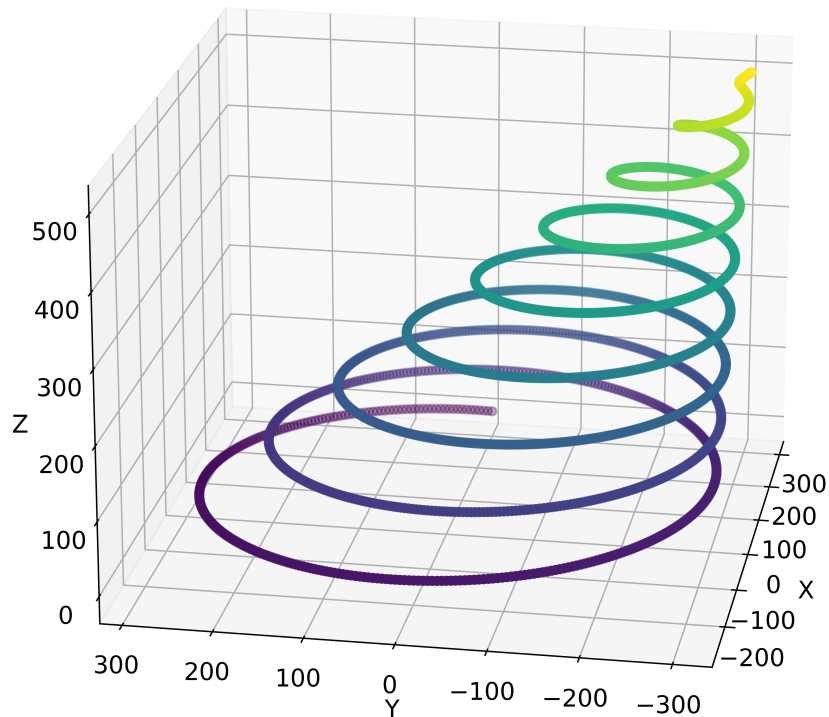


**Figure 4.3:** Toolpath 1: Converging spiral

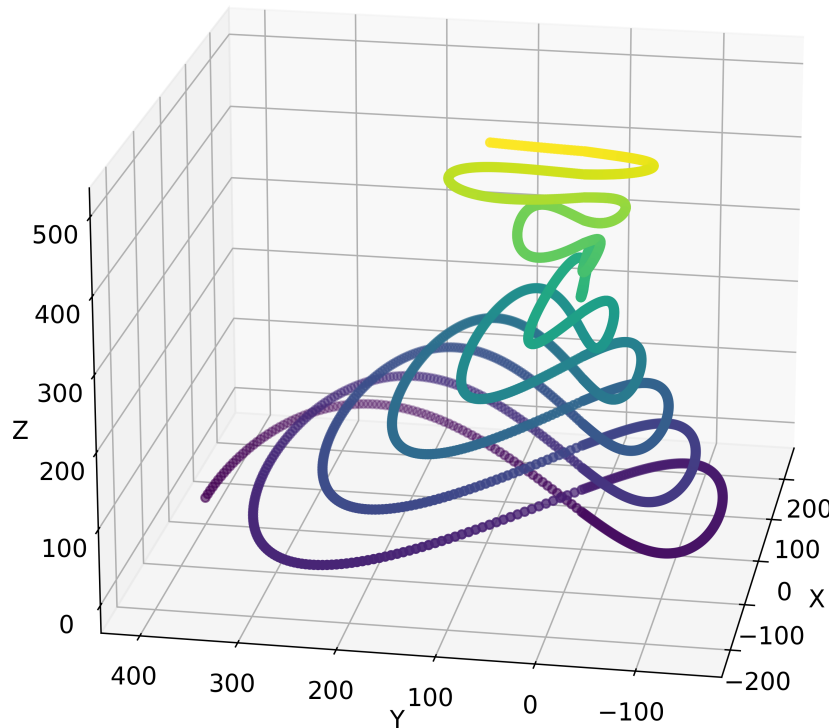


**Figure 4.4:** Toolpath 2: Converging infinity loop

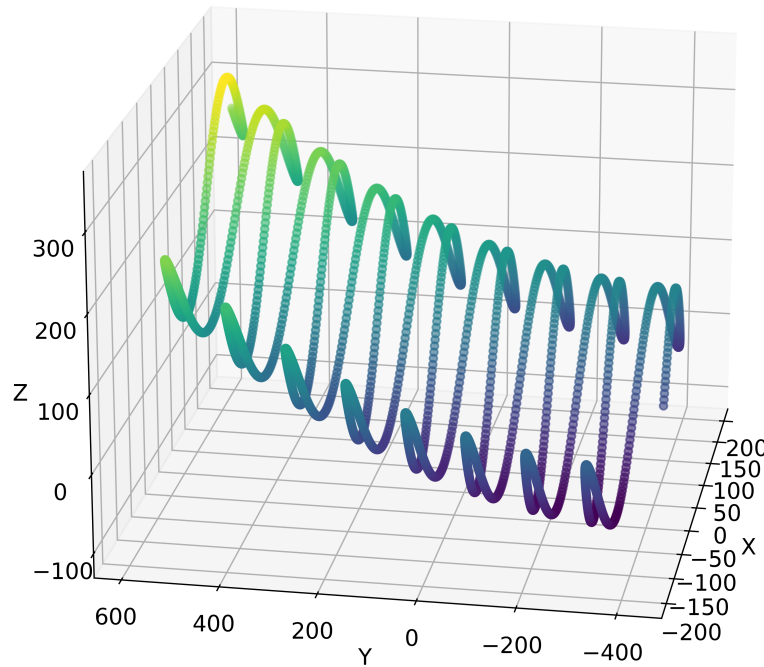


**Figure 4.5:** Toolpath 3: Forward moving pendulum oscillation

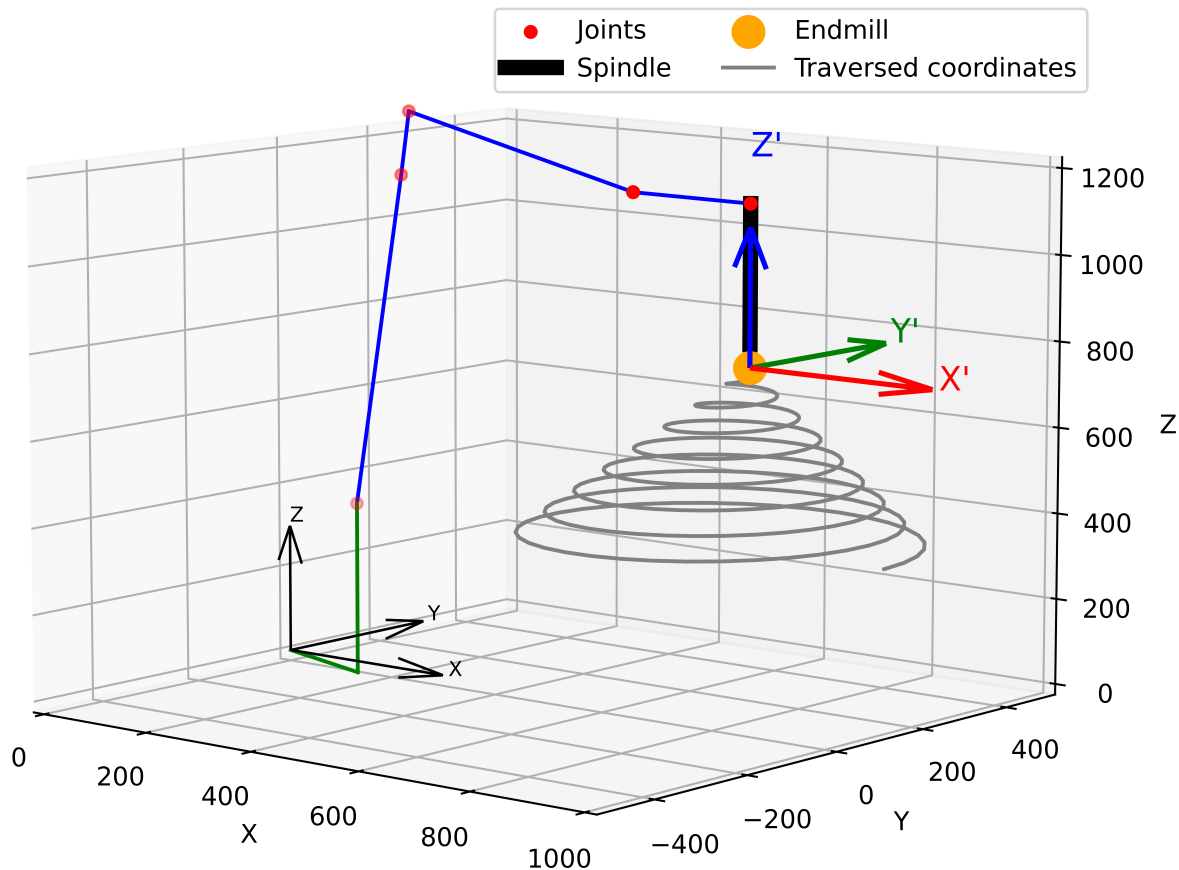


**Figure 4.6:** Traversing toolpath 1 with the modeled robot

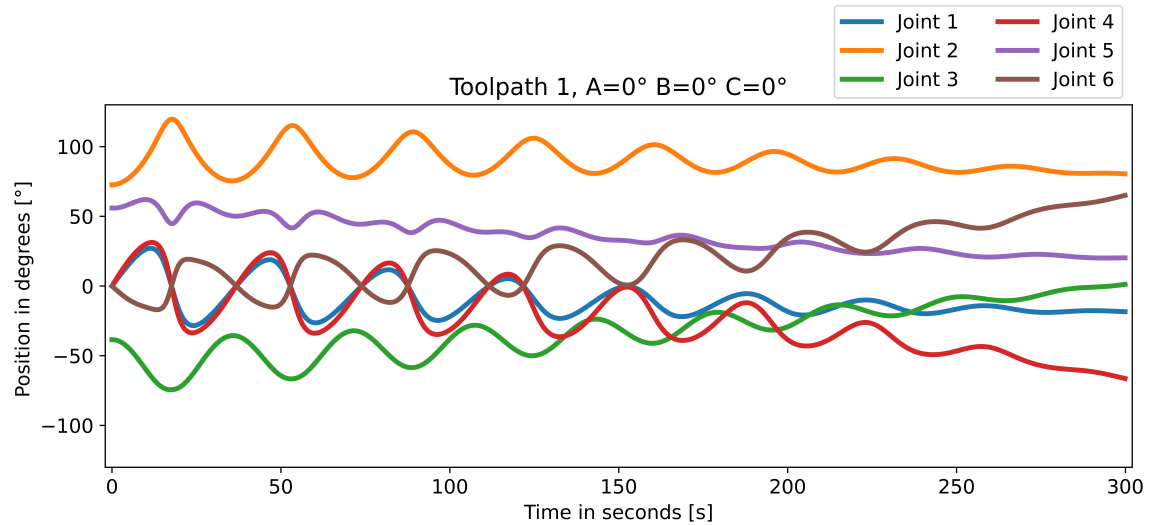
By utilizing the inverse kinematics algorithm from the Python library *visual\_kinematics*, the

joint angles for each coordinate can be computed. To achieve this, the rotations A, B, and C need to be defined. The outcome is a time-series that contains the corresponding joint positions. For all tests, all coordinates must be traversed in equidistant time steps. With this information, it becomes possible to calculate the velocity and other related variables. By transforming all the data from the time-series into scalar values and calculating the local rating, the local and global scores can be determined.

## 4.2 Testing and Validation

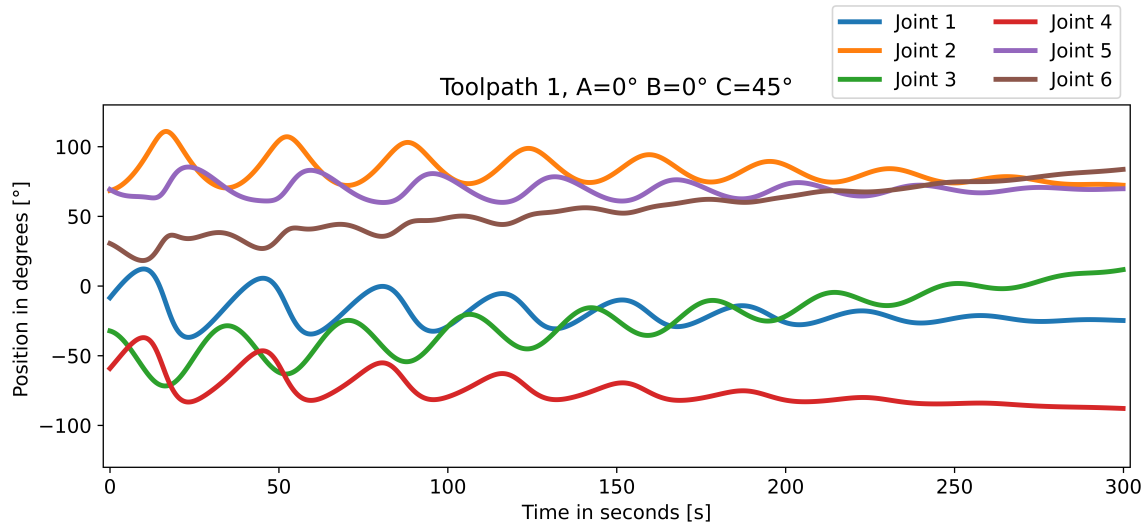
### 4.2.1 Toolpath Evaluation With one Redundant DoF

As discussed in Chapter 4.1.2, the toolpath remains constant with respect to the X-, Y-, and Z-coordinates. The fixed boundary conditions for the robot are that there are no rotations around the X and Y axes, resulting in A and B both being equal to zero. This condition is fixed for the entire toolpath. The user has the ability to set the DoF for the rotation around the Z-axis, which is the redundant DoF. Figure 4.7 displays the variation of each joint over time for toolpath 1. In this specific case, the rotations A, B, and C are all set to 0. The entire toolpath is traversed in 300 seconds.



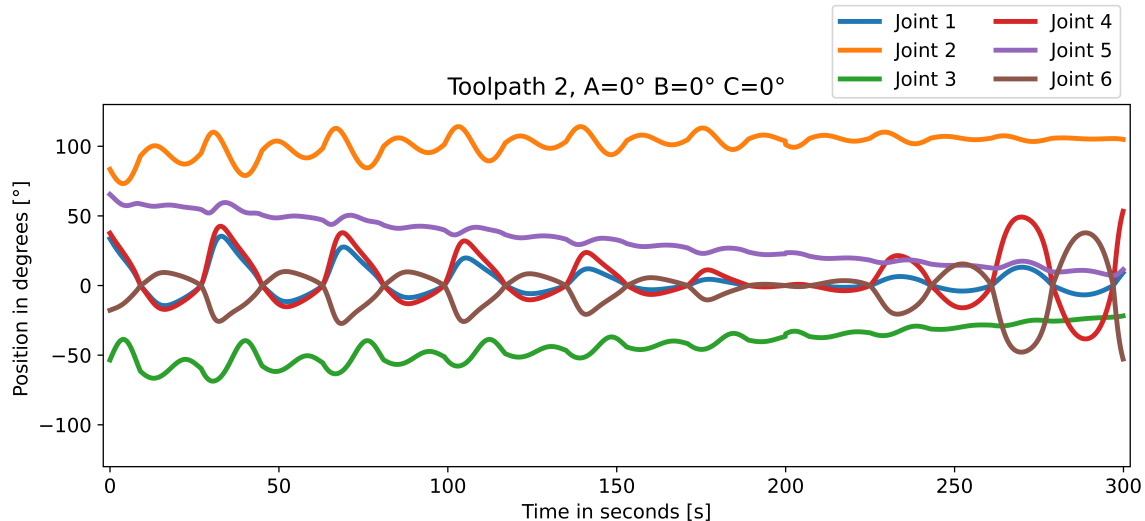
**Figure 4.7:** Visualization of the joint positions over time for toolpath 1 with  $C=0^\circ$

Figure 4.8 depicts the joint positions for all six joints over time for the same toolpath (toolpath 1) with a  $45^\circ$  rotation around the Z-axis ( $C = 45^\circ$ ). It is noticeable that joint 5 and joint 6 have undergone changes in their respective ranges and characteristics. Joint 1 and joint 3 have very similar trajectories in both cases. Additionally, joint 6 exhibits significantly smaller amplitudes at the beginning of the toolpath compared to the case with no rotation ( $C = 0^\circ$ ).



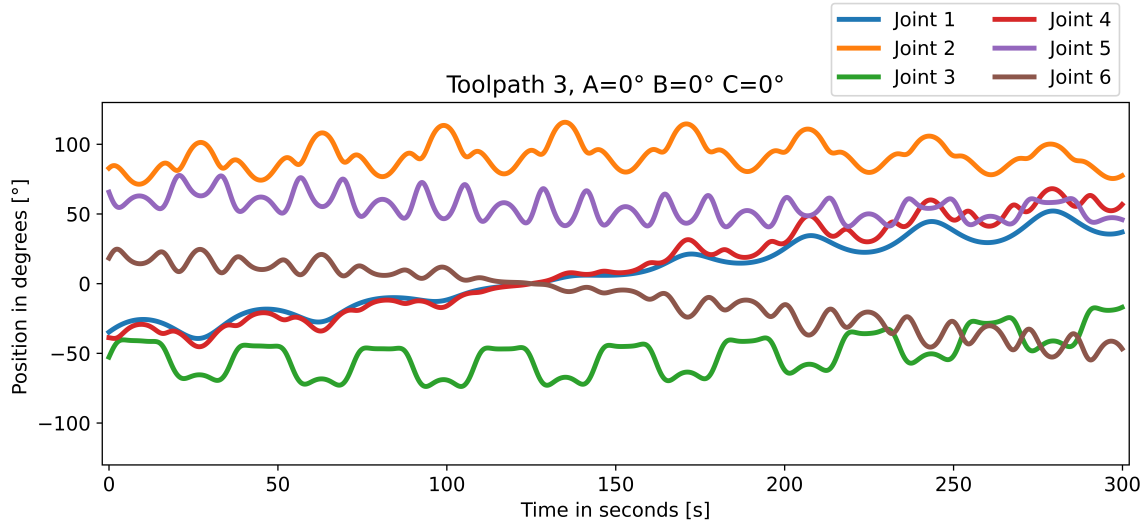
**Figure 4.8:** Visualization of the joint positions over time for toolpath 1 with C=45°

Figure 4.9 illustrates the variations in each joint over time for toolpath 2 without any rotation (A=B=C=0°). Unlike toolpath 1, the amplitudes in joint 4 and joint 1 noticeably decrease and then increase. This observation aligns with the distinct characteristics of different toolpaths.



**Figure 4.9:** Visualization of the joint positions over time for toolpath 2

Figure 4.10 visualizes the variations in each joint over time for toolpath 3. Again, the TCP coordinate system is held parallel to the world coordinate system resulting in A, B and C being zero. A clear oscillation over time is visible in every joint.



**Figure 4.10:** Visualization of the joint positions over time for toolpath 3

#### 4.2.2 Extracting Process Variables

The next step involves selecting the process variables of interest and assigning weights to each variable. For this first analysis, a basic case is discussed. As the user has the option to freely choose the process variables, the now chosen ones only serve an exemplary purpose and can be exchanged freely. The same applies to the selected importance factors. Additional process variables can also be added or removed from the analysis.

The selected process variables and importance factors are listed in Table 4.2. The total number of direction changes in all joints and the total distance traveled are chosen due to their ease of implementation. The number of direction changes is assigned an importance factor of 0.2. The total travel in all joints is combined and given an importance factor of 0.4. Additionally, the acceleration of joint 1 is analyzed. To obtain a scalar value for the acceleration, the individual acceleration values are squared and then summed up. The importance factor for acceleration in joint 1 is 0.4. Other process variables are disregarded.

**Table 4.2:** Selected process variables and their importance factors

Process variables	Importance factors
Direction changes in joints 1-6	0.2
Total travel in joints 1-6	0.4
Acceleration in joint 1	0.4

Since only one redundant DoF is being analyzed, it is possible to represent the individual local scores and global score as a one-dimensional graph. Firstly, toolpath 1 is analyzed by incrementing the redundant DoF (C-axis) by 5 degrees, starting from -135 degrees and ending at 135 degrees.

Figure 4.11 illustrates a case with a  $-45^\circ$  rotation around the Z-axis for toolpath 1. Similarly, Figure 4.12 displays a case with a  $+45^\circ$ . The traversed path is identical but the final pose of the robot and its movements while traversing the path are different.

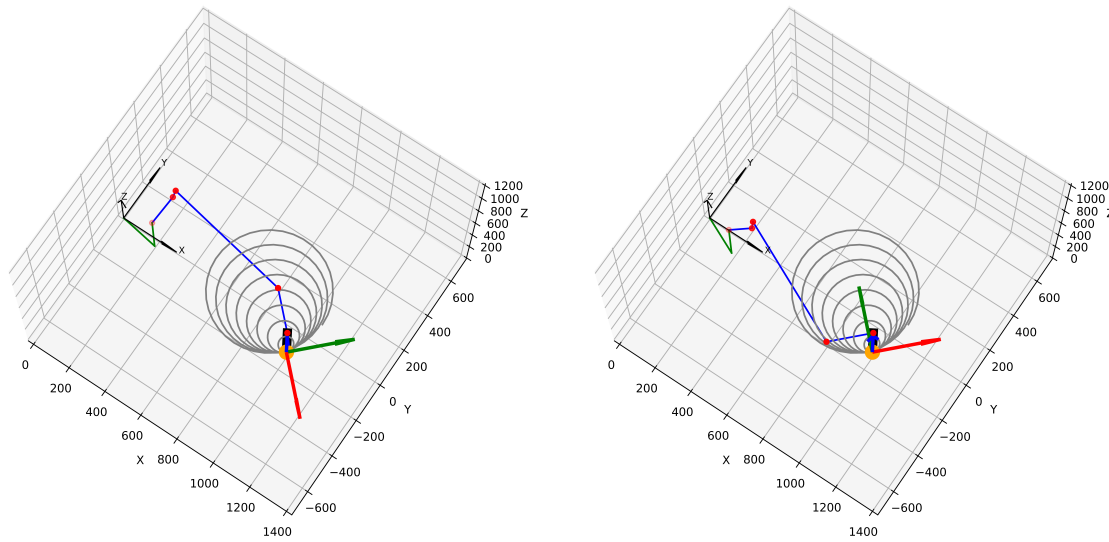


**Figure 4.11:** Toolpath 1 with  $A=0^\circ$ ,  $B=0^\circ$  and  $C=-45^\circ$

**Figure 4.12:** Toolpath 1 with  $A=0^\circ$ ,  $B=0^\circ$  and  $C=45^\circ$

A total of 55 time-series of joint positions are generated. On average, the inverse kinematics algorithm takes 35 seconds to calculate the joint values for all 3000 coordinates. The process variables are extracted and scaled in relation to each other, as described in Chapter 3.3.2. It is important to note that before scaling, the selected process variables are pre-multiplied by -1, as each value should be minimized. The arrays of local ratings are then multiplied by the weights selected in Table 4.2. Subsequently, the local scores of each process variable can be plotted as a one-dimensional graph, as shown in Figure 4.13.

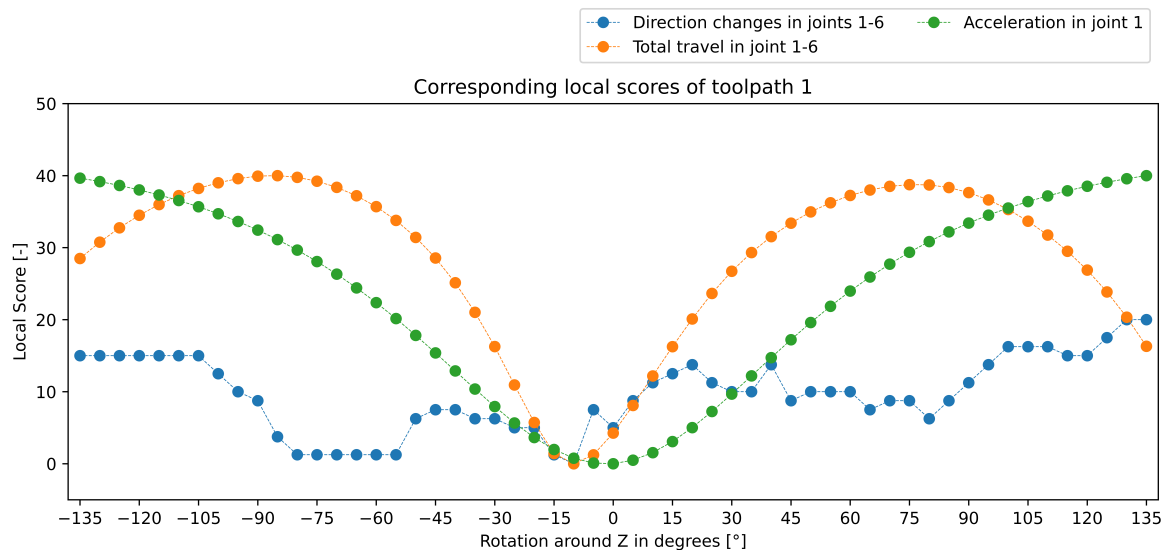


**Figure 4.13:** Local scores of each process variable for toolpath 1

The acceleration in joint 1 and the combined total travel in the joints display a smooth oscillating curve similar to a sine. The combined travel of the joints is maximized at  $C = -10^\circ$ , resulting in the lowest local score at that setting. Two maxima (minimal travel) are observed at  $C = -80^\circ$  and  $C = +75^\circ$ . The acceleration in joint 1 exhibits a symmetrical profile, similar to a sine, with the lowest score at  $C = 0^\circ$  and two maxima at the two outermost settings. The local score of the direction changes shows a non-smooth progression, with a plateau towards the negative end of the analyzed range. It is worth mentioning that the maximum value that the local score can reach is 40 for acceleration and total travel, while for direction changes, the maximum score is 20. This is due to the assigned importance factors.

Next, the local scores are summed up to calculate the global score. The resulting array, displayed in Figure 4.14, represents the global score achieved by varying the rotation around the Z-axis in relation to all other analyzed values. The orange star on the graph indicates the maximum attainable score and its corresponding rotation, compared to all analyzed boundary conditions.

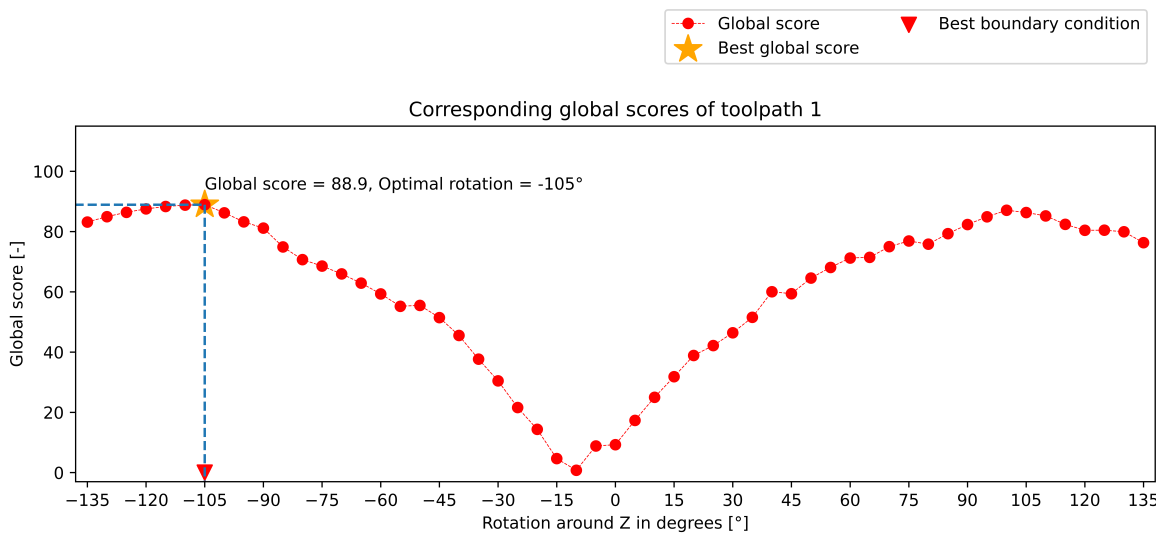
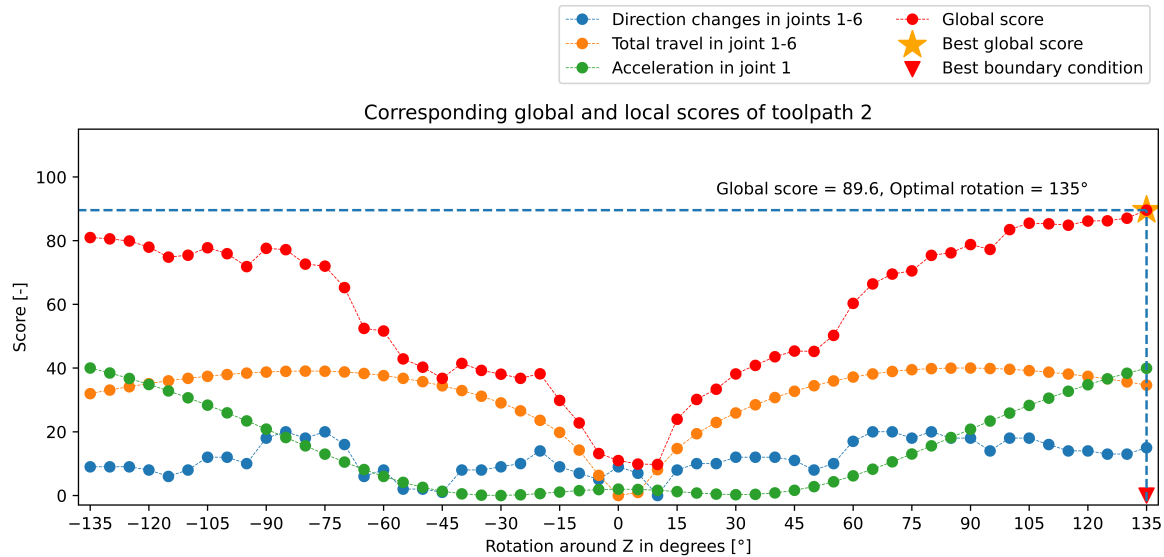


Figure 4.14: Global score for toolpath 1

In this particular case, the highest achievable score is 88.9 at  $-105^\circ$  degrees. This score indicates that setting the rotation C to  $-105^\circ$  degrees results in close to minimal direction changes, almost minimal total travel, and close to minimal acceleration in joint 1. It is crucial to emphasize that this rating is only in comparison to the other analyzed boundary conditions.

The same analysis, using identical process variables and weights, can be performed with toolpath 2 and toolpath 3. Figure 4.15 and Figure 4.16 display the global and local scores for each analyzed value of the redundant DoF. For toolpath 2, the best score is 89.6 at  $C=135^\circ$ , while for toolpath 3, the best score is 93.5 at  $C=105^\circ$ .



**Figure 4.15:** Global and local scores in toolpath 2 depending on the rotation around Z

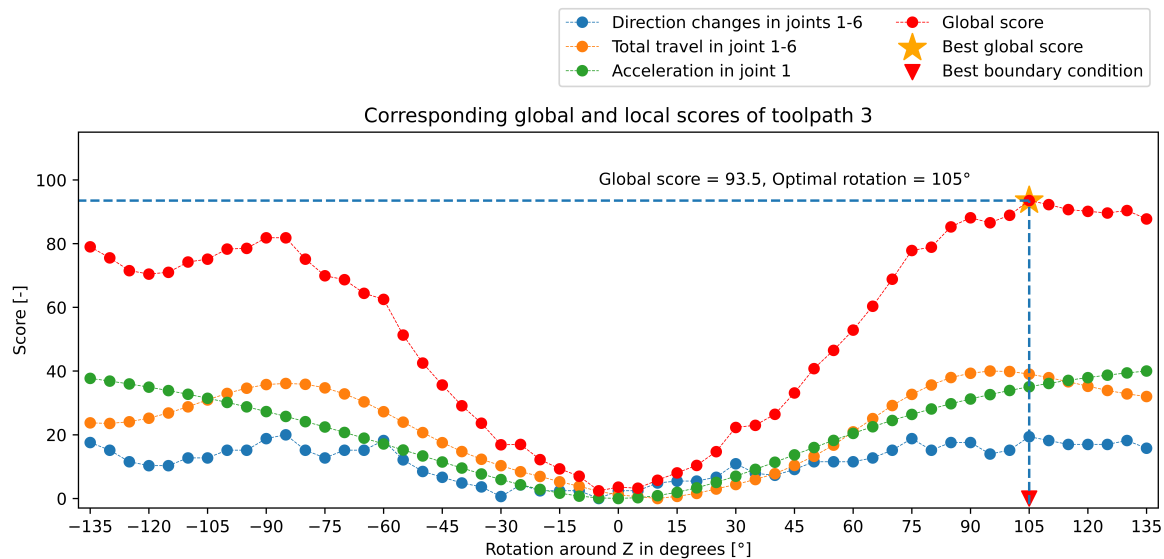


**Figure 4.16:** Global and local scores in toolpath 3 depending on the rotation around Z

It is noteworthy that even though all toolpaths have significantly different characteristics, all global scores analyzed process variables show a similar trend. The total travel and acceleration show a smooth and almost symmetric characteristic. High global scores are achieved by setting the rotation to high positive or high negative numbers, while low scores are achieved by setting the rotation close to 0°. This might be due to the robot's configuration, where the joints hinder the robot's movements. To continue on the predefined path, the robot has to quickly adjust the joints and reorient them to traverse the toolpath in the same time.

Additionally, it is important to note that when a local score reaches its maximum value, it does not imply that the corresponding variables, such as the number of direction changes, become zero. Instead, it signifies that the number of direction changes is at its lowest compared to

all other analyzed options. Based on the results, it is reasonable to conclude that optimizing the redundant DoFs can significantly improve the manufacturing process.

#### 4.2.3 Validation on a Production Grade Toolpath

In addition to the three simulated toolpaths, a toolpath that was used for the production of a WAAM component is now being used for validation. The toolpath has an organic structure that requires tilting of the rotary-tilt table to ensure that the material deposition process occurs in the direction of gravity. Thus, the position of the rotary-tilt table is not horizontal during the process. The redundant DoF remains the rotation around the Z-axis of the tool, as before. Figure 4.17 provides a visual representation of the analyzed toolpath. It consists of 28,000 coordinates and is modeled to be traversed in 2,800 seconds.

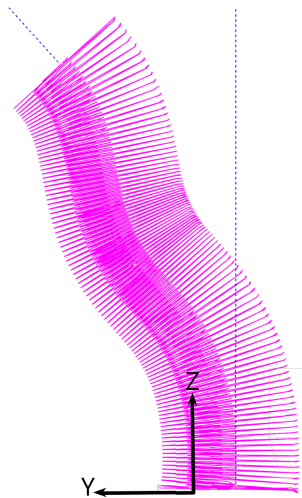


**Figure 4.17:** Organic toolpath (Reisch 2023)

The process variables for the analysis of this toolpath are defined in Table 4.3. As before, the selected process variables just serve a exemplary purpose and can be exchanged freely by the user. For the following, new process variables are selected compared to the first analysis (see Table 4.2), to further validate the elaborated method.

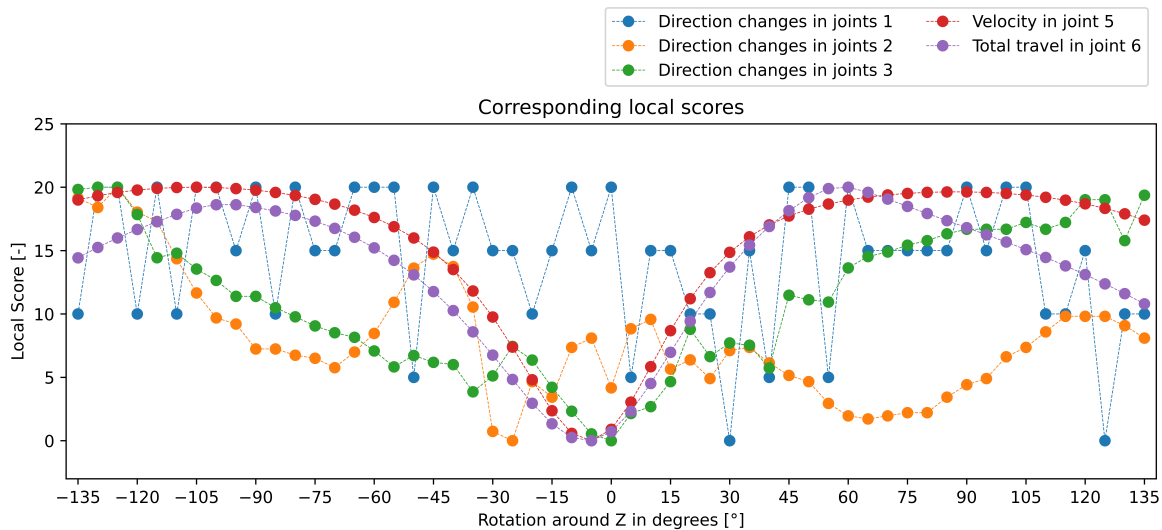
In this example, the direction changes in joints 1, 2, and 3 are all individually weighted with a factor of 0.2. The last two variables are the velocity in joint 5 and the total travel in joint 6. These variables are also weighted with an importance factor of 0.2. To obtain a scalar value for the velocity, all elements of the time-series are squared and summed up.

**Table 4.3:** Selected process variables and their importance factors for the organic toolpath

Process variables	Importance factors
Direction changes in joint 1	0.2
Direction changes in joint 2	0.2
Direction changes in joint 3	0.2
Velocity in joint 5	0.2
Total travel in joint 6	0.2

The redundant DoF is once again analyzed in  $5^\circ$  increments, starting from  $-135^\circ$  and ending at  $135^\circ$ . The resulting local scores are shown in Figure 4.18. It is evident that the velocity in joint 5 and the total travel in joint 6 exhibit a smooth and almost symmetrical behavior. The direction changes in joint 2 and 3 exhibit smooth progression in some section but are significantly jerkier than the analyzed velocity and total travel. When examining the local score of joint 1 for the direction changes, it is apparent that the individual scores only fall at 0, 5, 10, 15, or 20. This artifact arises from the fact that the direction changes in joint 1 can only reach five distinct equidistant numbers, which are: 630, 632, 634, 636, and 638. These values differ by a very small percentage relative to each other.

The difference in the count of direction changes can be attributed to the implemented process of calculating the joint angles in the inverse kinematics algorithm. The algorithm terminates the iterative calculation of the joint angles if the TCP is within 0.00001 mm of the defined coordinate. This can introduce rounding errors that result in different outcomes for process variables, even though the same number was expected.

**Figure 4.18:** Global and local score for WAAM toolpath

When analyzing the standard deviation of the individual process variables, as shown in Table 4.4, the stark contrast between them becomes apparent. To calculate the standard deviation of a process variable, all the individual values achieved by setting the redundant DoF to

the discrete analyzed values are utilized. It is important to note that the standard deviation is calculated based on the physical values before applying the Min-Max Scaler, rather than on the local score itself.

As mentioned in Chapter 3.3.2, the standard deviation of the direction changes in joint 1 is not sufficient to contribute to the analysis and optimization of the boundary condition. Therefore, this process variable is omitted from further analysis. It is worth noting that the higher the standard deviation of a process variable, the greater the potential for improvement in a physical sense. However, it is important to recognize that the global score is only influenced by the selected importance factors and does not take into account the physical nature of the process variables. The physical nature of the process variables is only reflected in the standard deviation.

**Table 4.4:** Standard deviation of the selected process parameters

Process variables	Standard deviation
Direction changes in joint 1	2.166
Direction changes in joint 2	38.513
Direction changes in joint 3	62.301
Velocity in joint 5	14795.394
Total travel in joint 6	546.560

Figure 4.19 illustrates the combined local scores in the form of the global score without the addition of the direction changes in joint 1. The highest global score is 75.6, which is achieved by setting the C-axis to  $-125^\circ$ . The fairly smooth progression of the global score in all analyzed toolpaths, serves as a strong indicator that an optimization algorithm will easily find an optimum setting for the redundant DoF.

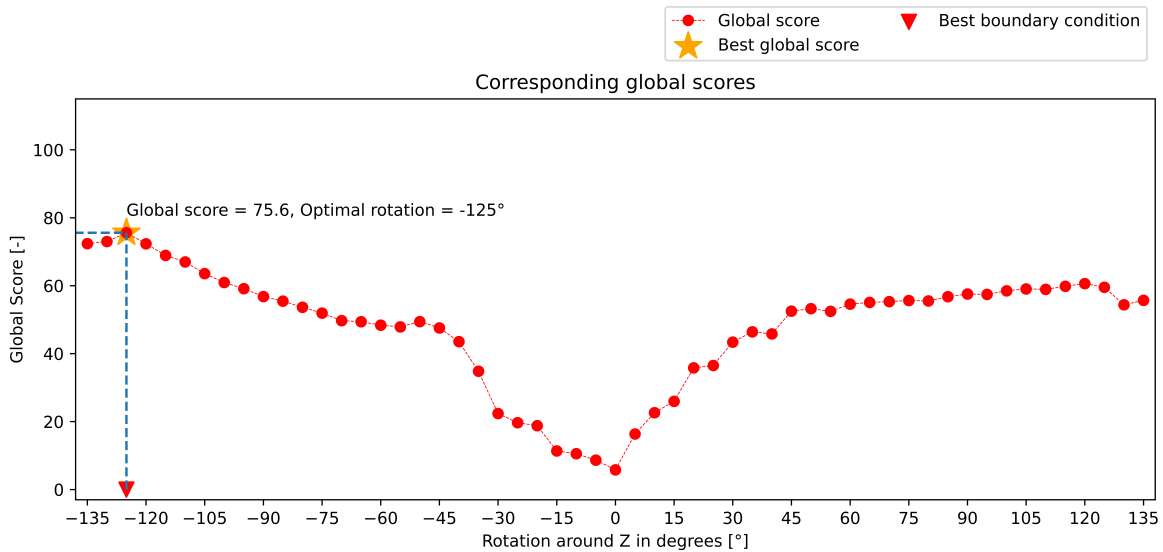


**Figure 4.19:** Global score for production toolpath

#### 4.2.4 Toolpath Evaluation With two Redundant DoF

To introduce an additional redundant DoF, a rotary-tilt table is simulated. Currently, only the tilting element is being analyzed. All coordinates of the toolpath can be rotated by a specified degree around the X-axis of the toolpath coordinate system. Figure 4.20 depicts toolpath 3 with no rotation around the X-axis, while Figure 4.21 illustrates a rotation of +25 degrees.

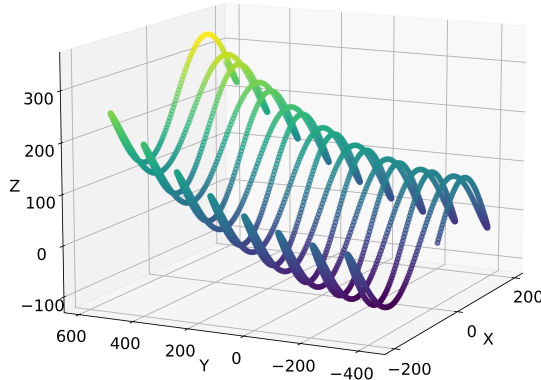


**Figure 4.20:** Toolpath 3 with no rotation around the X-axis

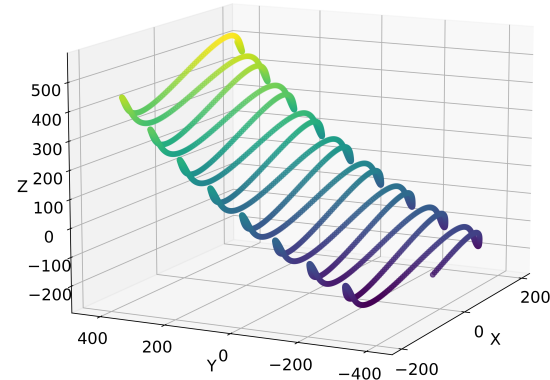


**Figure 4.21:** Toolpath 3 with a rotation of 25 degrees around the X-axis

Similar to the previous analysis, the same steps need to be followed. The newly selected process variables are presented in Table 4.5. The direction changes of the tilting joints (2+3+5) are combined and treated as one process variable, weighted with a factor of 0.3. Direction changes in joint 1 and acceleration in joint 4 are considered as individual variables, both individually weighted with 0.25. The final variable is the velocity in joint 6, weighted with 0.2. Just as before it is important to reiterate that these process variables serve a exemplary purpose and can be grouped and exchanged as desired.

**Table 4.5:** Selected process variables and their importance factors for two redundant DoFs

Process variables	Importance factors
Direction changes in joints 2+3+5	0.3
Direction changes in joints 1	0.25
Acceleration in joint 4	0.25
Velocity in joint 6	0.2

Figure 4.22 displays the robot and its orientation while following the tilted toolpath 3. It is crucial to note that since the toolpath is defined in 5 DoFs in its own frame, the frame of the TCP must also tilt by the same degree as the table. The two redundant DoFs in this

case are the rotation around the Z-axis in the frame of the tilted toolpath and the tilting of the toolpath itself. This introduces an additional dimension, as now two parameters can be adapted for optimization.

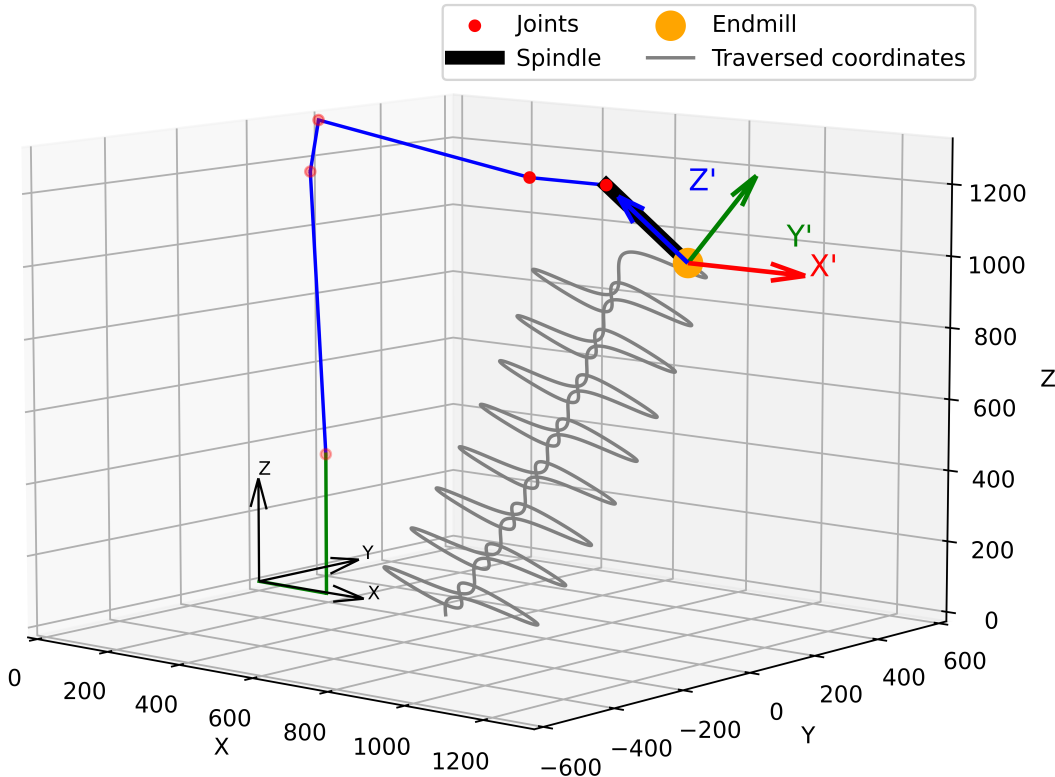


**Figure 4.22:** Robot following the tilted toolpath 3

The range of possible tilt positions ranges from  $-45^\circ$  to  $45^\circ$  in 2-degree increments. For every combination of tilt and rotation, the joint angles are generated using inverse kinematics. To speed up the computation, only every third coordinate is utilized in the inverse kinematic algorithm. This reduces the toolpath by 2000 points and speeds up calculation time. On average, it now takes only 10 seconds to calculate the joint positions. A total of 2530 individual combinations are analyzed.

The extracted process variables are again multiplied by -1, as the objective is to minimize them. Afterwards, the Min-Max scaler is applied. The individual values are aggregated and presented in the form of a matrix. The values of this matrix are visualized in Figure 4.23. The maximum achievable score from all possible combinations is 85.4, visualized by the red cross. This score was attained by setting the table tilt to  $-1^\circ$  and the rotation around the Z-axis of the tool to  $+115^\circ$ . The resulting hyperplane exhibits two distinct local maxima. The entire surface displays a smooth curvature.

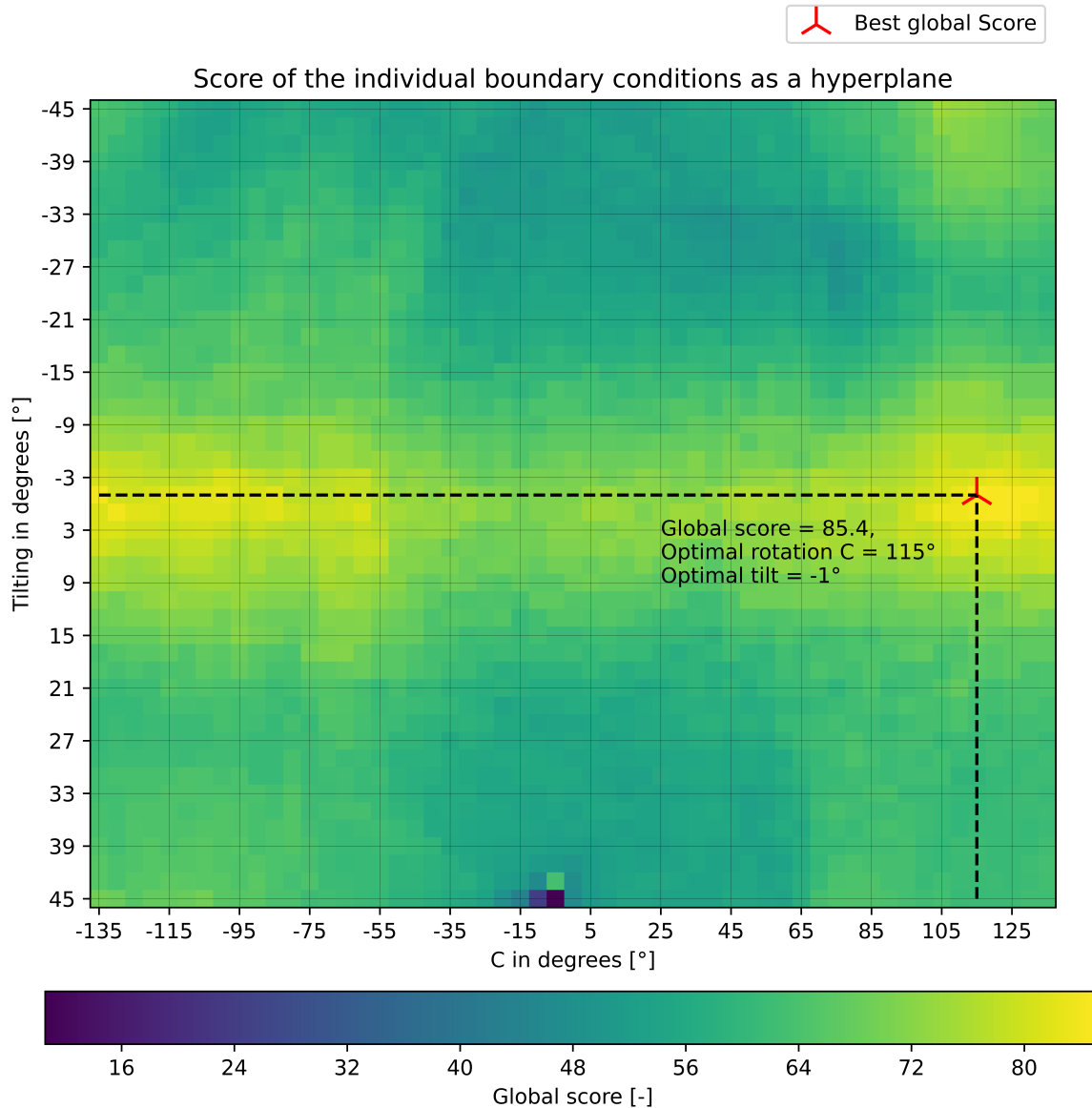


**Figure 4.23:** Hyperplane representing the global score of toolpath 3

The same analysis is performed with toolpath 1 and toolpath 2. The resulting matrix of the global scores for each possible boundary condition combination is shown in Figure 4.24 and Figure 4.25, respectively. The same process variables and weights (see Table 4.5) are used for the calculations.

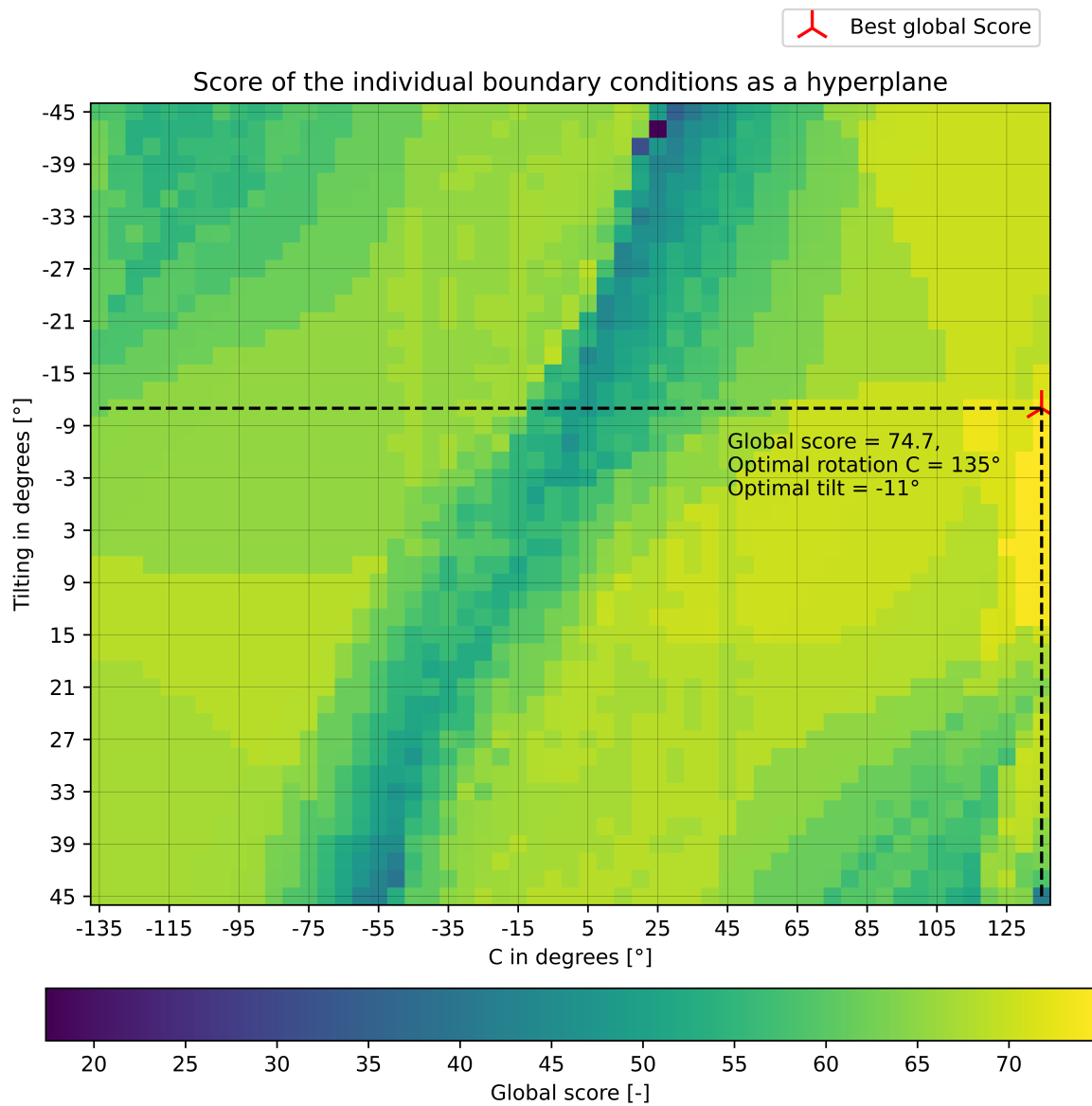


**Figure 4.24:** Hyperplane representing the global score of toolpath 1

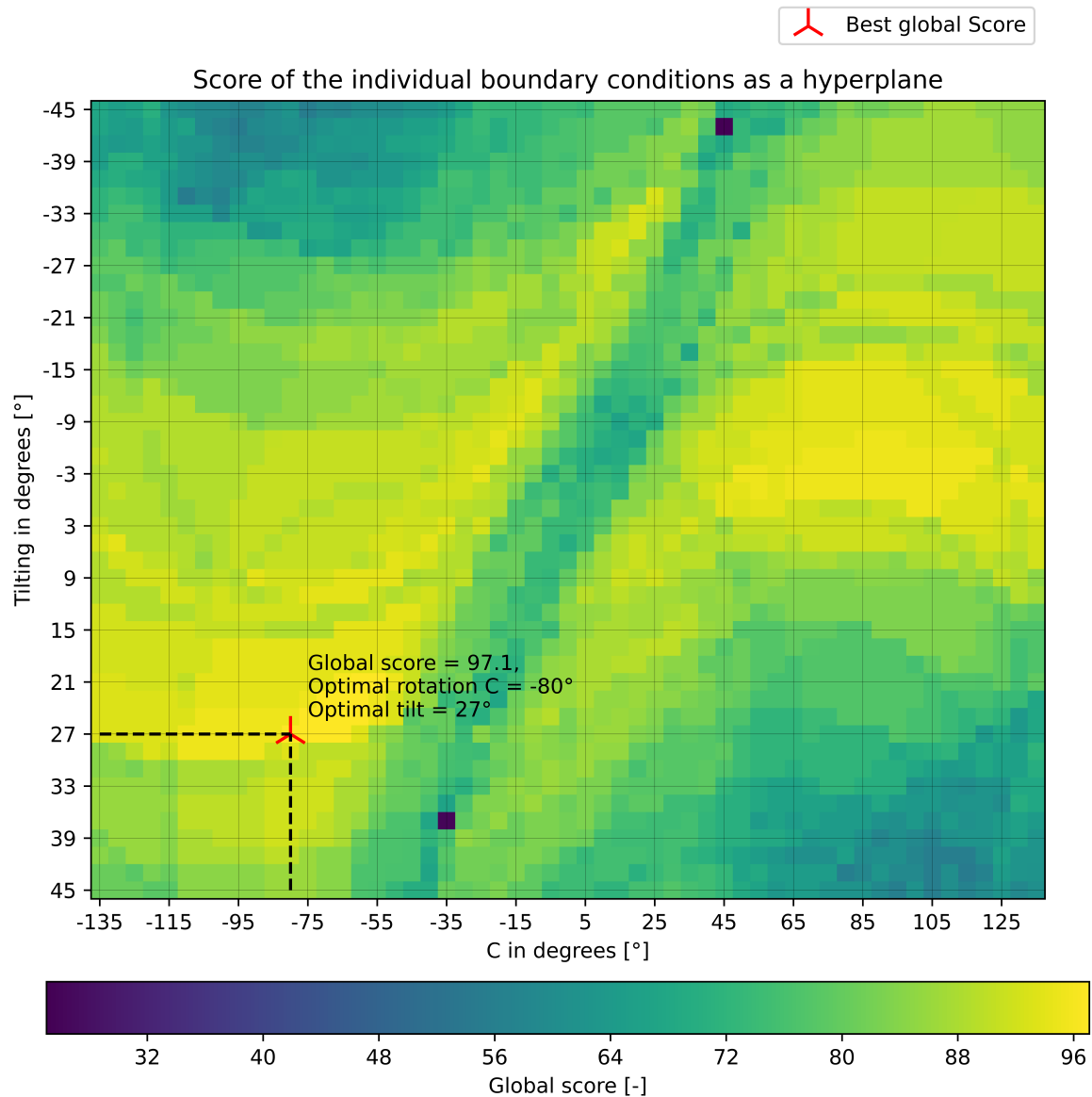


Figure 4.25: Hyperplane representing the global score of toolpath 2

#### 4.2.5 Boundary Condition Optimization

So far, only the analysis of different boundary conditions has been performed by exploring the entire range of possible settings for the redundant DoFs. However, this approach is very time-consuming and becomes exponentially more complex with additional redundant DoF and a finer step size. To address this issue and efficiently search the extensive solution space for optimal values of the redundant DoF, a PSO algorithm is proposed. In this algorithm, individual particles navigate the search space by adjusting their positions based on their own best position and the best position found by the entire swarm.

In more detail, each particle in a swarm optimization algorithm has an initial velocity, which represents its momentum or tendency to continue moving in the same direction. This velocity is adjusted based on several factors, including its current velocity, its own historical best position, and the best-known position of the entire swarm.

The mathematical procedure for adjusting the velocity of a particle is represented by the equation 4.1. In this equation,  $velocity_{current}(t+1)$  is the updated velocity of the particle at time  $t+1$ .  $velocity_{current}(t)$  is the current velocity of the particle at time  $t$ .  $c1$  and  $c2$  are cognitive and social constants, respectively, which are both typically set to 1.  $r1$  and  $r2$  are random values in the range  $(0,1)$ .  $position_{individualbest}$  represents the particle's own historical best position, and  $position_{globalbest}$  represents the best-known position of the entire swarm.

Additionally, the equation includes an inertia weight, denoted as  $w$ . This weight is used to balance the exploration and exploitation capabilities of the algorithm. A higher inertia weight allows for more exploration, while a lower inertia weight promotes exploitation. In most cases, the inertia weight is set to a value of 0.4.

$$\begin{aligned} velocity_{cognitive}(t) &= c1 * r1 * (position_{individualbest} - position_{current}(t)) \\ velocity_{social}(t) &= c2 * r2 * (position_{globalbest} - position_{current}(t)) \\ velocity_{current}(t + 1) &= w * velocity_{current}(t) + velocity_{cognitive}(t) + velocity_{social}(t) \\ position_{current}(t + 1) &= position_{current}(t) + velocity_{current}(t + 1) \end{aligned} \quad (4.1)$$

This procedure is iteratively applied to each particle in the swarm. This cooperative behavior enables the particles to explore the search space more effectively and converge towards the best solution (see Chapter 2.3).

The first test is conducted using the global score matrix of toolpath 3. Initially, 20 particles are randomly placed on the plane. Each particle's score is determined by the corresponding global score at its position. By increasing the number of particles and iterations, the search space can be analyzed more comprehensively. Figure 4.26 illustrates the randomly placed particles on the pre-calculated global score matrix of toolpath 3, considering the previously selected importance factors (see table 4.5).

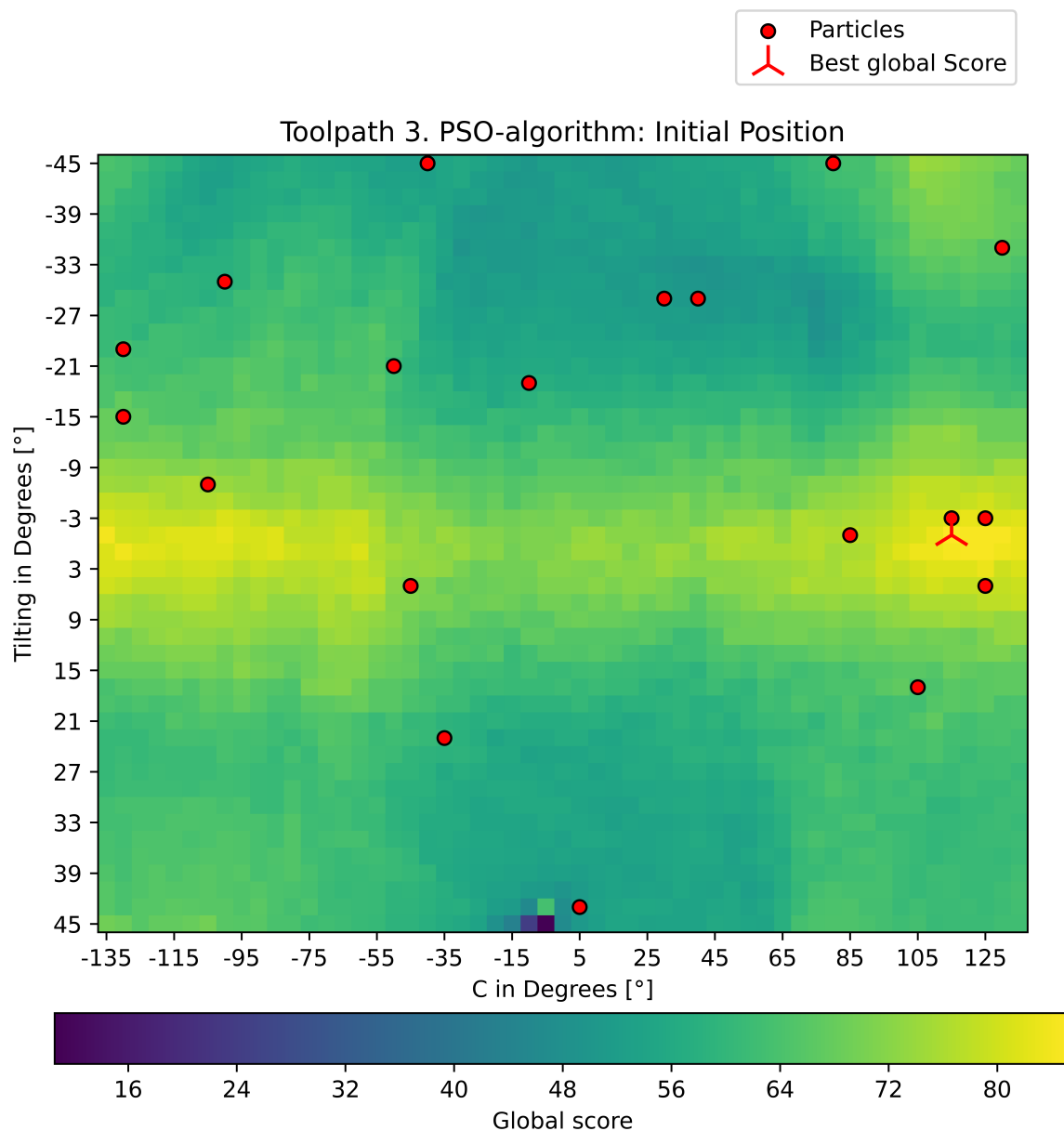


**Figure 4.26:** Distributed of particles at their initial positions

It is important to clarify that the individual particles in the PSO algorithm do not have access to the entire global score matrix. The visualization of the global score matrix is only provided for the benefit of the human reader to aid in understanding. In reality, each particle only has knowledge of the global score at its own position. The particles update their positions iteratively by comparing their positions with each other. Each particle determines a new position based on the best score observed so far by all particles and the best score observed by itself.

Figures 4.27 to 4.30 demonstrate the convergence of the particles towards the maximum global score. This convergence is achieved within 5 iterations. It is noteworthy that the best position of all 20 particles corresponds to the global maximum, as discussed in Chapter 4.2.4.

This example highlights the ability to explore a high-dimensional space without the need to compute all possible combinations.

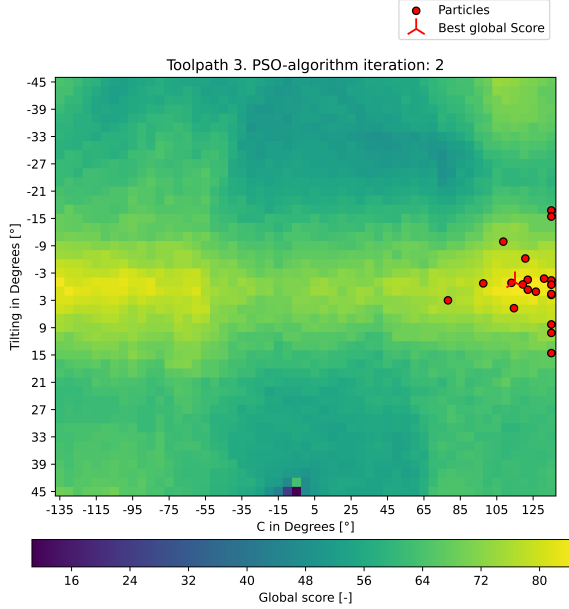


**Figure 4.27:** PSO Iteration 2 on toolpath 3

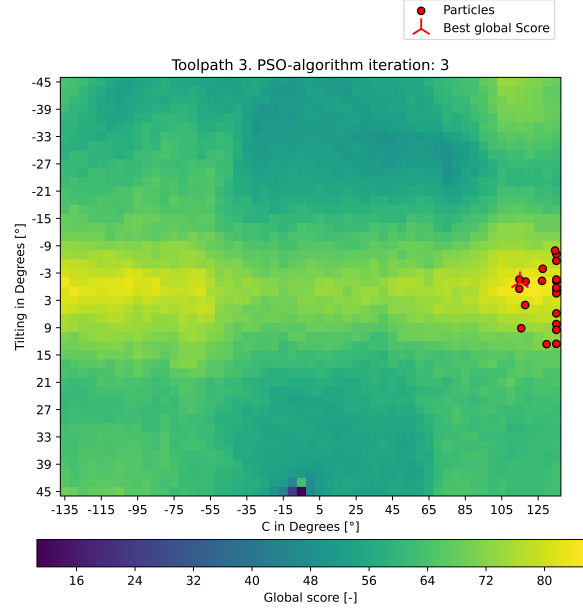


**Figure 4.28:** PSO Iteration 3 on toolpath 3

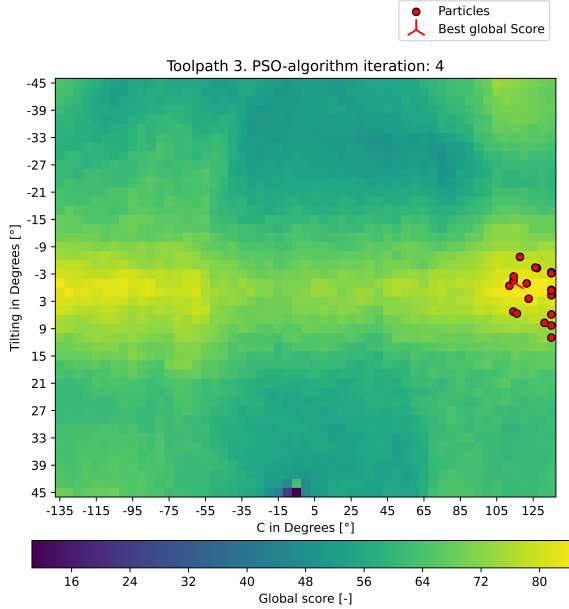


**Figure 4.29:** PSO Iteration 4 on toolpath 3

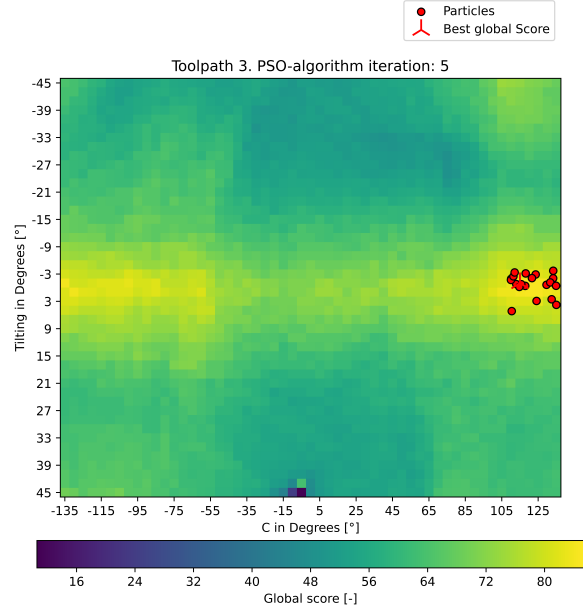


**Figure 4.30:** PSO Iteration 5 on toolpath 3

One important consideration in this test is, that the scores have already been calculated. The global score matrix is determined by evaluating all possible combinations of different boundary conditions. However, in the intended scenario where this method is used to find the optimal boundary condition, such a pre-calculated matrix does not exist.

Therefore, in each iteration, the scores of the individual particle positions need to be com-

pared relative to each other, taking into account the previous iterations. This process is illustrated in Figure 4.31. Initially, a predetermined number of particles is randomly placed on the plane, with the X and Y values representing the selected boundary conditions. For each selected boundary condition, the joint angles are calculated using the inverse kinematic approach. The analyzed process variables are then extracted and the joint angles are stored. The score for each current position is calculated relative to all other stored toolpaths.

It is possible that in an early iteration, a particle had a position with a significantly higher score compared to the other available toolpaths. Therefore, after each iteration, it is necessary to update the score of the particle's most optimal position as more boundary conditions are analyzed. This is done to ensure that a score, which may have been mistakenly chosen as the best, does not influence the subsequent search directions.

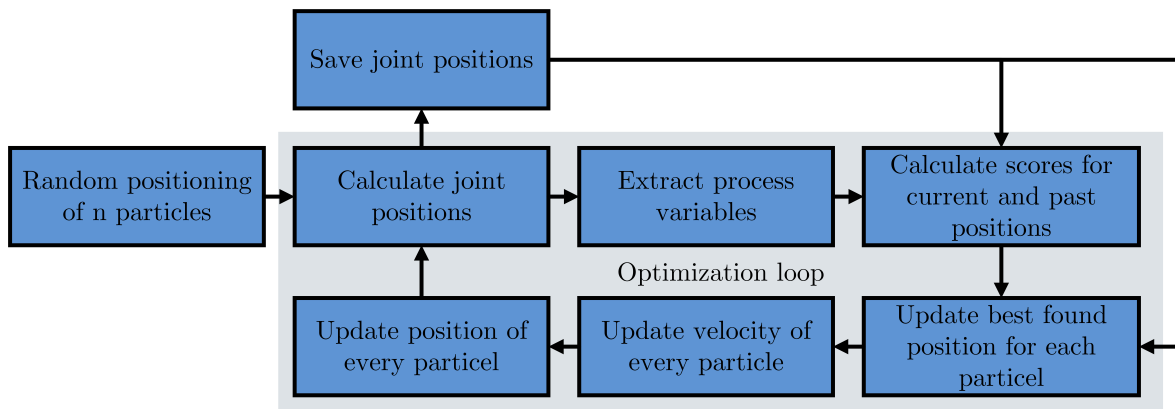


**Figure 4.31:** PSO-Loop

By utilizing this approach, the following results have been obtained. It is important to emphasize that the precalculated values of the global score matrix are not accessible to the PSO algorithm. They are only used for evaluating the behavior of the particles and aiding in visualization. Figures 4.32 to 4.35 illustrate the evolution of the individual particles. The green circle represents the overall best position discovered by the particles up to that point.

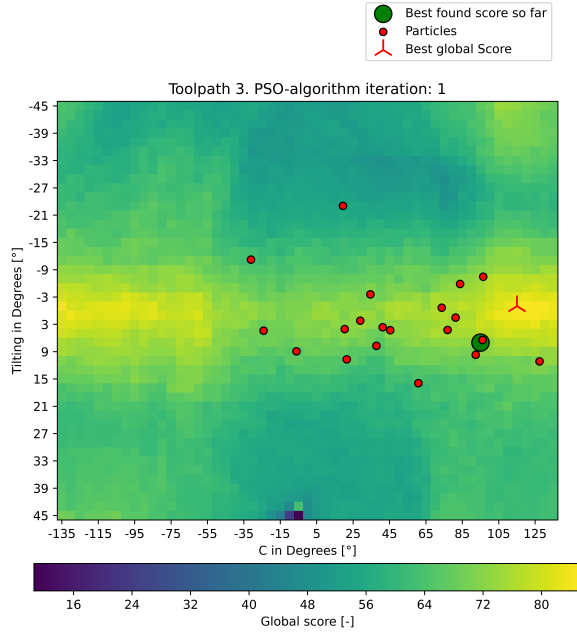


Figure 4.32: PSO Iteration 1 on toolpath 3

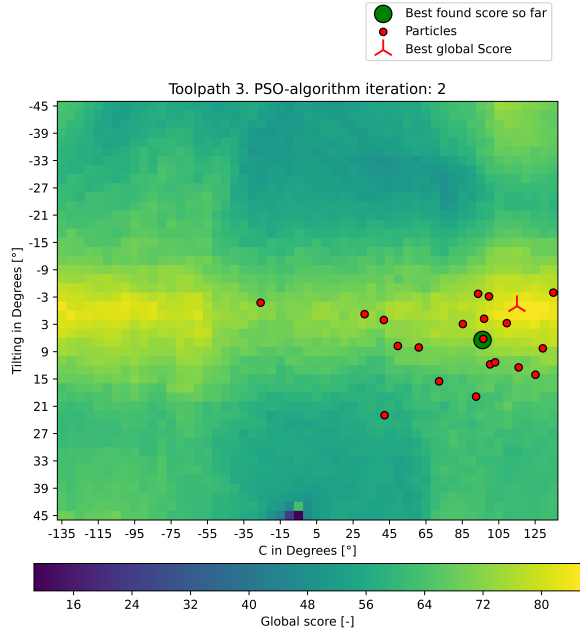


Figure 4.33: PSO Iteration 2 on toolpath 3

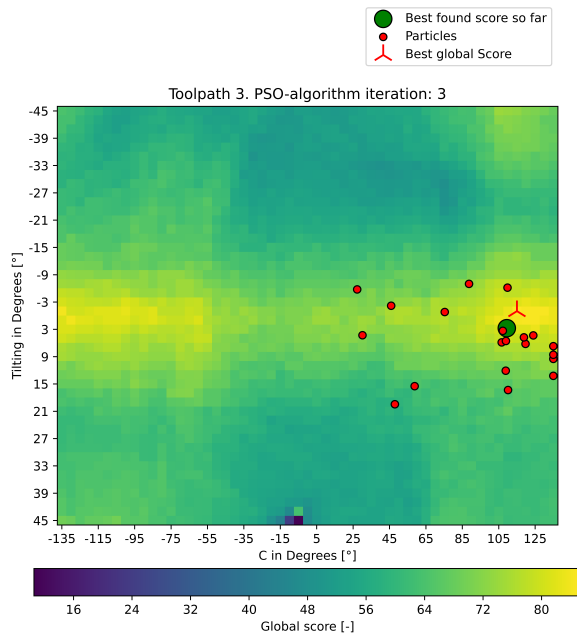


Figure 4.34: PSO Iteration 3 on toolpath 3

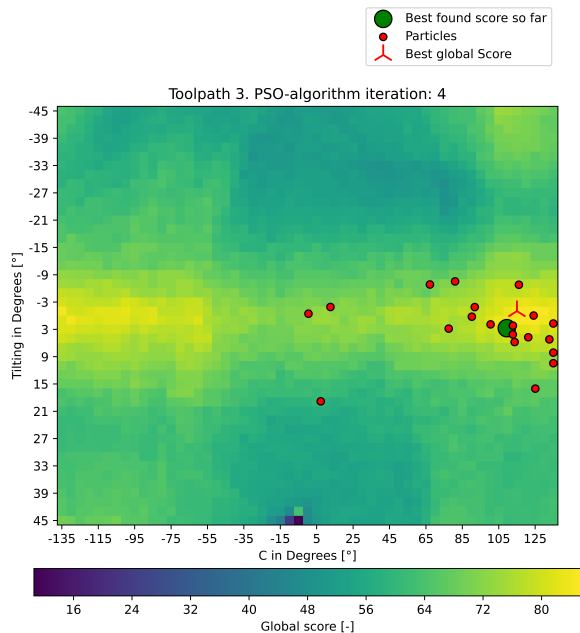
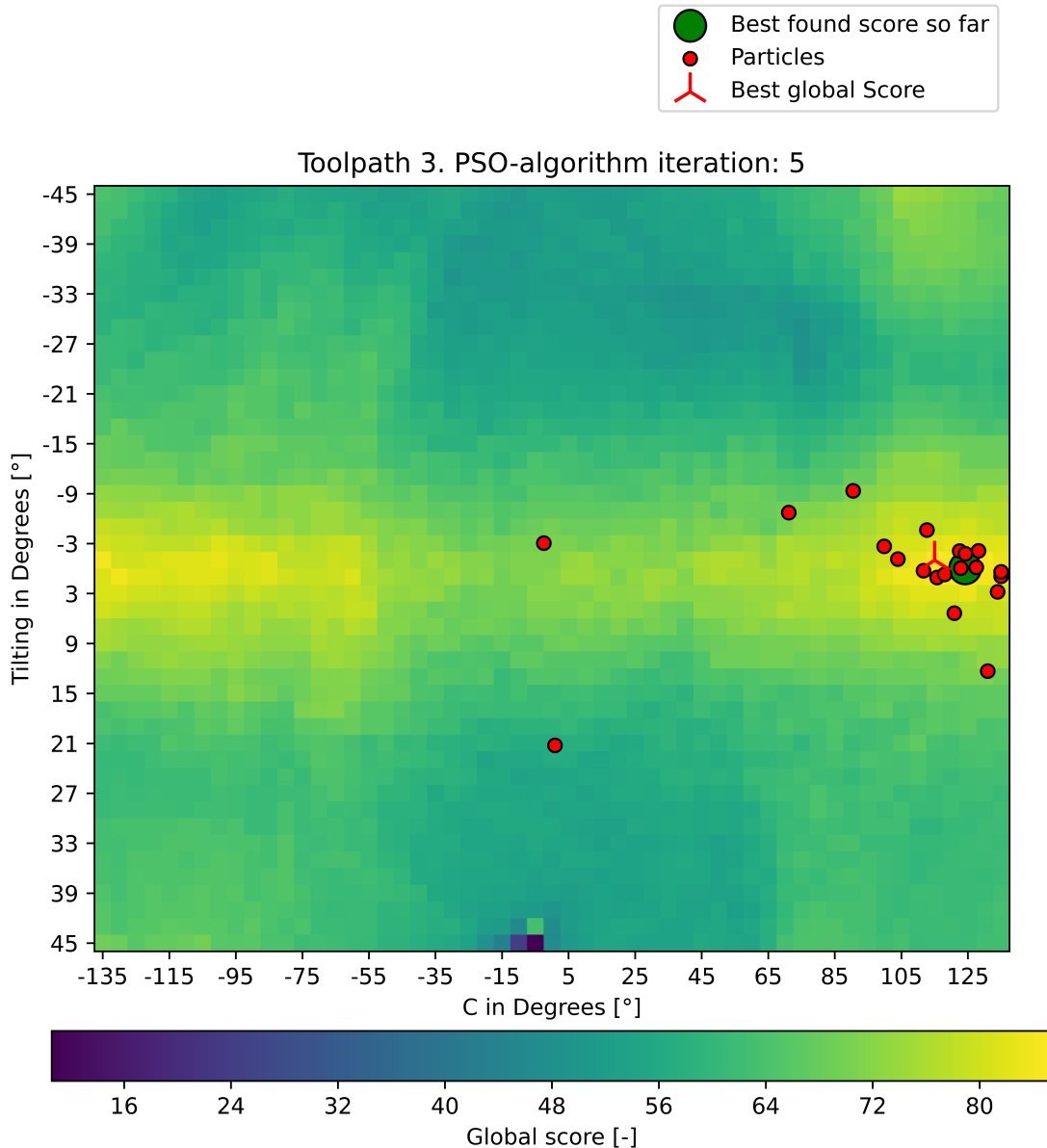


Figure 4.35: PSO Iteration 4 on toolpath 3

The backtracking comparison of all previously visited positions by the particles is clearly evident in the movement of the green dot, which represents the best position found so far. As more points are visited by the particles, the calculation of the best boundary conditions improves. Even without the precalculated global score matrix, the particles are able to converge to the global optimum. Figure 4.36 illustrates the positions of the particles after the fifth and final iteration. It is important to clarify that the global maximum is formed by a plateau and has multiple solutions for the redundant DoF. The red cross marks the first position of

the plateau according to mathematical convention (first row, then column), while the green dot marks the first found maximum. These two positions are not necessarily equal, but they achieve the same global score.



**Figure 4.36:** PSO iteration 5 on toolpath 3

The same optimization process can be applied to toolpath 1 and toolpath 2. The same process variables and weights are selected as for toolpath 3 (see Table 4.5). Once again, 20 particles are analyzed over 5 iterations. Figures 4.37 and 4.38 depict the positions of the particles after the first and final iteration when analyzing the first toolpath, while Figures 4.39 and 4.40 showcase the initial and final positions of the particles when analyzing the second toolpath. In both cases, the PSO algorithm successfully converges very closely towards the optimal boundary condition.

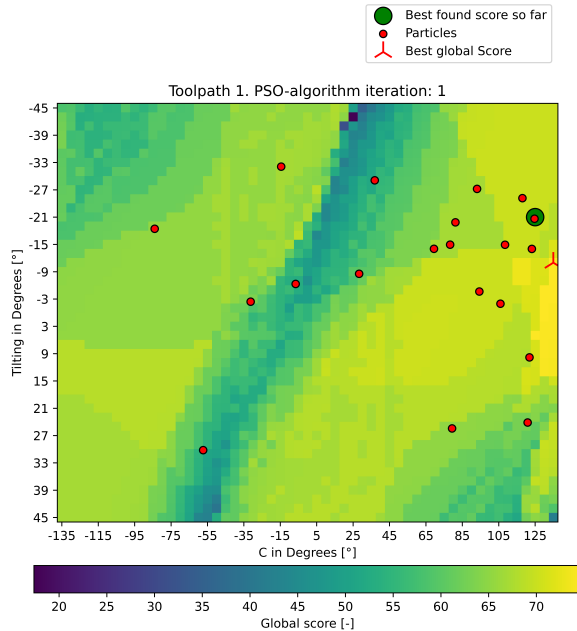


**Figure 4.37:** PSO Iteration 1 on toolpath 1

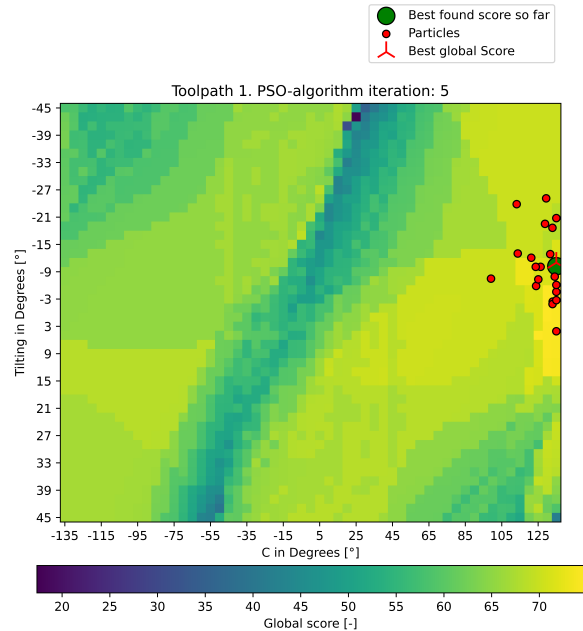


**Figure 4.38:** PSO Iteration 5 on toolpath 1

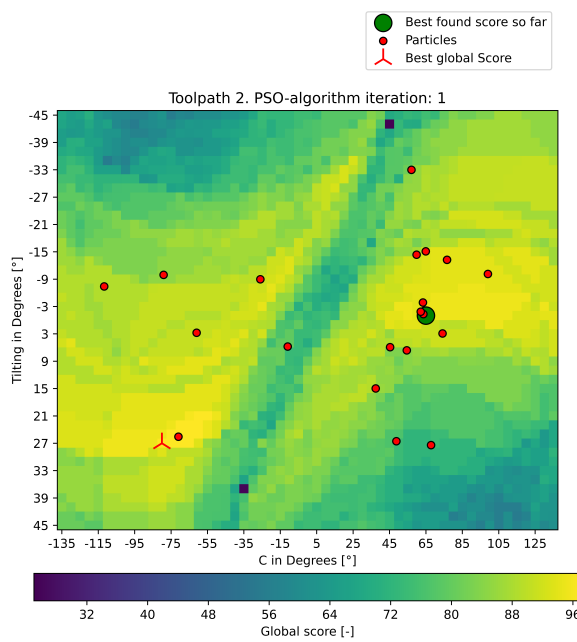


**Figure 4.39:** PSO Iteration 1 on toolpath 2

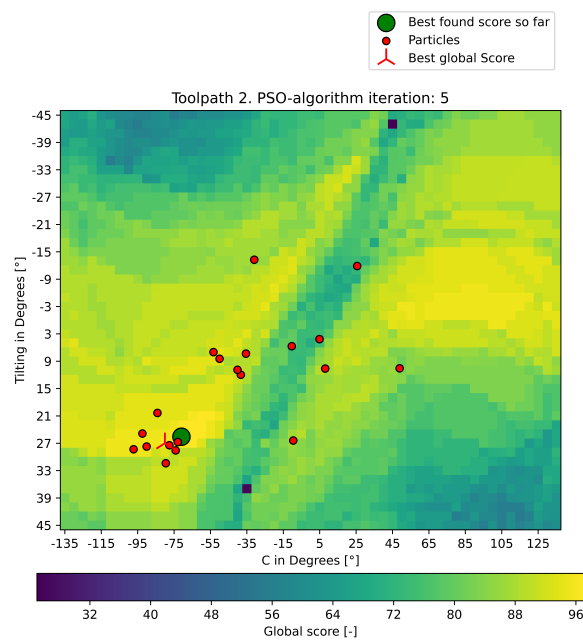


**Figure 4.40:** PSO Iteration 5 on toolpath 2

## 4.3 Analysis and Discussion of the Results

In the following, the results of the performed validation are analyzed in detail as well as critically discussed. In general, the presented validation does provide a solid basis as a proof of concept for the proposed method. Additional implementations and tests can further provide the necessary validation for successful implementation in an industrial environment.

### 4.3.1 One Redundant DoF

When analyzing only one redundant DoF, specifically the rotation around the Z-axis (see Figure 4.14, Figure 4.15, and Figure 4.16), it becomes evident that there is significant potential for improvement in the robots movement. In this initial test, multiple process variables are analyzed. The local score for total travel in all joints and acceleration in joint 1 both exhibit a very continuous change and almost symmetrical behavior over the entire analyzed range. Low scores are achieved in the range from  $-15^\circ$  to  $+15^\circ$  for the rotation around the Z-axis. This property may be attributed to the robots' joint configuration. In order to stay on the pre-defined path, the robot needs to swiftly adapt its joints and realign them to effectively sweep the toolpath with the predefined feedrate. For that reason, the overall travel in the joints and their acceleration are increased. The smooth change in the local score, is a clear indication that optimization algorithms are a reasonable choice for finding the optimal boundary condition when it comes to boundary condition optimization. When analyzing the direction changes, a irregular progression is visible. The local score of the direction changes does not exhibit any symmetry. Additionally, multiple plateaus are visible where the local score has the same value. This could be attributed to the specific approach used in the inverse kinematics algorithm. In this algorithm, the iteration process terminates when the TCP is within 0.00001 mm proximity of the defined coordinate. However, this termination condition can introduce rounding errors, resulting in varying outcomes for the analyzed process variables, especially for the direction changes. Another drawback of the selected inverse kinematics algorithm, is that its not designed for optimal high-performance calculations, making it infeasible to use when dealing with toolpaths that have millions of coordinates. Additionally, the algorithm calculates the joint position numerically rather than analytically, which can result in unexpected robot poses. CAM software such as *Siemens NX* or *Master CAM* offer advanced inverse kinematics algorithms that can be used to fine-tune the behavior of the robot. In the time-frame of this thesis it was not possible to access the internal algorithms of those CAM programs and use them in the validation process.

### 4.3.2 Production Grade Toolpath

To further validate the proposed method for analyzing process variables, a production grade G-Code is examined (see Figure 4.18) with newly selected process variables. This G-Code consists of 28,000 points and takes significantly longer to analyze. Just as in the artificial toolpaths, the velocity in joint 5 and total travel in joint 6 show a symmetrical curve over the analyzed range. The direction changes in joint 2 and 3 have a less smooth progression. The local score of joint 1 on the other hand, shows a very distinct characteristic where the local score only varies between five values and doesn't follow any pattern. As explained before, the difference in the count of direction changes can be attributed to the implemented process of calculating the joint angles in the inverse kinematics algorithm. The termination condition can introduce rounding errors that result in different outcomes for process variables, even though the same number was expected. This assumption is verified by analyzing the individual values and calculating the standard deviation. As the standard deviation is very low in comparison to the other analyzed process variables, it save to assume that this process variable does not provide enough potential for improvement and is thus omitted from the global score. The resulting global score shows a fairly smooth curve with a distinct global minima and global maxima.

Even though a different set of process variables is selected compared to the analysis before, the graph of the global score still shows a similarity to the global score of the three manually created toolpaths. This can suggest that in the case where the redundant DoF is the same and the rotation A and B are the same, the optimal boundary condition of one toolpath is transferable to all other toolpaths and will result in high global scores.

### 4.3.3 Two Redundant DoF

When considering the scenario where two DoF can be set, it is observed that toolpath 1 and toolpath 2 have a very similar global score matrix (see Figure 4.24 and Figure 4.25). This suggests that these two toolpaths do not differ significantly from each other when considering the process variables alone. A distinct streak is visible in both matrices. Additionally there are distinct points that show a significantly lower score than their surrounding. This may be due to the rounding errors in the inverse kinematics algorithm or an overlap of many low local scores. Many sections of the hyperplane consist out of plateaus where the global score is the same. This can suggest that the individual step sizes of the two redundant DoF can be increased, and thus significantly reduce computation time.

Analyzing the hyperplane of toolpath 3 (Figure 4.23), it is clearly visible that most of the possible combinations result in a global score in the range from 50 to 70. The combinations that lead to a low local score form a single area that is clearly visible in the lower part in the center. The visualization the matrix shows an almost symmetrical hyperplane. Two local optima are visible on the left and right sides. Such hyperplane with generally high global

scores can result due to the fact that the very low scores present, shift all other scores towards the upper limit. The found low global score can again be either a artifact of rounding errors or a overlap of many low local scores.

#### 4.3.4 PSO Optimization

Based on the results obtained from the PSO algorithm (see Figure 4.36), it can be concluded that achieving a close-to-optimal result is feasible when the global score matrix yields smooth surfaces. The number of particles is selected to be as high as possible while also considering the computational costs. Rather than increasing the number of particles and iterations, a trade-off between number of particles and iterations is selected. The number of iterations is set to 5 in order to enable convergence towards the global optima. The number of particles is set to 20 to saturate the whole search space in the initial random placing. Adding more iterations only resulted in the particles movement around the found global maxima. Increasing the number of particles does help significantly with the search of the global maxima but also requires significantly more computation. The selected parameters clearly show that convergence is possible even with the presence of large plateaus. By implementing this approach with the selected hyper-parameters, a significant reduction in computation time is possible. Instead of calculating the entire matrix, only 100 toolpaths need to be computed using the inverse kinematics algorithm.

Nonetheless, when analyzing multiple process variables, it is not guaranteed that the resulting surface of the global score matrix will be smooth and optimal for the selected optimization algorithm. Additionally, when working with a PSO algorithm, the final result strongly depends on the initial distribution of the particles. If the optimum is a very tight and sharp spike, the probability of finding the optimal boundary condition is significantly lower. This is particularly true in systems with 3 or more redundant DoF, where simple optimization algorithms can lead to suboptimal results or require unfeasibly long computation times. In future work with multiple redundant DoF, it is necessary to analyze if an increase in population size will improve the convergence rate without significantly impact computation time.

#### Conclusion

In conclusion, the analysis of a single redundant DoF revealed significant potential for improvement in the robot's movement. The smooth and symmetrical behavior of process variables suggests that optimization algorithms are suitable for finding the optimal boundary condition. The validation of the proposed method using a production-grade G-Code further supported the effectiveness of analyzing process variables. When considering the scenario with two DoFs, toolpath 1 and toolpath 2 showed similar global score matrices, indicating minimal differences in the space of process variables alone. On the other hand, toolpath 3 exhibited an almost symmetrical hyperplane with clearly distinct global maxima and min-

ima. The existing plateaus in the global score matrix highlight the possibility to increase the step size in the analyzed DoF and significantly reduce computation time. The results obtained from the PSO algorithm demonstrated that achieving close-to-optimal results is feasible when the global score matrix exhibits smooth surfaces. By implementing this approach, a significant reduction in computation time can be achieved. The analysis highlights the potential for improving the robot's movement through optimization algorithms and validates the effectiveness of analyzing process variables. The findings provide valuable insights for optimizing toolpaths and reducing computation time.

The obtained results show that the presented method, with the help of its adaptability, serves as a robust proof of concept. It is demonstrated that the effectiveness of the approach is not bound to a specific analyzed toolpath or process variables. Additionally it can be extended to a broad spectrum of robotic systems by adapting the DH parameters. Even though the results show a very promising outcome, it is necessary to consider some additional factors. To validate this method in detail, it is necessary to use longer and more complex production G-codes with correctly modeled robotic systems and analyze whether it can be optimized. It should be noted that this work only provides a limited excerpt and does not analyze complex multi-axis operations with more than two redundant DoFs.

# **Chapter 5**

## **Conclusion**

### **5.1 Summary**

This thesis proposes a method for optimizing the execution of a toolpath on manufacturing machines with redundant DoFs. Firstly, the problem formulation (Chapter 1.2) highlights the flexibility and various issues that arise with redundant DoFs. It discusses how singularity avoidance can help industrial robots avoid sub-optimal poses that may lead to unexpected behavior. Redundant DoF can also affect joint accelerations and jerk, potentially causing excessive wear on parts and resulting in more downtime and sub-optimal part quality. Additionally, other factors such as extension control, precision, and energy usage are mentioned, and their impact on the manufacturing process is discussed.

The aim of this thesis (Chapter 1.3) is to propose and validate a systematic approach to leveraging these redundant DoFs in order to optimize towards a user-defined goal. Currently, there is no publication available that presents a general solution to this problem.

Chapter 2 provides a comprehensive discussion on the state of science and technology, aiming to provide a clear understanding of the individual components of manufacturing systems and optimization algorithms. Both subtractive and additive manufacturing are examined in detail, including a review of their respective strengths and weaknesses. An important focus is placed on one of the common processes in additive manufacturing, namely WAAM, which has a significant relationship with industrial robots. In Chapter 2.1.3, the functionality of these robots is described in detail, with special attention given to the issue of redundancy in such robotic systems. Chapter 2.4 focuses on a comparative analysis of published research papers related to singularity avoidance, optimization of joint acceleration and jerk, optimization of energy use, and optimization of stiffness. Each section highlights the available options and approaches for leveraging redundant DoFs to achieve improved performance in these specific areas. The examination of multiple methods serves as the foundation for understanding the current state of cutting-edge research and identifying any existing research gaps. Thus far, no global optimization approach has been proposed that can consider a user-defined input with specified goals, based on multiple process variables, and providing the optimal settings

for the redundant DoFs. This represents an important research opportunity in the field.

Chapter 3 presents a solution for the identified research gap. In order to address this problem, a carefully selected list of process variables is introduced and thoroughly discussed. These variables can be derived from the movement of a robots' arm and includes variables such as the rotational position of joints over time, as well as their subsequent derivatives and direction changes. After summarizing which process variables can be extracted from a toolpath traversed by a industrial robot, the two main parts of the method are validated. The validation process involves constructing a mathematical model that represents an industrial robot. Additionally, three artificial toolpaths are generated for the robot model to traverse. These toolpaths are defined in five DoFs, while the 6th DoF, rotation around the Z-axis, is not defined and can be chosen freely. The range of rotation is set from  $-135^\circ$  to  $+135^\circ$ , divided into  $5^\circ$  increments. For each possible setting of the rotation around the Z-axis, the inverse kinematics algorithm calculates the joint positions over time required to traverse the toolpaths. Subsequently, the process variables are extracted and compared. Based on their numerical values and user-defined importance factors, the global score for each setting is calculated. The same process is then performed on a larger production-grade toolpath. This approach allows for the analysis of different settings for the redundant DoF and the identification of the most optimal one. The same process is used to analyze the results when two different redundant DoFs are present. The first redundancy is in the form of the rotation around the Z-axis, and the second one is introduced as the tilting of a rotary-tilt table. In this scenario, the goal is to analyze how each combination of the two redundant DoFs affects the analyzed process variables. The resulting scores are shown in the form of a matrix. The matrices for the three different toolpaths exhibit different characteristics but generally result in a fairly smooth surface.

The second step in the presented method involves the optimization of the redundant DoF. Instead of calculating the joint positions for every possible setting, a PSO algorithm is utilized. This implementation saves a significant amount of time and has the capability to quickly converge to the global optima. The population size is set to 20, and the iterations are capped at five. As mentioned in the discussion of the results, the performance of the PSO algorithm depends on the initial positions of the individual particles. One of the proposed goals mentioned in the task for this thesis is the implementation of the optimization loop in CAM. This implementation would allow for the validation of the described optimization process in Chapter 3.7.2. However, due to the limited time-frame of the thesis and the unavailability of a developer version of the selected CAM software with the necessary API, this goal could not be achieved.

## 5.2 Outlook

This work focuses only on a select number of process variables, but this selection can be expanded to further optimize the real-world manufacturing process. One potential additional variable that can be optimized, is the stiffness value of the robotic system based on its current pose. Maintaining high stiffness in the orthogonal cutting direction is crucial for minimizing deviations. Low stiffness combined with high contact forces can result in significant dimensional errors. Finite-element analysis or multi-body simulation can be used to determine the stiffness value and optimize it for better performance by specifically constraining the redundant DoF.

Another important variable for future research is the collision index. The collision index is used to identify potential collisions between any part of the robot or the end-effector and the workpieces or other objects in the environment. This variable is particularly significant in scenarios involving WAAM systems, where loose wires can change their position depending on the robots pose. Preventing collisions is essential to avoid damage to the workpiece, the robot, or other equipment. As of now the optimization algorithm does not consider this possibility.

One area where the PSO optimization process can lead to significant advantages is section-wise optimization. The toolpath can be divided into sections, and for each section, the optimal settings of the redundant DoF can be determined. To make this approach work effectively, it is important to consider the boundary conditions at the transition points between the individual sections. Furthermore, implementing the proposed method in a CAM software can provide faster computation and enable the optimization of more complex toolpaths. Another option to speed up the computation is to program the algorithm in such a way that it is designed for multi-threading. Such implementation can result in significantly faster optimization.

Moving forward, it is necessary to conduct further validation processes, including real-world tests and simulations, to evaluate the performance and verify the effectiveness of the proposed methodology. Additionally, exploring the implementation of ML techniques for best-case calculations could be a valuable avenue for future research.



# List of Figures

2.1	3-Axis CNC Machine ( <i>CNC Masters</i> 2022) . . . . .	7
2.2	5-Axis CNC Machine ( <i>Manufacturing Guide</i> 2023) . . . . .	8
2.3	Schematic representation of WAAM ( <i>Chaurasia et al.</i> 2021) . . . . .	11
2.4	Part produced by WAAM with post machining ( <i>Lortek</i> 2023) . . . . .	11
2.5	Current and Voltage wave forms of a CMT process ( <i>Selvi et al.</i> 2018) . . . . .	12
2.6	Individual sections of a CMT cycle ( <i>Dalton</i> 2024) . . . . .	13
2.7	SCARA robot ( <i>Epson</i> 2024) . . . . .	14
2.8	Delta robot ( <i>Weiss</i> 2024) . . . . .	14
2.9	6-DoF industrial robot ( <i>Hoai Nam et al.</i> 2018) . . . . .	16
2.10	Industrial robots with an additional linear axis ( <i>KUKA</i> 2023) . . . . .	17
2.11	7-DoF robot ( <i>Hagane et al.</i> 2022) . . . . .	17
2.12	Desired path with constant velocity ( <i>Siemens</i> 2024) . . . . .	19
2.13	Influence of G-Code commands G64 and G60 ( <i>Siemens</i> 2024) . . . . .	19
2.14	Predetermined deviation of the programmed path ( <i>Siemens</i> 2024) . . . . .	20
2.15	Influence of commands G601 and G602 ( <i>Siemens</i> 2024) . . . . .	20
2.16	Interface of Siemens NX (NX 2015) . . . . .	23
2.17	Three exemplary tool paths for iso-planar milling ( <i>Zhao et al.</i> 2018) . . . . .	24
2.18	Passing through a wrist singularity ( <i>Mecademic Industrial Robotics</i> 2023) . . . . .	26
3.1	Interdependence of various parameters and elements . . . . .	33
3.2	Parameter flowchart . . . . .	37
3.3	Calculation of the local score through variation . . . . .	38
3.4	Variations of a process variable with low standard deviation . . . . .	39
3.5	Variations of a process variable with high standard deviation . . . . .	39
3.6	Additional information for angular position of each joint . . . . .	40

3.7 Two option for recording the joint position in a time-series . . . . .	41
3.8 Summing up the rotation in the clockwise and anti-clockwise direction . . . . .	41
3.9 Calculating direction changes from a time-series . . . . .	42
3.10 Two time-series with equal number of direction changes but different characteristics . . . . .	43
3.11 Hard and soft limits with desired range . . . . .	44
3.12 Calculating velocity from the joint position over time . . . . .	45
3.13 Overstepping the threshold value . . . . .	45
3.14 Exemplary methods for energy usage calculations . . . . .	47
3.15 Turn-on and turn-off points in the G-code used in WAAM . . . . .	48
3.16 Rotation around the C-axis of a welding torch . . . . .	49
3.17 Two examples for optimal alignments along a vector in 2D . . . . .	50
3.18 Example of optimal and non-optimal tilt in the welding torch . . . . .	52
3.19 Evaluation of a toolpath . . . . .	53
3.20 Process of evaluating a defined boundary condition . . . . .	54
3.21 Schematic process of optimization without CAM software in the loop . . . . .	56
3.22 Variation of the redundant DoF in the G-code . . . . .	57
3.23 Schematic process of optimization with CAM software in the loop . . . . .	58
4.1 Schematics of the modeled robot . . . . .	62
4.2 Visualization of the modeled robot in Python . . . . .	63
4.3 Toolpath 1: Converging spiral . . . . .	64
4.4 Toolpath 2: Converging infinity loop . . . . .	64
4.5 Toolpath 3: Forward moving pendulum oscillation . . . . .	65
4.6 Traversing toolpath 1 with the modeled robot . . . . .	65
4.7 Visualization of the joint positions over time for toolpath 1 with C=0° . . . . .	66
4.8 Visualization of the joint positions over time for toolpath 1 with C=45° . . . . .	67
4.9 Visualization of the joint positions over time for toolpath 2 . . . . .	67
4.10 Visualization of the joint positions over time for toolpath 3 . . . . .	68
4.11 Toolpath 1 with A=0°, B=0° and C=-45° . . . . .	69
4.12 Toolpath 1 with A=0°, B=0° and C=45° . . . . .	69
4.13 Local scores of each process variable for toolpath 1 . . . . .	69

4.14 Global score for toolpath 1 . . . . .	70
4.15 Global and local scores in toolpath 2 depending on the rotation around Z . . . . .	71
4.16 Global and local scores in toolpath 3 depending on the rotation around Z . . . . .	71
4.17 Organic toolpath ( <i>Reisch 2023</i> ) . . . . .	72
4.18 Global and local score for WAAM toolpath . . . . .	73
4.19 Global score for production toolpath . . . . .	74
4.20 Toolpath 3 with no rotation around the X-axis . . . . .	75
4.21 Toolpath 3 with a rotation of 25 degrees around the X-axis . . . . .	75
4.22 Robot following the tilted toolpath 3 . . . . .	76
4.23 Hyperplane representing the global score of toolpath 3 . . . . .	77
4.24 Hyperplane representing the global score of toolpath 1 . . . . .	78
4.25 Hyperplane representing the global score of toolpath 2 . . . . .	79
4.26 Distributed of particles at their initial positions . . . . .	81
4.27 PSO Iteration 2 on toolpath 3 . . . . .	82
4.28 PSO Iteration 3 on toolpath 3 . . . . .	82
4.29 PSO Iteration 4 on toolpath 3 . . . . .	82
4.30 PSO Iteration 5 on toolpath 3 . . . . .	82
4.31 PSO-Loop . . . . .	83
4.32 PSO Iteration 1 on toolpath 3 . . . . .	84
4.33 PSO Iteration 2 on toolpath 3 . . . . .	84
4.34 PSO Iteration 3 on toolpath 3 . . . . .	84
4.35 PSO Iteration 4 on toolpath 3 . . . . .	84
4.36 PSO iteration 5 on toolpath 3 . . . . .	85
4.37 PSO Iteration 1 on toolpath 1 . . . . .	86
4.38 PSO Iteration 5 on toolpath 1 . . . . .	86
4.39 PSO Iteration 1 on toolpath 2 . . . . .	86
4.40 PSO Iteration 5 on toolpath 2 . . . . .	86



## Bibliography

- ABDULHAMEED, O., AL-AHMARI, A., AMEEN, W., and MIAN, S. H., (2019). “Additive manufacturing: Challenges, trends, and applications”. In: *Advances in Mechanical Engineering* 11.2. DOI: 10.1177/1687814018822880.
- AHANGAR, S., MEHRABANI, M. V., POURANSARI SHORIJEH, A., and MASOULEH, M. T., (2019). “Design a 3-DOF Delta Parallel Robot by One Degree Redundancy along the Conveyor Axis, A Novel Automation Approach”. In: *2019 5th Conference on Knowledge Based Engineering and Innovation (KBEI)*. IEEE. DOI: 10.1109/kbei.2019.8734975.
- AMANULLAH, A., MURSHIDUZZAMAN, SALEH, T., and KHAN, R., (2017). “Design and Development of a Hybrid Machine Combining Rapid Prototyping and CNC Milling Operation”. In: 1877-7058 184, pp. 163–170. ISSN: 1877-7058. DOI: 10.1016/j.proeng.2017.04.081.
- ANJUM, Z., SAMO, S., NIGHAT, A., NISA, A. U., SOOMRO, M. A., and ALAYI, R., (2022). “Design and Modeling of 9 Degrees of Freedom Redundant Robotic Manipulator”. In: *Journal of Robotics and Control (JRC)* 3.6, pp. 800–808. ISSN: 2715-5056. DOI: 10.18196/jrc.v3i6.15958. URL: <https://journal.umy.ac.id/index.php/jrc/article/view/15958>.
- ASLAN, D. and ALTINTAS, Y., (2018). “On-line chatter detection in milling using drive motor current commands extracted from CNC”. In: *International Journal of Machine Tools and Manufacture* 132, pp. 64–80. ISSN: 0890-6955. DOI: 10.1016/j.ijmachtools.2018.04.007. URL: <https://www.sciencedirect.com/science/article/pii/s0890695518300841>.
- ATTARAN, M., (2017). “The rise of 3-D printing: The advantages of additive manufacturing over traditional manufacturing”. In: *Business Horizons* 60.5, pp. 677–688. ISSN: 0007-6813. DOI: 10.1016/j.bushor.2017.05.011. URL: <https://www.sciencedirect.com/science/article/pii/s0007681317300897>.
- AYTEN, K. K., SAHINKAYA, M. N., and DUMLU, A., (2016). “Optimum Trajectory Generation for Redundant/Hyper-Redundant Manipulators”. In: *IFAC-PapersOnLine* 49.21, pp. 493–500. ISSN: 2405-8963. DOI: 10.1016/j.ifacol.2016.10.651. URL: <https://www.sciencedirect.com/science/article/pii/s2405896316322637>.
- BÄCK, T. and SCHWEFEL, H.-P., (1993). “An Overview of Evolutionary Algorithms for Parameter Optimization”. In: *Evolutionary Computation* 1.1, pp. 1–23. ISSN: 1063-6560. DOI: 10.1162/evco.1993.1.1.1.
- BANDYOPADHYAY, A., (2020). *Additive Manufacturing, Second Edition*. 2nd ed. Milton: Taylor & Francis Group. ISBN: 9780429881022.

- BEDROSSIAN, N. S., (2002). "Classification of singular configurations for redundant manipulators". In: *Proceedings, IEEE International Conference on Robotics and Automation*. New York: IEEE, pp. 818–823. ISBN: 0-8186-9061-5. DOI: 10.1109/ROBOT.1990.126089.
- BI, Z., (2021). "Computer-Aided Manufacturing (CAM)". In: *Practical Guide to Digital Manufacturing*. Springer, Cham, pp. 223–320. DOI: 10.1007/978-3-030-70304-2{\textunderscore}4. URL: [https://link.springer.com/chapter/10.1007/978-3-030-70304-2\\_4](https://link.springer.com/chapter/10.1007/978-3-030-70304-2_4).
- BI, Z. and WANG, X., (2020). *Computer aided design and manufacturing*. 1st edition. Wiley-ASME press series. Hoboken, New Jersey and West Sussex, England: Wiley and ASME Press. ISBN: 9781119534211.
- BIBBY, L. and DEHE, B., (2018). "Defining and assessing industry 4.0 maturity levels – case of the defence sector". In: *Production Planning & Control* 29.12, pp. 1030–1043. DOI: 10.1080/09537287.2018.1503355.
- BILLARD, A. and KRAGIC, D., (2019). "Trends and challenges in robot manipulation". In: *Science* 364.6446. DOI: 10.1126/science.aat8414.
- BONEV, I., (2001). *Delta parallel robot-the story of success*. Newsletter, available at <http://www.parallelmic.org>. URL: <http://www.robotics.caltech.edu/~jwb/courses/me115/handouts/deltarobothistory.pdf>.
- BOSCAROLI, P., CARACCIOLI, R., RICHIEDEI, D., and TREVISANI, A., (2020). "Energy Optimization of Functionally Redundant Robots through Motion Design". In: *Applied Sciences* 10.9, p. 3022. DOI: 10.3390/app10093022.
- BOSCAROLI, P. and RICHIEDEI, D., (2019). "Energy Saving in Redundant Robotic Cells: Optimal Trajectory Planning". In: Springer, Cham, pp. 268–275. DOI: 10.1007/978-3-030-00365-4{\textunderscore}32. URL: [https://link.springer.com/chapter/10.1007/978-3-030-00365-4\\_32](https://link.springer.com/chapter/10.1007/978-3-030-00365-4_32).
- BOSE, S., KE, D., SAHASRABUDHE, H., and BANDYOPADHYAY, A., (2018). "Additive manufacturing of biomaterials". In: *Progress in materials science* 93, pp. 45–111. ISSN: 0079-6425. DOI: 10.1016/j.pmatsci.2017.08.003.
- BOSSCHER, P. and HEDMAN, D., (2011). "Real-time collision avoidance algorithm for robotic manipulators". In: *Industrial Robot: An International Journal* 38.2, pp. 186–197. DOI: 10.1108/01439911111106390. URL: <https://www.emerald.com/insight/content/doi/10.1108/01439911111106390/full/pdf>.
- BOUJELBENE, M., MOISAN, A., TOUNSI, N., and BRENIER, B., (2004). "Productivity enhancement in dies and molds manufacturing by the use of C1 continuous tool path". In: *International Journal of Machine Tools and Manufacture* 44.1, pp. 101–107. ISSN: 0890-6955. DOI: 10.1016/j.ijmachtools.2003.08.005.
- BRECHER, C. and LOHSE, W., (2013). "Evaluation of toolpath quality: User-assisted CAM for complex milling processes". In: *CIRP Journal of Manufacturing Science and Technology* 6.4, pp. 233–245. ISSN: 1755-5817. DOI: 10.1016/j.cirpj.2013.07.002. URL: <https://www.sciencedirect.com/science/article/pii/s1755581713000539>.
- BUI, H., PIERSON, H. A., NURRE, S. G., and SULLIVAN, K. M., (2019). "Tool Path Planning Optimization for Multi-Tool Additive Manufacturing". In: *2351-9789* 39, pp. 457–464.

- ISSN: 2351-9789. DOI: 10.1016/j.promfg.2020.01.389. URL: <https://www.sciencedirect.com/science/article/pii/s2351978920304601>.
- CALLEJA, A., BO, P., GONZÁLEZ, H., BARTOŇ, M., and LÓPEZ DE LACALLE, LUIS NORBERTO, (2018). "Highly accurate 5-axis flank CNC machining with conical tools". In: *The International Journal of Advanced Manufacturing Technology* 97.5-8, pp. 1605–1615. ISSN: 1433-3015. DOI: 10.1007/s00170-018-2033-7. URL: <https://link.springer.com/article/10.1007/s00170-018-2033-7>.
- Chaurasia *et al.* (2021). Mayank Chaurasia and Manoj Kumar Sinha: Investigations on Process Parameters of Wire Arc Additive Manufacturing (WAAM): A Review. URL: [https://www.researchgate.net/publication/348465062\\_Investigations\\_on\\_Process\\_Parameters\\_of\\_Wire\\_Arc\\_Additive\\_Manufacturing\\_WAAM\\_A\\_Review](https://www.researchgate.net/publication/348465062_Investigations_on_Process_Parameters_of_Wire_Arc_Additive_Manufacturing_WAAM_A_Review).
- CHEN-GANG, LI-TONG, CHU-MING, XUAN, J.-Q., and XU, S.-H., (2014). "Review on kinematics calibration technology of serial robots". In: *International Journal of Precision Engineering and Manufacturing* 15.8, pp. 1759–1774. ISSN: 2005-4602. DOI: 10.1007/s12541-014-0528-1. URL: <https://link.springer.com/article/10.1007/s12541-014-0528-1>.
- CNC Masters (2022). CNC Machine Buyer's Guide: Types, Uses, Price, & Definitions. URL: <https://www.cncmasters.com/cnc-machine-buyers-guide/>.
- CONG, B., OUYANG, R., QI, B., and DING, J., (2016). "Influence of Cold Metal Transfer Process and Its Heat Input on Weld Bead Geometry and Porosity of Aluminum-Copper Alloy Welds". In: *Rare Metal Materials and Engineering* 45.3, pp. 606–611. ISSN: 1875-5372. DOI: 10.1016/S1875-5372(16)30080-7. URL: <https://www.sciencedirect.com/science/article/pii/s1875537216300807>.
- CUNNINGHAM, C. R., FLYNN, J. M., SHOKRANI, A., DHOKIA, V., and NEWMAN, S. T., (2018). "Invited review article: Strategies and processes for high quality wire arc additive manufacturing". In: *Additive Manufacturing* 22, pp. 672–686. ISSN: 2214-8604. DOI: 10.1016/j.addma.2018.06.020. URL: <https://www.sciencedirect.com/science/article/pii/s2214860418303920>.
- CVITANIC, T., NGUYEN, V., and MELKOTE, S. N., (2020). "Pose optimization in robotic machining using static and dynamic stiffness models". In: *Robotics and Computer-Integrated Manufacturing* 66, p. 101992. ISSN: 0736-5845. DOI: 10.1016/j.rcim.2020.101992. URL: <https://www.sciencedirect.com/science/article/pii/s0736584520302039>.
- DAI, C., LEFEBVRE, S., YU, K.-M., GERAEDTS, J. M. P., and WANG, C. C. L., (2020). "Planning Jerk-Optimized Trajectory With Discrete Time Constraints for Redundant Robots". In: *IEEE Transactions on Automation Science and Engineering* 17.4, pp. 1711–1724. ISSN: 1545-5955. DOI: 10.1109/TASE.2020.2974771.
- Dalton (2024). Imaging CMT Welding with a Weld Camera and Last Access: 05.01.2024. URL: <https://blog.xiris.com/blog/imaging-cmt-welding-with-a-weld-camera>;
- DAS, M. T. and CANAN DÜLGER, L., (2005). "Mathematical modelling, simulation and experimental verification of a scara robot". In: *Simulation Modelling Practice and Theory* 13.3, pp. 257–271. ISSN: 1569-190X. DOI: 10.1016/j.simpat.2004.11.004. URL: <https://www.sciencedirect.com/science/article/pii/s1569190x04001200>.

- DILBEROGLU, U. M., GHAREHPAPAGH, B., YAMAN, U., and DOLEN, M., (2017). “The Role of Additive Manufacturing in the Era of Industry 4.0”. In: *Procedia Manufacturing* 11, pp. 545–554. ISSN: 2351-9789. DOI: 10.1016/j.promfg.2017.07.148. URL: <https://www.sciencedirect.com/science/article/pii/s2351978917303529>.
- DIN EN ISO/ASTM 52900, (2022). In: *Additive Fertigung - Grundlagen - Terminologie (ISO/ASTM 52900:2021); Deutsche Fassung EN ISO/ASTM 52900:2021*. DOI: 10.31030/3290011.
- DING, D., PAN, Z., CUIURI, D., and LI, H., (2015). “Wire-feed additive manufacturing of metal components: technologies, developments and future interests”. In: *The International Journal of Advanced Manufacturing Technology* 81.1-4, pp. 465–481. ISSN: 1433-3015. DOI: 10.1007/s00170-015-7077-3. URL: <https://link.springer.com/article/10.1007/s00170-015-7077-3>.
- DOAN, N. C. N., TAO, P. Y., and LIN, W., (2016). “Optimal redundancy resolution for robotic arc welding using modified particle swarm optimization”. In: *2016 IEEE International Conference on Advanced Intelligent Mechatronics (AIM)*. IEEE. DOI: 10.1109/aim.2016.7576826.
- DOMAE, Y., (2019). “Recent Trends in the Research of Industrial Robots and Future Outlook”. In: *Journal of Robotics and Mechatronics* 31.1, pp. 57–62. ISSN: 1883-8049. DOI: 10.20965/jrm.2019.p0057. URL: [https://www.jstage.jst.go.jp/article/jrobomech/31/1/31\\_57/\\_article/-char/ja/](https://www.jstage.jst.go.jp/article/jrobomech/31/1/31_57/_article/-char/ja/).
- DUBOVSKA, R., JAMBOR, J., and MAJERIK, J., (2014). “Implementation of CAD/CAM System CATIA V5 in Simulation of CNC Machining Process”. In: *1877-7058* 69, pp. 638–645. ISSN: 1877-7058. DOI: 10.1016/j.proeng.2014.03.037. URL: <https://www.sciencedirect.com/science/article/pii/s1877705814002835>.
- DUONG, X. B., (2021). “On the Effect of the End-effector Point Trajectory on the Joint Jerk of the Redundant Manipulators”. In: *Journal of Applied and Computational Mechanics* 7.3, pp. 1575–1582. ISSN: 2383-4536. DOI: 10.22055/jacm.2021.35350.2635. URL: [https://jacm.scu.ac.ir/article\\_16660.html](https://jacm.scu.ac.ir/article_16660.html).
- DUTRA, J. C., GONÇALVES E SILVA, R. H., and MARQUES, C., (2015). “Melting and welding power characteristics of MIG–CMT versus conventional MIG for aluminium 5183”. In: *Welding International* 29.3, pp. 181–186. DOI: 10.1080/09507116.2014.932974.
- Epson (2024). Epson SCARA LS10-B802S/RC-90B | SCARA Robots | Roboter | Produkte | Epson Deutschland and Last Access: 05.01.2024. URL: [https://www.epson.de/de\\_DE/produkte/roboter/scara-robots/epson-scara-ls10-b802s-rc-90b/p/28174](https://www.epson.de/de_DE/produkte/roboter/scara-robots/epson-scara-ls10-b802s-rc-90b/p/28174).
- ERDŐS, G., KOVÁCS, A., and VÁNCZA, J., (2016). “Optimized joint motion planning for redundant industrial robots”. In: *CIRP Annals* 65.1, pp. 451–454. ISSN: 00078506. DOI: 10.1016/j.cirp.2016.04.024. URL: <https://www.sciencedirect.com/science/article/pii/s0007850616300245>.
- FALUDI, J., BAYLEY, C., BHOGAL, S., and IRIBARNE, M., (2015). “Comparing environmental impacts of additive manufacturing vs traditional machining via life-cycle assessment”. In: *Rapid Prototyping Journal* 21.1, pp. 14–33. DOI: 10.1108/RPJ-07-2013-0067. URL: <https://www.emerald.com/insight/content/doi/10.1108/rpj-07-2013-0067/full/pdf>.

- FARIA, C., FERREIRA, F., ERLHAGEN, W., MONTEIRO, S., and BICHO, E., (2018). “Position-based kinematics for 7-DoF serial manipulators with global configuration control, joint limit and singularity avoidance”. In: *Mechanism and Machine Theory* 121, pp. 317–334. ISSN: 0094-114X. DOI: 10.1016/j.mechmachtheory.2017.10.025. URL: <https://www.sciencedirect.com/science/article/pii/s0094114x17306559>.
- FELDHAUSEN, T., HEINRICH, L., SALEEBY, K., BURL, A., POST, B., MACDONALD, E., SALDANA, C., and LOVE, L., (2022). “Review of Computer-Aided Manufacturing (CAM) strategies for hybrid directed energy deposition”. In: *Additive Manufacturing* 56, p. 102900. ISSN: 2214-8604. DOI: 10.1016/j.addma.2022.102900.
- GADALETÀ, M., PELLICCIARI, M., and BERSELLI, G., (2019). “Optimization of the energy consumption of industrial robots for automatic code generation”. In: *Robotics and Computer-Integrated Manufacturing* 57, pp. 452–464. ISSN: 0736-5845. DOI: 10.1016/j.rcim.2018.12.020. URL: <https://www.sciencedirect.com/science/article/pii/s0736584518301856>.
- GASPARETTO, A. and ZANOTTO, V., (2010). “Optimal trajectory planning for industrial robots”. In: *Advances in Engineering Software* 41.4, pp. 548–556. ISSN: 0965-9978. DOI: 10.1016/j.advengsoft.2009.11.001. URL: <https://www.sciencedirect.com/science/article/pii/s0965997809002464>.
- GHOBAKHLOO, M., (2020). “Industry 4.0, digitization, and opportunities for sustainability”. In: *Journal of Cleaner Production* 252, p. 119869. ISSN: 0959-6526. DOI: 10.1016/j.jclepro.2019.119869. URL: <https://www.sciencedirect.com/science/article/pii/s0959652619347390>.
- GIORGIO BORT, C. M., LEONESIO, M., and BOSETTI, P., (2016). “A model-based adaptive controller for chatter mitigation and productivity enhancement in CNC milling machines”. In: *Robotics and Computer-Integrated Manufacturing* 40, pp. 34–43. ISSN: 0736-5845. DOI: 10.1016/j.rcim.2016.01.006. URL: <https://www.sciencedirect.com/science/article/pii/s0736584516300242>.
- GOEL, R. and GUPTA, P., (2020). “Robotics and Industry 4.0”. In: *A Roadmap to Industry 4.0: Smart Production, Sharp Business and Sustainable Development*. Springer, Cham, pp. 157–169. DOI: 10.1007/978-3-030-14544-6\_9. URL: [https://link.springer.com/chapter/10.1007/978-3-030-14544-6\\_9](https://link.springer.com/chapter/10.1007/978-3-030-14544-6_9).
- GU, X. and KOREN, Y., (2018). “Manufacturing system architecture for cost-effective mass-individualization”. In: *Manufacturing Letters* 16, pp. 44–48. ISSN: 2213-8463. DOI: 10.1016/j.mfglet.2018.04.002. URL: <https://www.sciencedirect.com/science/article/pii/s2213846317300974>.
- Hagane et al. (2022). Hagane, Shohei and Venture, Gentiane: Robotic Manipulator’s Expressive Movements Control Using Kinematic Redundancy. DOI: 10.3390/machines10121118.
- HÄGELE, M., NILSSON, K., PIRES, J. N., and BISCHOFF, R., (2016). “Industrial Robotics”. In: *Springer Handbook of Robotics*. Springer, Cham, pp. 1385–1422. DOI: 10.1007/978-3-319-32552-1\_54. URL: [https://link.springer.com/chapter/10.1007/978-3-319-32552-1\\_54](https://link.springer.com/chapter/10.1007/978-3-319-32552-1_54).

- HALEEM, A. and JAVAID, M., (2019). "Additive Manufacturing Applications in Industry 4.0: A Review". In: *Journal of Industrial Integration and Management* 04.04, p. 1930001. ISSN: 2424-8622. DOI: 10.1142/S2424862219300011.
- HALEVI, Y., CARPANZANO, E., MONTALBANO, G., and KOREN, Y., (2011). "Minimum energy control of redundant actuation machine tools". In: *CIRP Annals* 60.1, pp. 433–436. ISSN: 00078506. DOI: 10.1016/j.cirp.2011.03.032.
- HANAFUSA, H., YOSHIKAWA, T., and NAKAMURA, Y., (1981). "Analysis and Control of Articulated Robot Arms with Redundancy". In: *IFAC Proceedings Volumes* 14.2, pp. 1927–1932. ISSN: 1474-6670. DOI: 10.1016/S1474-6670(17)63754-6. URL: <https://www.sciencedirect.com/science/article/pii/s1474667017637546>.
- HEIMANN, O. and GUHL, J., (2020). "Industrial Robot Programming Methods: A Scoping Review". In: *2020 25th IEEE International Conference on Emerging Technologies and Factory Automation (ETFA)*. IEEE. DOI: 10.1109/etfa46521.2020.9211997.
- HESSE, D. F. and MARKERT, B., (2019). "Tool wear monitoring of a retrofitted CNC milling machine using artificial neural networks". In: *Manufacturing Letters* 19, pp. 1–4. ISSN: 2213-8463. DOI: 10.1016/j.mfglet.2018.11.001. URL: <https://www.sciencedirect.com/science/article/pii/s2213846318301524>.
- HEYER, C., (2010). "Human-robot interaction and future industrial robotics applications". In: *2010 IEEE/RSJ International Conference on Intelligent Robots and Systems*. IEEE. DOI: 10.1109/iros.2010.5651294.
- Hoai Nam et al. (2018). Huynh Hoai Nam, Edouard Riviere, and Olivier Verlinden: Multi-body modelling of a flexible 6-axis robot dedicated to robotic machining. URL: [https://www.researchgate.net/profile/huynh-hoai-nam/publication/326106790\\_multibody\\_modelling\\_of\\_a\\_flexible\\_6-axis\\_robot\\_dedicated\\_to\\_robotic\\_machining](https://www.researchgate.net/profile/huynh-hoai-nam/publication/326106790_multibody_modelling_of_a_flexible_6-axis_robot_dedicated_to_robotic_machining).
- HUO, L. and BARON, L., (2008). "The joint-limits and singularity avoidance in robotic welding". In: *Industrial Robot: An International Journal* 35.5, pp. 456–464. DOI: 10.1108/01439910810893626. URL: <https://www.emerald.com/insight/content/doi/10.1108/01439910810893626/full/pdf>.
- HUYNH, H. N., ASSADI, H., RIVIÈRE-LORPHÈVRE, E., VERLINDEN, O., and AHMADI, K., (2020). "Modelling the dynamics of industrial robots for milling operations". In: *Robotics and Computer-Integrated Manufacturing* 61, p. 101852. ISSN: 0736-5845. DOI: 10.1016/j.rcim.2019.101852. URL: <https://www.sciencedirect.com/science/article/pii/s0736584519301784>.
- IGLESIAS, I., SEBASTIÁN, M. A., and ARES, J. E., (2015). "Overview of the State of Robotic Machining: Current Situation and Future Potential". In: *1877-7058* 132, pp. 911–917. ISSN: 1877-7058. DOI: 10.1016/j.proeng.2015.12.577. URL: <https://www.sciencedirect.com/science/article/pii/s1877705815044896>.
- IQBAL, A., ZHAO, G., SUHAIMI, H., HE, N., HUSSAIN, G., and ZHAO, W., (2020). "Readiness of subtractive and additive manufacturing and their sustainable amalgamation from the perspective of Industry 4.0: a comprehensive review". In: *The International Journal of Advanced Manufacturing Technology* 111.9-10, pp. 2475–2498. ISSN: 1433-3015. DOI: 10.1007/s00170-020-06287-6. URL: <https://link.springer.com/article/10.1007/s00170-020-06287-6>.

- IVÁNTABERNERO, PASKUAL, A., ÁLVAREZ, P., and SUÁREZ, A., (2018). “Study on Arc Welding Processes for High Deposition Rate Additive Manufacturing”. In: 2212-8271 68, pp. 358–362. ISSN: 2212-8271. DOI: 10.1016/j.procir.2017.12.095. URL: <https://www.sciencedirect.com/science/article/pii/s2212827117310363>.
- JAIN, R., NAYAB ZAFAR, M., and MOHANTA, J. C., (2019). “Modeling and Analysis of Articulated Robotic Arm for Material Handling Applications”. In: *IOP Conference Series: Materials Science and Engineering* 691.1, p. 012010. ISSN: 1757-899X. DOI: 10.1088/1757-899X/691/1/012010. URL: <https://iopscience.iop.org/article/10.1088/1757-899x/691/1/012010/meta>.
- JANDYAL, A., CHATURVEDI, I., WAZIR, I., RAINA, A., and UL HAQ, M. I., (2022). “3D printing – A review of processes, materials and applications in industry 4.0”. In: 2666-4127 3, pp. 33–42. ISSN: 2666-4127. DOI: 10.1016/j.susoc.2021.09.004. URL: <https://www.sciencedirect.com/science/article/pii/s2666412721000441>.
- JAYAWARDANE, H., DAVIES, I. J., GAMAGE, J. R., JOHN, M., and BISWAS, W. K., (2023). “Sustainability perspectives – a review of additive and subtractive manufacturing”. In: *Sustainable Manufacturing and Service Economics* 2, p. 100015. ISSN: 2667-3444. DOI: 10.1016/j.smse.2023.100015.
- JI, W. and WANG, L., (2019). “Industrial robotic machining: a review”. In: *The International Journal of Advanced Manufacturing Technology* 103.1-4, pp. 1239–1255. ISSN: 1433-3015. DOI: 10.1007/s00170-019-03403-z. URL: <https://link.springer.com/article/10.1007/s00170-019-03403-z>.
- JIA, Z.-y., MA, J.-w., SONG, D.-n., WANG, F.-j., and LIU, W., (2018). “A review of contouring-error reduction method in multi-axis CNC machining”. In: *International Journal of Machine Tools and Manufacture* 125, pp. 34–54. ISSN: 0890-6955. DOI: 10.1016/j.ijmachtools.2017.10.008.
- JIANG, L., LU, S., GU, Y., and ZHAO, J., (2017). “Time-Jerk Optimal Trajectory Planning for a 7-DOF Redundant Robot Using the Sequential Quadratic Programming Method”. In: 2017, pp. 343–353. DOI: 10.1007/978-3-319-65298-6\_32.
- JOSHI, K., MELKOTE, S. N., ANDERSON, M., and CHAUDHARI, R., (2021). “Investigation of cycle time behavior in the robotic grinding process”. In: *CIRP Journal of Manufacturing Science and Technology* 35, pp. 315–322. ISSN: 1755-5817. DOI: 10.1016/j.cirpj.2021.06.021. URL: <https://www.sciencedirect.com/science/article/pii/s1755581721001139>.
- JUNG, J. H. and LIM, D.-G., (2020). “Industrial robots, employment growth, and labor cost: A simultaneous equation analysis”. In: 0040-1625 159, p. 120202. ISSN: 0040-1625. DOI: 10.1016/j.techfore.2020.120202. URL: <https://www.sciencedirect.com/science/article/pii/s0040162520310283>.
- KADAM, O. B., PIRAYESH, A., and FATAHI VALILAI, O., (2023). “Technological Insights of Interoperable Models for Integration of CAD/PLM/PDM and ERP Modules in Engineering Change Management”. In: Springer, Cham, pp. 556–564. DOI: 10.1007/978-3-031-17629-6\_58. URL: [https://link.springer.com/chapter/10.1007/978-3-031-17629-6\\_58](https://link.springer.com/chapter/10.1007/978-3-031-17629-6_58).

- KAPPMEYER, G. and NOVOMIC, D., (2021). "Production technology research – Building blocks for competitiveness and solution for future challenges in aerospace component manufacturing". In: *2212-8271* 101, pp. 62–68. ISSN: 2212-8271. DOI: 10.1016/j.procir.2020.09.189. URL: <https://www.sciencedirect.com/science/article/pii/s2212827121006570>.
- KATOCH, S., CHAUHAN, S. S., and KUMAR, V., (2021). "A review on genetic algorithm: past, present, and future". In: *Multimedia Tools and Applications* 80.5, pp. 8091–8126. ISSN: 1573-7721. DOI: 10.1007/s11042-020-10139-6. URL: <https://link.springer.com/article/10.1007/s11042-020-10139-6>.
- KIM, H. S. and TSAI, L.-W., (2003). "Design Optimization of a Cartesian Parallel Manipulator". In: *Journal of Mechanical Design* 125.1, pp. 43–51. ISSN: 1050-0472. DOI: 10.1115/1.1543977.
- KIRÉANSKI, M. V. and PETROVIÉ, T. M., (1993). "Combined Analytical- Pseudoinverse Inverse Kinematic Solution for Simple Redundant Manipulators and Singularity Avoidance". In: *The International Journal of Robotics Research* 12.2, pp. 188–196. ISSN: 0278-3649. DOI: 10.1177/027836499301200207.
- KUBELA, T., POCHYLY, A., and SINGULE, V., (2016). "Assessment of industrial robots accuracy in relation to accuracy improvement in machining processes". In: *2016 IEEE International Power Electronics and Motion Control Conference (PEMC)*. IEEE. DOI: 10.1109/epepemc.2016.7752083.
- KUKA (2023). KUKA linear units and Last access: 30.10.2023. URL: <https://www.kuka.com/en-de/products/robot-systems/robot-periphery/linear-units>.
- KUMAR, K., RANJAN, C., and DAVIM, J. P., (2020). *CNC Programming for Machining*. 1st ed. 2020. Materials Forming, Machining and Tribology. Cham: Springer International Publishing and Imprint: Springer. ISBN: 978-3-030-41278-4. DOI: 10.1007/978-3-030-41279-1.
- KUMAR, L. J., PANDEY, P. M., and WIMPENNY, D. I., eds., (2019). *3D Printing and Additive Manufacturing Technologies*. Springer eBook Collection. Singapore: Springer Singapore. ISBN: 9789811303050. DOI: 10.1007/978-981-13-0305-0.
- KYRATSIS, P., KAKOULIS, K., and MARKOPOULOS, A. P., (2020). "Advances in CAD/CAM/CAE Technologies". In: *Machines* 8.1, p. 13. ISSN: 2075-1702. DOI: 10.3390/machines8010013. URL: <https://www.mdpi.com/2075-1702/8/1/13/htm>.
- LALIT NARAYAN, K., MALLIKARJUNA RAO, K., and SARCAR, M. M. M., (2013). *Computer aided design and manufacturing*. Second printing. Delhi: PHI Learning Private Limited. ISBN: 9788120333420.
- LAMBORA, A., GUPTA, K., and CHOPRA, K., (2019). "Genetic Algorithm- A Literature Review". In: *2019 International Conference on Machine Learning, Big Data, Cloud and Parallel Computing (COMITCon)*. IEEE. DOI: 10.1109/comitcon.2019.8862255.
- LI, B., ZHANG, H., and YE, P., (2018). "Error constraint optimization for corner smoothing algorithms in high-speed CNC machine tools". In: *The International Journal of Advanced Manufacturing Technology* 99.1-4, pp. 635–646. ISSN: 1433-3015. DOI: 10.1007/s00170-018-2489-5.

- LI, F., CHEN, S., WU, Z., and YAN, Z., (2018). “Adaptive process control of wire and arc additive manufacturing for fabricating complex-shaped components”. In: *The International Journal of Advanced Manufacturing Technology* 96.1-4, pp. 871–879. ISSN: 1433-3015. DOI: 10.1007/s00170-018-1590-0. URL: <https://link.springer.com/article/10.1007/s00170-018-1590-0>.
- LI, J. Z., ALKAHARI, M. R., ROSLI, N. A. B., HASAN, R., SUDIN, M. N., and RAMLI, F. R., (2019). “Review of Wire Arc Additive Manufacturing for 3D Metal Printing”. In: *International Journal of Automation Technology* 13.3, pp. 346–353. ISSN: 1883-8022. DOI: 10.20965/ijat.2019.p0346. URL: [https://www.jstage.jst.go.jp/article/ijat/13/3/13\\_346/\\_article/-char/ja/](https://www.jstage.jst.go.jp/article/ijat/13/3/13_346/_article/-char/ja/).
- LIBERMAN, Y. L. and GORBUNOVA, L. N., (2021). “Selection of Positioning Devices for the Components of CNC Machines”. In: *Russian Engineering Research* 41.11, pp. 1067–1070. ISSN: 1934-8088. DOI: 10.3103/S1068798X21110204. URL: <https://link.springer.com/article/10.3103/s1068798x21110204>.
- LIN, J., YE, C., YANG, J., ZHAO, H., DING, H., and LUO, M., (2022). “Contour error-based optimization of the end-effector pose of a 6 degree-of-freedom serial robot in milling operation”. In: *Robotics and Computer-Integrated Manufacturing* 73, p. 102257. ISSN: 0736-5845. DOI: 10.1016/j.rcim.2021.102257. URL: <https://www.sciencedirect.com/science/article/pii/s073658452100137x>.
- LIN, Y., ZHAO, H., and DING, H., (2023). “Real-time path correction of industrial robots in machining of large-scale components based on model and data hybrid drive”. In: *Robotics and Computer-Integrated Manufacturing* 79, p. 102447. ISSN: 0736-5845. DOI: 10.1016/j.rcim.2022.102447. URL: <https://www.sciencedirect.com/science/article/pii/s0736584522001302>.
- LIU, C., LI, Y., and HAO, X., (2017). “An adaptive machining approach based on in-process inspection of interim machining states for large-scaled and thin-walled complex parts”. In: *The International Journal of Advanced Manufacturing Technology* 90.9-12, pp. 3119–3128. ISSN: 1433-3015. DOI: 10.1007/s00170-016-9647-4.
- LIU, L., GUO, F., ZOU, Z., and DUFFY, V. G., (2022). “Application, Development and Future Opportunities of Collaborative Robots (Cobots) in Manufacturing: A Literature Review”. In: *International Journal of Human-Computer Interaction*, pp. 1–18. DOI: 10.1080/10447318.2022.2041907.
- LIU, Y., WAN, M., QIN, X.-B., XIAO, Q.-B., and ZHANG, W.-H., (2020). “FIR filter-based continuous interpolation of G01 commands with bounded axial and tangential kinematics in industrial five-axis machine tools”. In: *International Journal of Mechanical Sciences* 169, p. 105325. ISSN: 00207403. DOI: 10.1016/j.ijmecsci.2019.105325.
- Lortek (2023). Fabricación aditiva en metales - WAAM and Last access: 30.10.2023. URL: <https://www.lortek.es/en/technological-areas/metal-additive-manufacturing/waam>.
- MAITI, C. K., (2017). *Introducing technology computer-aided design (TCAD): Fundamentals, simulations and applications*. Temasek Boulevard, Singapore: Pan Stanford Publishing. ISBN: 9789814745529.

- MALYSHEV, D. I., RYBAK, L. A., PISARENKO, A. S., and CHERKASOV, V. V., (2022). "Analysis of the Singularities Influence on the Forward Kinematics Solution and the Geometry of the Workspace of the Gough-Stewart Platform". In: *Advances in Service and Industrial Robotics*. Ed. by MÜLLER, A. and BRANDSTÖTTER, M. Vol. 120. Mechanisms and Machine Science. Cham: Springer International Publishing and Imprint: Springer, pp. 60–67. ISBN: 978-3-031-04869-2. DOI: 10.1007/978-3-031-04870-8{\textunderscore}8.
- Manufacturing Guide* (2023). 5-axis milling, Last access: 30.10.2023. URL: <https://www.manufacturingguide.com/en/5-axis-milling>.
- Mecademic Industrial Robotics* (2023). What are Singularities in a Six-Axis Robot Arm? | Mecademic Robotics and Last access: 02.11.2023. URL: [https://www.mecademic.com/academic\\_articles/singularities-6-axis-robot-arm/](https://www.mecademic.com/academic_articles/singularities-6-axis-robot-arm/).
- MEIER, C., PENNY, R. W., ZOU, Y., GIBBS, J. S., and HART, A. J., (2017). "THERMOPHYSICAL PHENOMENA IN METAL ADDITIVE MANUFACTURING BY SELECTIVE LASER MELTING: FUNDAMENTALS, MODELING, SIMULATION, AND EXPERIMENTATION". In: *Annual Review of Heat Transfer* 20.1, pp. 241–316. ISSN: 1049-0787. DOI: 10.1615/AnnualRevHeatTransfer.2018019042. URL: <https://www.dl.begellhouse.com/references/5756967540dd1b03,562e7b3835dec96e,0860d4f32b9f248d.html>.
- MILENKOVIC, P., (2021). "Wrist singularity avoidance with a robot end-effector adding an oblique, redundant axis". In: *Mechanism and Machine Theory* 162, p. 104355. ISSN: 0094-114X. DOI: 10.1016/j.mechmachtheory.2021.104355. URL: <https://www.sciencedirect.com/science/article/pii/s0094114x21001130>.
- NAGASAI, B. P., MALARVIZHI, S., and BALASUBRAMANIAN, V., (2022). "Effect of welding processes on mechanical and metallurgical characteristics of carbon steel cylindrical components made by wire arc additive manufacturing (WAAM) technique". In: *CIRP Journal of Manufacturing Science and Technology* 36, pp. 100–116. ISSN: 1755-5817. DOI: 10.1016/j.cirpj.2021.11.005. URL: <https://www.sciencedirect.com/science/article/pii/s1755581721001887>.
- NEE, A. Y. C., (2015). *Handbook of Manufacturing Engineering and Technology*. 1st ed. 2015. London: Springer London and Imprint: Springer. ISBN: 978-1-4471-4669-8. DOI: 10.1007/978-1-4471-4670-4.
- NX (2015). Hybrid Additive Manufacturing with NX CAM Overview - NX Manufacturing and Last access: 30.10.2023. URL: <https://blogs.sw.siemens.com/nx-manufacturing/hybrid-additive-manufacturing-with-nx-cam-overview/>.
- OU, W., MUKHERJEE, T., KNAPP, G. L., WEI, Y., and DEBROY, T., (2018). "Fusion zone geometries, cooling rates and solidification parameters during wire arc additive manufacturing". In: *International Journal of Heat and Mass Transfer* 127, pp. 1084–1094. ISSN: 0017-9310. DOI: 10.1016/j.ijheatmasstransfer.2018.08.111. URL: <https://www.sciencedirect.com/science/article/pii/s0017931018323974>.
- PAN, Z., POLDEN, J., LARKIN, N., VAN DUIN, S., and NORRISH, J., (2012). "Recent progress on programming methods for industrial robots". In: *Robotics and Computer-Integrated Manufacturing* 28.2, pp. 87–94. ISSN: 0736-5845. DOI: 10.1016/j.rcim.2011.08.004. URL: <https://www.sciencedirect.com/science/article/pii/s0736584511001001>.

- PARYANTO, BROSSOG, M., BORNSCHLEGL, M., and FRANKE, J., (2015). "Reducing the energy consumption of industrial robots in manufacturing systems". In: *The International Journal of Advanced Manufacturing Technology* 78.5-8, pp. 1315–1328. ISSN: 1433-3015. DOI: 10.1007/s00170-014-6737-z. URL: <https://link.springer.com/article/10.1007/s00170-014-6737-z>.
- PICKIN, C. G., WILLIAMS, S. W., and LUNT, M., (2011). "Characterisation of the cold metal transfer (CMT) process and its application for low dilution cladding". In: *Journal of Materials Processing Technology* 211.3, pp. 496–502. ISSN: 0924-0136. DOI: 10.1016/j.jmatprotec.2010.11.005. URL: <https://www.sciencedirect.com/science/article/pii/s0924013610003456>.
- PICKIN, C. G. and YOUNG, K., (2006). "Evaluation of cold metal transfer (CMT) process for welding aluminium alloy". In: *Science and Technology of Welding and Joining* 11.5, pp. 583–585. DOI: 10.1179/174329306X120886.
- PLOCHER, J. and PANESAR, A., (2019). "Review on design and structural optimisation in additive manufacturing: Towards next-generation lightweight structures". In: *Materials & Design* 183, p. 108164. ISSN: 02641275. DOI: 10.1016/j.matdes.2019.108164.
- PRAKASH, K. S., NANCHARAIH, T., and RAO, V. S., (2018). "Additive Manufacturing Techniques in Manufacturing -An Overview". In: *Materials Today: Proceedings* 5.2, pp. 3873–3882. ISSN: 2214-7853. DOI: 10.1016/j.matpr.2017.11.642. URL: <https://www.sciencedirect.com/science/article/pii/s2214785317329152>.
- R.V. DUBEY, J.A. EULER, and S.M. BABCOCK, (1988). *Robotics and Automation, 5th IEEE International Conference on, 1988: Proceedings*. Los Alamitos: IEEE Computer Society Press. ISBN: 0818608528. URL: <http://ieeexplore.ieee.org/servlet/opac?punumber=202>.
- RAHUL, S. G., DHIVYASRI, G., KAVITHA, P., ARUNGALAI VENDAN, S., KUMAR, K. R., GARG, A., and GAO, L., (2018). "Model reference adaptive controller for enhancing depth of penetration and bead width during Cold Metal Transfer joining process". In: *Robotics and Computer-Integrated Manufacturing* 53, pp. 122–134. ISSN: 0736-5845. DOI: 10.1016/j.rcim.2018.03.013. URL: <https://www.sciencedirect.com/science/article/pii/s0736584517304519>.
- RAMAZANOV, S., BABENKO, V., HONCHARENKO, O., MOISIEIEVA, N., and DYKAN, V., (2020). "Integrated Intelligent Information and Analytical System of Management of a Life Cycle of Products of Transport Companies". In: *Journal of Information Technology Management* 12.3, pp. 26–33. ISSN: 2008-5893. DOI: 10.22059/jitm.2020.76291. URL: [https://jitm.ut.ac.ir/article\\_76291\\_0.html](https://jitm.ut.ac.ir/article_76291_0.html).
- Reisch (2023). Prozessorientierter Digitaler Zwilling für die Additive Fertigung mittels Lichtbogenauftragschweißen (Dissertation) and Reisch, Raven.
- REITER, A., MULLER, A., and GATTRINGER, H., (2016). "Inverse kinematics in minimum-time trajectory planning for kinematically redundant manipulators". In: *IECON 2016 - 42nd Annual Conference of the IEEE Industrial Electronics Society*. IEEE. DOI: 10.1109/iecon.2016.7793436.
- RUDER, S., (2017). *An overview of gradient descent optimization algorithms*.

- SAXENA, P., STAVROPOULOS, P., KECHAGIAS, J., and SALONITIS, K., (2020). "Sustainability Assessment for Manufacturing Operations". In: *Energies* 13.11, p. 2730. ISSN: 1996-1073. DOI: 10.3390/en13112730. URL: <https://www.mdpi.com/1996-1073/13/11/2730>.
- SCHMITZ, M., WIARTALLA, J., GELFGREN, M., MANN, S., CORVES, B., and HÜSING, M., (2021). "A Robot-Centered Path-Planning Algorithm for Multidirectional Additive Manufacturing for WAAM Processes and Pure Object Manipulation". In: *Applied Sciences* 11.13, p. 5759. DOI: 10.3390/app11135759. URL: <https://www.mdpi.com/2076-3417/11/13/5759>.
- SCOTTI, F. M., TEIXEIRA, F. R., DA SILVA, L. J., ARAÚJO, D. B. de, REIS, R. P., and SCOTTI, A., (2020). "Thermal management in WAAM through the CMT Advanced process and an active cooling technique". In: *Journal of Manufacturing Processes* 57, pp. 23–35. ISSN: 1526-6125. DOI: 10.1016/j.jmapro.2020.06.007. URL: <https://www.sciencedirect.com/science/article/pii/s1526612520303807>.
- SELVI, S., VISHVAKSENAN, A., and RAJASEKAR, E., (2018). "Cold metal transfer (CMT) technology - An overview". In: *2214-9147* 14.1, pp. 28–44. ISSN: 2214-9147. DOI: 10.1016/j.dt.2017.08.002. URL: <https://www.sciencedirect.com/science/article/pii/s2214914717301022>.
- Selvi et al.* (2018). Selvi, S., Vishvaksenan, A., and Rajasekar, E.: Cold metal transfer (CMT) technology - An overview. DOI: 10.1016/j.dt.2017.08.002. URL: <https://www.sciencedirect.com/science/article/pii/s2214914717301022>.
- SHAHZADEH, A., KHOSRAVI, A., ROBINETTE, T., and NAHAVANDI, S., (2018). "Smooth path planning using biclothoid fillets for high speed CNC machines". In: *International Journal of Machine Tools and Manufacture* 132, pp. 36–49. ISSN: 0890-6955. DOI: 10.1016/j.ijmachtools.2018.04.003. URL: <https://www.sciencedirect.com/science/article/pii/s0890695518300804>.
- SHERWANI, F., ASAD, M. M., and IBRAHIM, B., (2020). "Collaborative Robots and Industrial Revolution 4.0 (IR 4.0)". In: *2020 International Conference on Emerging Trends in Smart Technologies (ICETST)*. IEEE. DOI: 10.1109/icetst49965.2020.9080724.
- SHI, X., GUO, Y., CHEN, X., CHEN, Z., and YANG, Z., (2021). "Kinematics and Singularity Analysis of a 7-DOF Redundant Manipulator". In: *Sensors* 21.21, p. 7257. ISSN: 1424-8220. DOI: 10.3390/s21217257. URL: <https://www.mdpi.com/1424-8220/21/21/7257>.
- SICILIANO, B. and KHATIB, O., (2016). *Springer handbook of robotics: With 1375 figures and 109 tables*. 2nd edition. Berlin and Heidelberg: Springer. ISBN: 978-3-319-32550-7. DOI: 10.1007/978-3-319-32552-1.
- Siemens* (2024). Continuous-path mode (G64, G641, G642, G643, G644, G645, ADIS, ADIS-POS) - SINUMERIK ... - ID: 28705635 - Industry Support Siemens and Last Access: 24/10/2023. URL: <https://support.industry.siemens.com/cs/mdm/28705635?c=19192781067&lc=en-AO>.
- SIMONIS, K., GLOY, Y.-S., and GRIES, T., (2016). "INDUSTRIE 4.0 - Automation in weft knitting technology". In: *IOP Conference Series: Materials Science and Engineering* 141.1, p. 012014. ISSN: 1757-899X. DOI: 10.1088/1757-899X/141/1/012014. URL: <https://iopscience.iop.org/article/10.1088/1757-899x/141/1/012014/meta>.

- SINGH, M., FUENMAYOR, E., HINCHY, E., QIAO, Y., MURRAY, N., and DEVINE, D., (2021). “Digital Twin: Origin to Future”. In: *Applied System Innovation* 4.2, p. 36. ISSN: 2571-5577. DOI: 10.3390/asi4020036. URL: <https://www.mdpi.com/2571-5577/4/2/36>.
- SINGH, R., KUKSHAL, V., and YADAV, V. S., (2021). “A Review on Forward and Inverse Kinematics of Classical Serial Manipulators”. In: *Advances in Engineering Design*. Ed. by RAKESH, P. K., SHARMA, A. K., and SINGH, I. Lecture Notes in Mechanical Engineering. Singapore: Springer Singapore and Imprint: Springer, pp. 417–428. ISBN: 978-981-33-4017-6. DOI: 10.1007/978-981-33-4018-3{\textunderscore}39.
- SIVANANDAM, S. N. and DEEPA, S. N., (2007). “Genetic Algorithm Optimization Problems”. In: *Introduction to genetic algorithms*. Ed. by SIVANANDAM, S. N. and DEEPA, S. N. Berlin u.a.: Springer, pp. 165–209. ISBN: 978-3-540-73189-4. DOI: 10.1007/978-3-540-73190-0{\textunderscore}7.
- SRINIVASAN, D., SEVVEL, P., JOHN SOLOMON, I., and TANUSHKUMAAR, P., (2022). “A review on Cold Metal Transfer (CMT) technology of welding”. In: *Materials Today: Proceedings* 64, pp. 108–115. ISSN: 2214-7853. DOI: 10.1016/j.matpr.2022.04.016. URL: <https://www.sciencedirect.com/science/article/pii/s2214785322021289>.
- STEVENSON, R., SHIRINZADEH, B., and ALICI, G., (2002). “Singularity avoidance and aspect maintenance in redundant manipulators”. In: pp. 857–862. DOI: 10.1109/ICARCV.2002.1238536. URL: <https://ieeexplore.ieee.org/abstract/document/1238536>.
- SUN, S. and ALTINTAS, Y., (2021). “A G3 continuous tool path smoothing method for 5-axis CNC machining”. In: *CIRP Journal of Manufacturing Science and Technology* 32, pp. 529–549. ISSN: 1755-5817. DOI: 10.1016/j.cirpj.2020.11.002. URL: <https://www.sciencedirect.com/science/article/pii/s1755581720301280>.
- SVETLIZKY, D., DAS, M., ZHENG, B., VYATSKIKH, A. L., BOSE, S., BANDYOPADHYAY, A., SCHÖENUNG, J. M., LAVERNIA, E. J., and ELIAZ, N., (2021). “Directed energy deposition (DED) additive manufacturing: Physical characteristics, defects, challenges and applications”. In: *Materials Today* 49, pp. 271–295. ISSN: 1369-7021. DOI: 10.1016/j.mattod.2021.03.020. URL: <https://www.sciencedirect.com/science/article/pii/s1369702121001139>.
- TAKEUCHI, Y., (2014). “Current State of the Art of Multi-Axis Control Machine Tools and CAM System”. In: *Journal of Robotics and Mechatronics* 26.5, pp. 529–539. ISSN: 1883-8049. DOI: 10.20965/jrm.2014.p0529. URL: [https://www.jstage.jst.go.jp/article/jrobomech/26/5/26\\_529/\\_article/-char/ja/](https://www.jstage.jst.go.jp/article/jrobomech/26/5/26_529/_article/-char/ja/).
- TIEN, D. H., DUC, Q. T., VAN, T. N., NGUYEN, N.-T., DO DUC, T., and DUY, T. N., (2021). “Online monitoring and multi-objective optimisation of technological parameters in high-speed milling process”. In: *The International Journal of Advanced Manufacturing Technology* 112.9-10, pp. 2461–2483. ISSN: 1433-3015. DOI: 10.1007/s00170-020-06444-x. URL: <https://link.springer.com/article/10.1007/s00170-020-06444-x>.
- TOMAZ, I., GUPTA, M. K., and PIMENOV, D. Y., (2021). “Subtractive Manufacturing of Different Composites”. In: *Additive and Subtractive Manufacturing of Composites*. Springer, Singapore, pp. 137–165. DOI: 10.1007/978-981-16-3184-9{\textunderscore}6. URL: [https://link.springer.com/chapter/10.1007/978-981-16-3184-9\\_6](https://link.springer.com/chapter/10.1007/978-981-16-3184-9_6).

- TUNC, L. T. and STODDART, D., (2017). “Tool path pattern and feed direction selection in robotic milling for increased chatter-free material removal rate”. In: *The International Journal of Advanced Manufacturing Technology* 89.9-12, pp. 2907–2918. ISSN: 1433-3015. DOI: 10.1007/s00170-016-9896-2. URL: <https://link.springer.com/article/10.1007/s00170-016-9896-2>.
- UHLMANN, E., REINKOBER, S., and HOLLERBACH, T., (2016). “Energy Efficient Usage of Industrial Robots for Machining Processes”. In: 2212-8271 48, pp. 206–211. ISSN: 2212-8271. DOI: 10.1016/j.procir.2016.03.241. URL: <https://www.sciencedirect.com/science/article/pii/s2212827116305303>.
- VALENTE, A., BARALDO, S., and CARPANZANO, E., (2017). “Smooth trajectory generation for industrial robots performing high precision assembly processes”. In: *CIRP Annals* 66.1, pp. 17–20. ISSN: 00078506. DOI: 10.1016/j.cirp.2017.04.105. URL: <https://www.sciencedirect.com/science/article/pii/s0007850617301051>.
- VAN LE, T., PARIS, H., and MANDIL, G., (2017). “Environmental impact assessment of an innovative strategy based on an additive and subtractive manufacturing combination”. In: *Journal of Cleaner Production* 164, pp. 508–523. ISSN: 0959-6526. DOI: 10.1016/j.jclepro.2017.06.204. URL: <https://www.sciencedirect.com/science/article/pii/s0959652617313732>.
- VANDE WEGHE, M., FERGUSON, D., and SRINIVASA, S. S., (2007). “Randomized path planning for redundant manipulators without inverse kinematics”. In: *2007 7th IEEE-RAS International Conference on Humanoid Robots*. IEEE. DOI: 10.1109/ichr.2007.4813913.
- WAN, S., LI, X., SU, W., YUAN, J., HONG, J., and JIN, X., (2019). “Active damping of milling chatter vibration via a novel spindle system with an integrated electromagnetic actuator”. In: *Precision Engineering* 57, pp. 203–210. ISSN: 0141-6359. DOI: 10.1016/j.precisioneng.2019.04.007. URL: <https://www.sciencedirect.com/science/article/pii/s0141635918307931>.
- WANG, J., GOYANES, A., GAISFORD, S., and BASIT, A. W., (2016). “Stereolithographic (SLA) 3D printing of oral modified-release dosage forms”. In: *International Journal of Pharmaceutics* 503.1-2, pp. 207–212. ISSN: 0378-5173. DOI: 10.1016/j.ijpharm.2016.03.016. URL: <https://www.sciencedirect.com/science/article/pii/s0378517316302150>.
- WANG, L., LIU, Y., YU, Y., ZHANG, J., and SHU, B., (2022). “Optimization of redundant degree of freedom in robotic milling considering chatter stability”. In: *The International Journal of Advanced Manufacturing Technology* 121.11-12, pp. 8379–8394. ISSN: 1433-3015. DOI: 10.1007/s00170-022-09889-4.
- WANG, W., GUO, Q., YANG, Z., JIANG, Y., and XU, J., (2023). “A state-of-the-art review on robotic milling of complex parts with high efficiency and precision”. In: *Robotics and Computer-Integrated Manufacturing* 79, p. 102436. ISSN: 0736-5845. DOI: 10.1016/j.rcim.2022.102436. URL: <https://www.sciencedirect.com/science/article/pii/s073658452200120x>.
- WATSON, J. K. and TAMINGER, K. M. B., (2015). “A decision-support model for selecting additive manufacturing versus subtractive manufacturing based on energy consumption”. In: *Journal of Cleaner Production* 176, pp. 1316–1322. ISSN: 0959-6526. DOI: 10.1016/j.jclepro.2015.01.030.

- j.jclepro.2015.12.009. URL: <https://www.sciencedirect.com/science/article/pii/s0959652615018247>.
- WEI, Y., JIAN, S., HE, S., and WANG, Z., (2014). “General approach for inverse kinematics of nR robots”. In: *Mechanism and Machine Theory* 75, pp. 97–106. ISSN: 0094-114X. DOI: 10.1016/j.mechmachtheory.2014.01.008.
- Weiss (2024). DR Delta Robots. URL: <https://www.weiss-world.com/gb-en/products/robots-10327/delta-robots-211;%20Last%20Access:%2005.01.2024>.
- WICKRAMASINGHE, S., DO, T., and TRAN, P., (2020). “FDM-Based 3D Printing of Polymer and Associated Composite: A Review on Mechanical Properties, Defects and Treatments”. In: *Polymers* 12.7, p. 1529. ISSN: 2073-4360. DOI: 10.3390/polym12071529. URL: <https://www.mdpi.com/2073-4360/12/7/1529>.
- WU, B., PAN, Z., DING, D., CUIURI, D., LI, H., XU, J., and NORRISH, J., (2018). “A review of the wire arc additive manufacturing of metals: properties, defects and quality improvement”. In: *Journal of Manufacturing Processes* 35, pp. 127–139. ISSN: 1526-6125. DOI: 10.1016/j.jmapro.2018.08.001. URL: <https://www.sciencedirect.com/science/article/pii/s1526612518310739>.
- WU, K., LI, J., ZHAO, H., and ZHONG, Y., (2022). “Review of Industrial Robot Stiffness Identification and Modelling”. In: *Applied Sciences* 12.17, p. 8719. DOI: 10.3390/app12178719. URL: <https://www.mdpi.com/2076-3417/12/17/8719>.
- XIONG, G., DING, Y., and ZHU, L., (2019). “Stiffness-based pose optimization of an industrial robot for five-axis milling”. In: *Robotics and Computer-Integrated Manufacturing* 55, pp. 19–28. ISSN: 0736-5845. DOI: 10.1016/j.rcim.2018.07.001. URL: <https://www.sciencedirect.com/science/article/pii/s0736584517304556>.
- XU, T., CHEN, Z., LI, J., and YAN, X., (2015). “Automatic tool path generation from structuralized machining process integrated with CAD/CAPP/CAM system”. In: *The International Journal of Advanced Manufacturing Technology* 80.5-8, pp. 1097–1111. ISSN: 1433-3015. DOI: 10.1007/s00170-015-7067-5. URL: <https://link.springer.com/article/10.1007/s00170-015-7067-5>.
- YANG, B., ZHANG, G., RAN, Y., and YU, H., (2019). “Kinematic modeling and machining precision analysis of multi-axis CNC machine tools based on screw theory”. In: *Mechanism and Machine Theory* 140, pp. 538–552. ISSN: 0094-114X. DOI: 10.1016/j.mechmachtheory.2019.06.021. URL: <https://www.sciencedirect.com/science/article/pii/s0094114x19307992>.
- YANG, J. and YUEN, A., (2017). “An analytical local corner smoothing algorithm for five-axis CNC machining”. In: *International Journal of Machine Tools and Manufacture* 123, pp. 22–35. ISSN: 0890-6955. DOI: 10.1016/j.ijmachtools.2017.07.007.
- YANG, X.-S., (2011). “Metaheuristic Optimization: Algorithm Analysis and Open Problems”. In: Springer, Berlin, Heidelberg, pp. 21–32. DOI: 10.1007/978-3-642-20662-7{\textunderscore}2. URL: [https://link.springer.com/chapter/10.1007/978-3-642-20662-7\\_2](https://link.springer.com/chapter/10.1007/978-3-642-20662-7_2).
- YE, W., (2022). “Exploring the Use of Industrial Robots in CNC Machine Tool Programming and Operation Courses”. In: *2022 7th International Conference on Mechatronics System and Robots (ICMSR)*. IEEE. DOI: 10.1109/icmsr2020.2022.00017.

- YUAN, L., PAN, Z., DING, D., HE, F., VAN DUIN, S., LI, H., and LI, W., (2020). “Investigation of humping phenomenon for the multi-directional robotic wire and arc additive manufacturing”. In: *Robotics and Computer-Integrated Manufacturing* 63, p. 101916. ISSN: 0736-5845. doi: 10.1016/j.rcim.2019.101916. URL: <https://www.sciencedirect.com/science/article/pii/s0736584519304260>.
- YUE, C., GAO, H., LIU, X., LIANG, S. Y., and WANG, L., (2019). “A review of chatter vibration research in milling”. In: *1000-9361* 32.2, pp. 215–242. ISSN: 1000-9361. doi: 10.1016/j.cja.2018.11.007. URL: <https://www.sciencedirect.com/science/article/pii/s1000936119300147>.
- ZHANG, Y., WANG, T., DONG, J., PENG, P., LIU, Y., and KE, R., (2020). “An analytical G3 continuous corner smoothing method with adaptive constraints adjustments for five-axis machine tool”. In: *The International Journal of Advanced Manufacturing Technology* 109.3-4, pp. 1007–1026. ISSN: 1433-3015. doi: 10.1007/s00170-020-05402-x.
- ZHAO, H., ZHANG, B., YIN, X., ZHANG, Z., XIA, Q., and ZHANG, F., (2021). “Singularity Analysis and Singularity Avoidance Trajectory Planning for Industrial Robots”. In: *2021 China Automation Congress (CAC)*. IEEE. doi: 10.1109/cac53003.2021.9727497.
- Zhao et al. (2018). DSCarver: Zhao, Haisen et al. doi: 10.1145/3197517.3201338.

## **Disclaimer**

I hereby declare that this thesis is entirely the result of my own work except where otherwise indicated. I have only used the resources given in the list of references.

Garching, March 04, 2024

---

(Signature)